UNIVERSITY OF CALIFORNIA SAN DIEGO

Techniques for Measuring the Mechanical Properties of Organic Semiconductors

A Dissertation submitted in partial satisfaction of the requirements for the degree of

Doctor of Philosophy

in

Nanoengineering

by

Daniel Rodriquez Jr

Committee in charge:

Professor Darren J. Lipomi, Chair
Professor Shengqiang Cai
Professor Tina Ng
Professor Jan Talbot
Professor Sheng Xu

2018

The Dissertation of Daniel Rodriquez Jr is approved, and it is acceptable in quality and form for publication on microfilm and electronically:

_____

_____

_____

_____

_____

Chair

University of California San Diego

2018

DEDICATION

This thesis is dedicated to my mother, Janie.

EPIGRAPH

You can’t predict the waves, but you can learn to surf.

TABLE OF CONTENTS

LIST OF FIGURES

LIST OF TABLES

ACKNOWLEDGEMENTS

My PhD was the culmination of a nine year journey and a ride I never imagined taking. If you would've told me fourteen years ago that I would one day be writing and defending a doctoral thesis, I would have fiercely denied it. Whether it was fate or fortune that allowed me to reach these heights, there are a number of events and people in my life that have contributed to my success. The relationships and knowledge I have gained professionally and personally will last a lifetime and I am truly grateful.

Joining the U.S Navy after high school was pivotal for my growth and maturity. I learned so much about life outside of my hometown of Fresno, CA. The exposure to such a diverse range of personalities and cultures improved my ability to empathize and a gave me global perspective. The navy also taught me discipline and how to follow a plan to reach my goals. Joseph Ugalde was the first friend I made in the navy. Thank you for being a good friend and sparking my academic journey by encouraging me to complete my associate degree while we were serving. Russell Meyer and I met while I was stationed in Bahrain and we had a blast going to see cover bands and playing pool. Russell is not only a good friend, but he is also the person that first introduced me to the field of engineering. It makes me happy to see other veterans pursue college and become successful engineers. David Hellstrom is a good friend that I met at my last duty station, the USS Preble. Some of my best memories in the navy come from traveling the western pacific with David on my first (and last) sea deployment. David continues to be a good friend and great source of encouragement and support.

I met Ernesto Magaña at community college shortly after separating from the navy and we have been friends ever since. Thanks for debating with me and always being DTS. Nate Velez, Steven Accardo, and Jesus Zavala thanks for keeping me sane throughout undergrad with a good

mix of fun and study sessions. I still can't believe that each of us was a veteran from a different branch of the military! Han Nguyen thanks for the study sessions and the good humor.

The Lipomi Research Group. Suchol Savagatrup thank you for being a great mentor and ultimately a friend. Your work ethic and example provided the framework that helped make my PhD so successful. Adam Printz thank you for your knowledge and continued support throughout the years, your presence in the lab has certainly been missed, by absolutely no one. Brandon Marin I am really glad we met, your sense of humor is one of a kind. Thank you for being a source of guidance and deep laughs. It's great to see others from our culture and background thrive and prosper. Julian Ramirez I can always count on you to understand my sense of humor and debate about music or sports; I look forward to continuing our friendship in the years to come. Sam Root thank you for the good times and awesome collaborations, you are a simulation god. Cody Carpenter thank you for your wisdom of coffee, the great conversations, and reminding me to keep my hip flexors stretched. The walks and talks with you and Sam were some really good times. Mohammad Alkhadra you will forever be a boss and a friend. You taught me a lot about personal discipline, but then again that's nothing to a boss. Rachel O., Andrew C., Anne C., Armando U., and Madeleine R. thank you for being awesome mentees and a joy to work with. Dana Jimenez thank you for being one of the nicest and most helpful people in the Nanoengineering department.

Darren Lipomi, it has been great having you as an advisor. Thank you for helping me see that I was capable and qualified to pursue a PhD. Your knowledge and innovation are inspiring and you helped shape the scientist and engineer that I am today. I'm going to miss the lab culture, friends, and work environment that I have grown accustom to in the Lipomi group. I look forward to continuing our friendship outside of the lab.

There are no words sufficient enough to describe the love and support that I have received from my mother, Janie. Mom thank you for showing me strength, resilience, and true unconditional love. I am only able to reach these heights because I stand on your shoulders, I love you. To my stepdad, Sam, thank you for showing me what it means to work hard and take care of a family. I attribute my tenacious work ethic to you. My siblings Christopher, Jonathan, and Elizabeth your relentless teasing (love) reminds me to never take anything too seriously and the importance of family; each of you make me proud. Thank you for being there through the good times and the bad, together we can overcome anything. Sarah, Sammy, Prince, and Jessica thank you for always being encouraging and supportive throughout my life. To my in-laws Jennifer, Stephen, Cassie, and Whitley thank you for your support, you have shown me nothing but love and encouragement. Alec and Noelle thanks for welcoming me into your family and treating me like an older brother. To my nieces and nephews Leah, Avery, Violet, Coen, and Joey, I love seeing each of you grow and become your own person. To Annie, David, Mary, Cathy, Juan Carlos, Mary Ann, Caroline, Teresa, and Sonia thank you for always being there in times of need. I love you all.

To my wife, Briana, I love you more every day. You are my best friend, gym partner, travel buddy, gaming buddy, and favorite person to get food and coffee with. It's been amazing to grow with you as two separate people and become one. Thank you for showing me what it means to be loved and for being a continuous, never-ending source of support. I can't wait to start this next chapter in our lives and continue our incredible journey!

I also include the following acknowledgements below as required by the University of California, San Diego.

Chapter 1, in full, is a reprint of the material as it appears in Chemistry of Materials, 2015, 27, 3902-3911. Suchol Savagatrup, Daniel Rodriquez, Adam D. Printz, Alexander B. Sieval, Jan

C. Hummelen, and Darren J. Lipomi. American Chemical Society, 2015. Suchol Savagatrup was the primary investigator and author of this paper.

Chapter 2, in full, is a reprint of the material as it appears in *ACS Applied Materials & Interfaces*, 2016, 8, 11649-11657. Daniel Rodriquez, Suchol Savagatrup, Eduardo Valle, Christopher M. Proctor, Caitlin McDowell, Guillermo C. Bazan, Thuc-Quyen Nguyen, and Darren J. Lipomi. American Chemical Society, 2016. The dissertation author was the primary investigator and author of this paper.

Chapter 3, in full, is a reprint of the material as it appears in *ACS Applied Materials & Interfaces*, 2017, 9, 8855-8862. Daniel Rodriquez, Jae-Han Kim, Samuel E. Root, Zhuping Fei, Pierre Boufflet, Martin Heeney, Taek-Soo Kim, and Darren J. Lipomi. American Chemical Society, 2017. The dissertation author was the primary investigator and author of this paper.

Chapter 4, in part, has been submitted for publication of the material as it may appear in ACS Macro Letters, 2018. Daniel Rodriquez, James G. Kohl, Pierre Morel, Kyle Burrows, Grégory Favaro, Samuel E. Root, Julian Ramirez, Mohammad A. Alkhadra, Cody W. Carpenter, Zhuping Fei, Pierre Boufflet, Martin Heeney, Darren J. Lipomi. American Chemical Society, 2018. The dissertation author was the primary investigator and author of this paper.

VITA

2004 – 2009	Information Systems Technician, 2nd Class. United States Navy
2009	Associate of Arts, National University
2014	Bachelor of Science in Nanoengineering, University of California San Diego
2015	Teaching Assistant, Department of Electrical Engineering, University of California San Diego
2015	Master of Science in Nanoengineering, University of California San Diego
2013–2018	Graduate Researcher, University of California San Diego
2018	Doctor of Philosophy in Nanoengineering, University of California San Diego

PUBLICATIONS

Rodriquez, D. Kohl, J. G., Morel, P., Burrows, K., Favaro, G., Root, S. E., Ramirez, J., Alkhadra, M. A., Fei, Z., Boufflet, P., Heeney, M., and Lipomi, D. J. "*Measurement of Cohesion and Adhesion of Semiconducting Polymers by Scratch Testing: Effect of Side-Chain Length and Degree of Polymerization.*" ACS Macro Letters, 2018, 7, 1003.

Sugiyama, F., Kleinschmidt, A., Kayser, L. V., **Rodriquez, D.**, Finn III, M., Alkhandra, M., Wan, J., Ramirez, J., Chiang, A., Root, S. E., Savagatrup, S., Lipomi, D. J. "*Effects of flexibility and branching of side chains on the mechanical properties of low-bandgap conjugated polymers.*" Polymer Chemistry, 2018, DOI: 10.1039/c8py00820e.

Sugiyama, F., Kleinschmidt, A., Kayser, L. V., Alkhandra, M., Wan, J., Chiang, A., **Rodriquez, D.**, Root, S., Savagatrup, S., Lipomi, D. J. "*Stretchable and Degradable Semiconducting Block Copolymers.*" Macromolecules, 2018, DOI: 10.1021/acs.macromol.8b00846.

Kayser, L. V., Russell, M. D., **Rodriquez, D.**, Abuhamdieh, S. N., Dhong, C., Khan, S., Stein, A. N., Ramírez, J., Lipomi, D.J. "*RAFT Polymerization of an Intrinsically Stretchable Water-Soluble Block Copolymer Scaffold for PEDOT*." Chemistry of Materials, 2018, 30, 13, 4459.

Ramirez, J., **Rodriquez, D.**, Qiao, F., Warchall, J., Rye, J., Aklile, E., Chiang, A. S-C., Marin, B., Mercier, P. P., Cheng, C., Hutcheson, K. A., Shinn, E. H., and Lipomi, D. J. "*Metallic Nanoislands on Graphene for Monitoring Swallowing Activity in Head and Neck Cancer Patients*." ACS Nano, 2018, 12, 6, 5913.

Alkhadra, M. A., Kleinschmidt, A. T., Root, S. E., **Rodriquez, D.**, Printz, A. D., Savagatrup, S., and Lipomi, D. J., "*Mechanical Properties of Semiconducting Polymers*," in *Handbook of Conducting Polymers*, 4th ed., Skotheim, T.A., Reynolds, J. R., Thompson, B. C., Invited book chapter, CRC Press, 2018 (in press)

Root, S. E., Carpenter C. W., Kayser, K. V., **Rodriquez, D.**, Davies, D. M., Wang, S., Tan S. T. M., Meng, S. Y., Lipomi, D. J., "*Ionotactile Stimulation: Nonvolatile Ionic Gels for Human–Machine Interfaces*." ACS Omega, 2018, 3, 1, 662.

Carpenter C. W., Dhong, C., Root, N. B., **Rodriquez, D.**, Abdo, E. E., Skelil, K., Alkhadra, M. A., Ramirez, J., Ramachandran, V. S., Lipomi, D. J., "*Human ability to discriminate surface chemistry by touch*." Materials Horizons, 2018, 5, 70.

Alkhadra, M. A., Root, S. E., Hilby, K. M., **Rodriquez, D.**, Sugiyama, F., Lipomi, D. J., "*Quantifying the Fracture Behavior of Brittle and Ductile Thin Films of Semiconducting Polymers*." Chemistry of Materials, 2017, 29, 23, 10139.

Root, S. E., Savagatrup, S., Printz, A. D., **Rodriquez, D.**, and Lipomi D. J., "*Mechanical Properties of Organic Semiconductors for Stretchable, Highly Flexible, and Mechanically Robust Electronics*." Chemical Reviews, 2017, 117, 9, 6467.

Rodriquez, D., Kim, J.H., Root, S. E., Fei, Z., Bouffet, P., Heeney, M., Kim, T.S., and Lipomi, D. J. "*Comparison of Methods for Determining the Mechanical Properties of Semiconducting Polymer Films for Stretchable Electronics*." ACS Applied Materials & Interfaces, 2017, 9, 10, 8855.

Root, S. E., Alkhadra, M. A., **Rodriquez, D.**, Printz, A. D., and Lipomi D. J., "*Measuring the Glass Transition Temperature of Conjugated Polymer Films with Ultraviolet–Visible Spectroscopy*." Chemistry of Materials, 2017, 29, 7, 2646.

Rodriquez, D., Savagatrup, S., Valle, E., Proctor, CM., McDowell, C., Bazan, G. C., Nguyen, TQ., and Lipomi, D. J. "*Mechanical Properties of Solution-Processed Small-Molecule Semiconductor Films*." ACS Applied Materials & Interfaces, 2016, 8, 18, 11649.

Savagatrup, S., **Rodriquez, D.**, Printz, A. D., Sieval, A. B., Hummelen, J. C., and Lipomi, D. J. "*[70]PCBM and incompletely separated grades of methanofullerenes produce bulk heterojunctions with increased robustness for ultra-flexible and stretchable electronics*." Chemistry of Materials, 2015, 27, 11, 3902.

Printz, A. D., Savagatrup, S., **Rodriquez, D.**, and Lipomi, D. J. "*Role of molecular mixing on the stiffness of polymer: fullerene bulk heterojunction films*." Solar Energy Materials and Solar Cells, 2015, 134, 64.

Savagatrup, S., Printz, A. D., O'Connor, T. F., Zaretski, A. V., **Rodriquez, D.**, Sawyer, E. J., Rajan, K., Acosta, R. I., Root, S. E., and Lipomi, D. J. "*Mechanical degradation and stability of*

organic solar cells: molecular and microstructural determinants." Energy and Environmental Science, 2015, 8, 1, 55.

Savagatrup, S., Chan, E., Renteria-Garcia, S. M., Printz, A. D., Zaretski, A. V., O'Connor, T. F., **Rodriquez, D.**, Valle, E., and Lipomi, D. J. "*Plasticization of PEDOT:PSS by common additives for mechanically robust organic solar cells and wearable sensors*." Advanced Functional Materials, 2015, 25, 3, 427.

Savagatrup, S., Printz, A. D., **Rodriquez, D.**, and Lipomi, D. J. "*Best of both worlds: conjugated polymers exhibiting good photovoltaic behavior and high tensile elasticity*." Macromolecules, 2014, 47, 6, 1981.

ABSTRACT OF THE DISSERTATION

Techniques for Measuring the Mechanical Properties of Organic Semiconductors

by

Daniel Rodriquez Jr

Doctor of Philosophy in Nanoengineering

University of California San Diego, 2018

Professor Darren J. Lipomi, Chair

Mechanical flexibility and deformability are at the core of the advantages offered by organic semiconductors. Therefore, an in-depth understanding of the mechanical properties of these materials is crucial to the design of robust organic electronic devices such as solar cells, sensors, and displays. Since these devices are typically fabricated as thin films, on the order of 200 nm, it can be difficult to measure the mechanical properties using traditional techniques, such as

tensile testing, that require bulk samples. This thesis examines and compares various methods of testing the mechanical properties of thin films and correlates the molecular structure of organic semiconductors to such properties. Chapter 1 and Appendix A use mechanical buckling and crack-onset strain techniques to measure the elastic modulus and the strain at fracture in fullerene-based semiconductors. These methods were used to examine the effect of incompletely separated grades of electron acceptors on the mechanical deformability of organic solar cells in an effort to simultaneously improve the mechanical robustness of the organic solar cells and reduce the energy of production. Chapter 2 and Appendix B use mechanical buckling, crack-onset strain, and the onset of wrinkles (collectively known as film-on-elastomer techniques) to show a decrease in the stiffness and an increase in the ductility of small-molecule semiconductors that bear side-chains in the backbone structure and compare the results to fullerene-based semiconductors. Chapter 3 and Appendix C compare the results from two different methods of measuring thin-film mechanical properties; film-on-elastomer and film-on-water methods. The film-on-water method uses water to support thin films while conducting a tensile test. These methods were used to measure the mechanical properties of poly(3-hexylthiophene) in a range of molecular weight and the results were directly compared. In Chapter 4 and Appendix D a technique known as scratch testing was used, for the first time, to measure the cohesion and adhesion of semiconducting polymers. The cohesive and adhesive strength were measured as a function of the length of the side chain in poly(3-alkylthiophenes) and molecular weight in poly(3-hexylthiophene).

Introduction

Techniques for Measuring the Mechanical Properties of Organic Semiconductors

Daniel Rodriquez Jr.[a]

[a] *Department of NanoEngineering, University of California, San Diego, 9500 Gilman Drive Mail Code 0448, La Jolla, CA 92093-0448.*

Overview

My thesis work is primarily composed of two parts (1) the discovering, implementing, and comparing of techniques for measuring the mechanical properties of thin-film organic semiconductors and (2) using these techniques to study structure-property relationships in organic semiconductors.

Mechanical Properties of Organic Semiconductors

Mechanical flexibility and deformability are at the core of the advantages offered by organic semiconductors. Most of the applications for which these materials are destined require some degree of mechanical compliance. For example, organic semiconductors are often associated with large-area and low-cost fabrication techniques such as screen, slot-die, and roll-to-roll printing.[1–3] Brittle materials cannot withstand the stresses caused by bending and thermal expansion during these processes. It has been shown, however, that organic semiconductors exhibit a wide range of mechanical behaviour from extremely brittle to highly ductile.[4] To survive the rigors of roll-to-roll printing, some degree of flexibility and durability is required. Additional applications include integration into fabrics and textiles[5,6] as well as skin-wearable sensors and displays.[7] These types of applications require an even larger degree of mechanical deformability and may even require stretchability. While the mechanical properties of these materials can be easily tuned, there is an interplay between mechanical deformability and the electronic performance. Oftentimes it has been shown that the most deformable organic semiconductors are also the worst performing. Therefore, there is a significant effort in literature to co-optimize both properties (mechanical and electronic) simultaneously to realize the full potential of organic semiconductors.[8]

There are several parameters that affect the mechanical properties of organic semiconductors.[4] For example, prior studies have shown that increasing the length of the side chain in P3ATs lowers the elastic modulus and increases the crack-onset strain.[9] This result is mainly due to a decrease in the density of the films and a suppression of the glass transition temperature, T_g, from above to below room temperature. The T_g is a measure of the mobility of polymer chains. Polymers that exist above their T_g are said to exhibit liquid-like behaviour and can easily slip past one another under an applied stress. Below the T_g the polymer chains behave like a glass and typically exhibit brittle behaviour. The molecular weight of polymer semiconductors can also have a profound impact on the mechanical properties.[10,11] Prior studies have shown that bulk P3HT tapes exhibit larger elongations and greater values of toughness at high molecular weight.[12] These increases are correlated to an increase in the density of entanglements, which are physical linkages of polymer chains, in the amorphous domains of the material. Furthermore, there is an increase in the number of tie-molecules, which occurs when one polymer chain becomes part of multiple crystallites, in the crystalline regions of the polymer. Overall these two effects improve the connectivity in the material and raise the energy required for polymer chains to slip past one another under an applied load. Additionally, the dispersity of a polymer network can affect the mechanical properties. This occurs due to smaller polymer chains behaving as small-molecules and plasticizing the material. Amorphous polymer semiconductor films are typically more stretchable than highly crystalline films.[13] This is due to the ability of the amorphous domains to rearrange and plastically deform in response to a stress.

Techniques for Measuring the Mechanical Properties of Thin Films

Organic semiconductors are typically fabricated as thin films, on the order of 50-500 nm thick. It is very difficult to manipulate free-standing films of this thickness without the material being supported by a substrate. Oftentimes the material will just crumble upon itself due to van der Waals forces. Due to their extreme thinness it is difficult to measure their mechanical properties using traditional techniques, such as tensile testing, that were intended for bulk samples. In addition, organic synthesis of these materials typically only yields small quantities on the order of milligrams. However, to attain bulk measurements gram scale quantities are needed which is beyond the capability of most academic laboratories. Therefore, alternate techniques have been developed to test the mechanical properties of especially thin films.

The Buckling-Based Metrology

One of the most widely used techniques for testing the mechanical properties of thin films is the buckling-based metrology. First demonstrated in 1998 by Whitesides and Hutchinson[14] and later perfected into a metrology technique by Stafford,[15,16] the buckling method uses pre-strained elastomeric substrates as a support for thin films. Upon release of this strain an instability is formed and manifests as sinusoidal wrinkles on the surface of the material in question. The wavelength of these buckles along with the thickness of the film, the elastic modulus of the substrate, and the Poisson's ratio of both the substrate and the film can be used to extract the elastic modulus of the thin film under study. This method requires a few assumptions to be considered valid; 1) the thickness of the substrate >> thickness of the thin film 2) the elastic modulus of the thin film >> the modulus of the substrate 3) pre-strain

is within the elastic region of the thin film and 4) the amplitude of the buckles << than their wavelength.

Onset of Buckles

Buckling can also be used to determine the yield point in thin film materials. The yield point is the strain at which plastic (permanent) deformation begins to occur. This method was first demonstrated in 2015 by Printz.[17] By laminating a thin film onto an unstrained elastomer and incrementally and cyclically, loading and unloading the film (i.e. 0 → 1% → 0%, 0 → 2% → 0%, 0 → 3% → 0%, etc.), surface wrinkles form upon surpassing of the yield point. Together with surface wrinkling these two methods can roughly estimate the linear region of a stress-strain curve for thin film materials. The area under this region will give a rough estimate of the modulus of resilience which is defined as the maximum amount of energy, per unit volume, that a material can absorb elastically.

Crack-onset strain

The strain at which materials fail is the strain at failure. However, for methods that use elastomers as substrates the strain at failure can be artificially high since the substrate can redistribute stress away from the film. Instead of labelling the strain at failure, crack-onset measurements label the first appearance of cracks in a thin film at a given magnification.[18] There are a few parameters that can affect this measurement such as the adhesion of the thin film to the substrate. Additionally, the modulus mismatch between the thin film and the elastomeric substrate can affect the measurement.[19] In general, a greater elastic mismatch will lead to the appearance of cracks at a lower strain.

Film-on-Elastomer (FOE) Methods

Collectively the buckling-based metrology, the onset of wrinkles, and the crack-onset strain measurements are referred to as film-on-elastomer methods. These techniques can be used to roughly estimate the key features of a stress-strain curve (elastic modulus, yield point, strain at failure). There is not a FOE method that can capture the plastic behaviour of thin films between the yield point and the crack-onset strain. However, by estimating a constant stress from the yield point to the crack-onset strain very rough estimates of the modulus of toughness can be extracted. The modulus of toughness is defined as the maximum amount of energy, per unit volume, that a material can absorb before rupturing.

Film-on-water (FOW) Method

In 2013, a new technique for measuring the mechanical properties of thin films was demonstrated by Kim.[20,21] In this method water is used as a pseudo-substrate for supporting thin-film materials. Water was chosen for its high surface tension and low viscosity. While the film is suspended on the water surface a load cell and a linear actuator can be attached using soft elastomeric grips that make van der Waals adhesion with the thin film. A tensile test can then be conducted, and a full stress-strain curve is produced. The stress-strain curve produced in this technique is not an estimation and is more accurate than the estimated curve in the FOE methods. Values for the modulus of resilience and the modulus of toughness can be precisely extracted from these curves. This technique is useful for thin-film materials that do not degrade or interact with water (i.e. swell or dissolve). However, there is still the possibility of using other liquids, such as glycerol, as pseudo-substrates for materials that are incompatible with water.

Scratch Testing of Thin Films and Coatings

Scratch testing is a well-known method that is used industrially to qualitatively characterize the cohesion and adhesion of thin films and coatings to substrates.[22,23] In a progressive load scratch test, a hard indenter tip (typically diamond) is impressed into a material with a force that increases linearly with position. Cohesive failure occurs due to tensile stress behind the stylus tip and can be observed as cracking or tearing in the material. Adhesive failure occurs due to compressive stress in front of the stylus tip and can be observed as chipping or delamination away from the substrate. The forces at which cohesive and adhesive failure occur are used to compare the cohesion and adhesion of the materials under study. Scratch testing is best used as a comparative analysis for the cohesion and adhesion of multiple materials to a single substrate or of one material to multiple substrates.

Alternate Methods

There are other techniques for measuring thin-film mechanical properties, but these methods were not explored in this thesis. A few of these methods will be briefly described here. Nano-indentation uses small cantilevers to impress into thin films and measure the force response from the material.[24,25] The penetration depth along with the shape of the cantilever can be used to extract the elastic modulus, stiffness, and hardness of a thin film. Nano dynamic mechanical analysis (NanoDMA) is like nano-indentation except the cantilever is oscillated at a specific frequency to extract values of the storage and loss modulus.[10] Four-point bend (FPB)[26,27] and double-cantilever beam (DCB)[28] measurements have been successfully used to extract the critical fracture energy, G_c, of thin films.

Organization of Chapters

Chapter 1 describes my co-author work on using mechanical buckling and crack-onset strain measurements (film-on-elastomer techniques) to study the effect of isomerism and purity on the mechanical properties of fullerene-based organic semiconductors and their blends with poly(3-hexylthiophene) (P3HT). This study also examines these effects on the solar cell performance of these materials when mixed with P3HT.

Chapter 2 uses film-on-elastomer techniques to measure the mechanical properties of non-fullerene small-molecule organic semiconductors that bear linear alkyl and branched alkyl side chains. The solar cell performance of these small-molecule semiconductors was also examined in this work. To co-optimize both solar cell performance and mechanical deformability, additives of high molecular weight polystyrene and 1,8-diiodooctane were used.

Chapter 3 is a comparison of two different methods of measuring the mechanical properties of thin-film organic semiconductors. The first is a collection of methods known as film-on-elastomer (FOE) techniques and is comprised of mechanical buckling (elastic modulus), onset of surface wrinkles (yield point), and crack-onset (strain at failure) measurements. Together these techniques can be used to roughly estimate the key features of a stress-strain curve. The second method, known as the film-on-water (FOW) technique, uses water as a pseudo-substrate to support thin films while conducting a tensile test and produces full stress-strain curves (not estimates). These techniques were used to measure the mechanical properties of P3HT in a range of molecular weights and the results were directly compared.

Chapter 4 utilizes a method known as scratch testing, for the first time, to measure the cohesion and adhesion of polymer semiconductors to substrates. This study examined the effect of side chain length of poly(3-alkylthiophenes) (P3ATs) and molecular weight of P3HT on the cohesion and adhesion of these materials to silicon substrates.

References

(1) Krebs, F. C. All Solution Roll-to-Roll Processed Polymer Solar Cells Free from Indium-Tin-Oxide and Vacuum Coating Steps. *Org. Electron. physics, Mater. Appl.* **2009**, *10* (5), 761–768.

(2) Krebs, F. C.; Tromholt, T.; Jørgensen, M. Upscaling of Polymer Solar Cell Fabrication Using Full Roll-to-Roll Processing. *Nanoscale* **2010**, *2* (6), 873–886.

(3) Carle, J. E.; Andersen, T. R.; Helgesen, M.; Bundgaard, E.; Jorgensen, M.; Krebs, F. C. A Laboratory Scale Approach to Polymer Solar Cells Using One Coating/Printing Machine, Flexible Substrates, No ITO, No Vacuum and No Spincoating. *Sol. Energy Mater. Sol. Cells* **2013**, *108*, 126–128.

(4) Root, S. E.; Savagatrup, S.; Printz, A. D.; Rodriquez, D.; Lipomi, D. J. Mechanical Properties of Organic Semiconductors for Stretchable, Highly Flexible, and Mechanically Robust Electronics. *Chem. Rev.* **2017**, *117* (9), 6467–6499.

(5) Ding, Y.; Invernale, M. A.; Sotzing, G. A. Conductivity Trends of Pedot-Pss Impregnated Fabric and the Effect of Conductivity on Electrochromic Textile. *ACS Appl. Mater. Interfaces* **2010**, *2* (6), 1588–1593.

(6) Bihar, E.; Roberts, T.; Ismailova, E.; Saadaoui, M.; Isik, M.; Sanchez-Sanchez, A.; Mecerreyes, D.; Hervé, T.; De Graaf, J. B.; Malliaras, G. G. Fully Printed Electrodes on Stretchable Textiles for Long-Term Electrophysiology. *Adv. Mater. Technol.* **2017**, 1600251.

(7) Liang, J.; Li, L.; Niu, X.; Yu, Z.; Pei, Q. Elastomeric Polymer Light-Emitting Devices and Displays. *Nat. Photonics* **2013**, *7* (10), 817–824.

(8) Savagatrup, S.; Printz, A. D.; Rodriquez, D.; Lipomi, D. J. Best of Both Worlds: Conjugated Polymers Exhibiting Good Photovoltaic Behavior and High Tensile Elasticity. *Macromolecules* **2014**, *47* (6), 1981–1992.

(9) Savagatrup, S.; Makaram, A. S.; Burke, D. J.; Lipomi, D. J. Mechanical Properties of Conjugated Polymers and Polymer-Fullerene Composites as a Function of Molecular Structure. *Adv. Funct. Mater.* **2014**, *24* (8), 1169–1181.

(10) Bruner, C.; Dauskardt, R. Role of Molecular Weight on the Mechanical Device Properties of Organic Polymer Solar Cells. *Macromolecules* **2014**, *47*, 1117–1121.

(11) Holmes, N. P.; Ulum, S.; Sista, P.; Burke, K. B.; Wilson, M. G.; Stefan, M. C.; Zhou, X.; Dastoor, P. C.; Belcher, W. J. The Effect of Polymer Molecular Weight on P3HT:PCBM Nanoparticulate Organic Photovoltaic Device Performance. *Sol. Energy Mater. Sol. Cells* **2014**, *128*, 369–377.

(12) Koch, F. P. V.; Rivnay, J.; Foster, S.; Müller, C.; Downing, J. M.; Buchaca-Domingo, E.; Westacott, P.; Yu, L.; Yuan, M.; Baklar, M.; et al. The Impact of Molecular Weight on Microstructure and Charge Transport in Semicrystalline Polymer Semiconductors-Poly(3-Hexylthiophene), a Model Study. *Prog. Polym. Sci.* **2013**, *38* (12), 1978–1989.

(13) Root, S. E.; Jackson, N.; Savagatrup, S.; Arya, G.; Lipomi, D. J. Modelling the Morphology and Thermomechanical Behaviour of Low-Bandgap Conjugated Polymers and Bulk Heterojunction Films. *Energy Environ. Sci.* **2016**, *10*, 558–569.

(14) Bowden, N.; Brittain, S.; Evans, A. G.; Hutchinson, J. W.; Whitesides, G. M. Spontaneous Formation of Ordered Structures in Thin. *Nature* **1998**, *393* (May), 146–149.

(15) Chung, J. Y.; Nolte, A. J.; Stafford, C. M. Surface Wrinkling: A Versatile Platform for Measuring Thin-Film Properties. *Adv. Mater.* **2011**, *23* (3), 349–368.

(16) Stafford, C. M.; Harrison, C.; Beers, K. L.; Karim, A.; Amis, E. J.; VanLandingham, M. R.; Kim, H. C.; Volksen, W.; Miller, R. D.; Simonyi, E. E. A Buckling-Based Metrology for Measuring the Elastic Moduli of Polymeric Thin Films. *Nat. Mater.* **2004**, *3* (8), 545–550.

(17) Printz, A. D.; Zaretski, A. V.; Savagatrup, S.; Chiang, A. S.-C.; Lipomi, D. J. Yield Point of Semiconducting Polymer Films on Stretchable Substrates Determined by Onset of Buckling. *ACS Appl. Mater. Interfaces* **2015**, *7*, 23257–23264.

(18) Lipomi, D. J. Stretchable Figures of Merit in Deformable Electronics. *Adv. Mater.* **2016**, *28* (22), 4180–4183.

(19) Alkhadra, M. A.; Root, S. E.; Hilby, K. M.; Rodriquez, D.; Sugiyama, F.; Lipomi, D. J. Quantifying the Fracture Behavior of Brittle and Ductile Thin Films of Semiconducting Polymers. *Chem. Mater.* **2017**, *29*, 10139–10149.

(20) Kim, J.-H.; Nizami, A.; Hwangbo, Y.; Jang, B.; Lee, H.-J.; Woo, C.-S.; Hyun, S.; Kim, T.-S. Tensile Testing of Ultra-Thin Films on Water Surface. *Nat. Commun.* **2013**, *4*, 2520.

(21) Kim, T.; Kim, J.-H.; Kang, T. E.; Lee, C.; Kang, H.; Shin, M.; Wang, C.; Ma, B.; Jeong, U.; Kim, T.-S.; et al. Flexible, Highly Efficient All-Polymer Solar Cells. *Nat. Commun.* **2015**, *6* (May), 8547.

(22) Kohl, J. G.; Randall, N. X.; Schwarzer, N.; Ngo, T. T.; Shockley, M. J.; Nair, R. P. An Investigation of Scratch Testing of Silicone Elastomer Coatings with a Thickness

Gradient. *J. Appl. Polym. Sci.* **2011**, *124*, 2978–2986.

(23) Kohl, J. G.; Singer, I. L.; Schwarzer, N.; Yu, V. Y. Effect of Bond Coat Modulus on the Durability of Silicone Duplex Coatings. *Prog. Org. Coatings* **2006**, *56* (2–3), 220–226.

(24) Li, X.; Bhushan, B. A Review of Nanoindentation Continuous Stiffness Measurement Technique and Its Applications. *Mater. Charact.* **2002**, *48* (1), 11–36.

(25) Fischer-Cripps, A. C. Critical Review of Analysis and Interpretation of Nanoindentation Test Data. *Surf. Coatings Technol.* **2006**, *200* (14–15), 4153–4165.

(26) Brand, V.; Bruner, C.; Dauskardt, R. H. Cohesion and Device Reliability in Organic Bulk Heterojunction Photovoltaic Cells. *Sol. Energy Mater. Sol. Cells* **2012**, *99*, 182–189.

(27) Balar, N.; O'Connor, B. T. Correlating Crack Onset Strain and Cohesive Fracture Energy in Polymer Semiconductor Films. *Macromolecules* **2017**, acs.macromol.7b01282.

(28) Dupont, S. R.; Oliver, M.; Krebs, F. C.; Dauskardt, R. H. Interlayer Adhesion in Roll-to-Roll Processed Flexible Inverted Polymer Solar Cells. *Sol. Energy Mater. Sol. Cells* **2012**, *97*, 171–175.

Chapter 1

[70]PCBM and incompletely separated grades of methanofullerenes produce bulk heterojunctions with increased robustness for ultra-flexible and stretchable electronics

Suchol Savagatrup,[a] Daniel Rodriquez,[a] Adam D. Printz,[a] Alexander B. Sieval,[b] Jan C. Hummelen,[b,c] and Darren J. Lipomi[a]

[a] *Department of NanoEngineering, University of California, San Diego, 9500 Gilman Drive Mail Code 0448, La Jolla, CA 92093-0448.*

[b] *Solenne BV, Zernikepark 6-8, 9747 AN Groningen, Netherlands*

[c] *Stratingh Institute for Chemistry and Zernike Institute for Advanced Materials, University of Groningen, Nijenborgh 4, 9747 AG Groningen, Netherlands*

Abstract

An organic solar cell based on a bulk heterojunction (BHJ) of a polymer and a methanofullerene ([60]PCBM or [70]PCBM) exhibits a complex morphology that controls both its photovoltaic and mechanical compliance (robustness, flexibility, and stretchability). Methanofullerenes are excellent electron acceptors, however they have relatively high cost and production energy (in the purest samples) compared to other small-molecule semiconductors. Moreover, [60]PCBM and [70]PCBM—typical of van der Waals solids—can be stiff and brittle. Stiffness and brittleness may lower the yield of working modules in roll-to-roll manufacturing, shorten the lifetime against mechanical failure in outdoor conditions, and jeopardize wearable and portable applications that demand stretchability or extreme flexibility. This paper tests the hypothesis that "technical grade" PCBM (incompletely separated but otherwise pure blends containing ≥90% [60]PCBM or [70]PCBM) could lower the cost of manufacturing organic solar cells while simultaneously increasing their mechanical stability. Measurements of tensile modulus of five methanofullerene samples, "technical grades" and 99% grades of both [60]PCBM and [70]PCBM, and a 1:1 mixture [60]PCBM and [70]PCBM, along with their blends with regioregular poly(3-hexylthiophene) (P3HT), lead to two important conclusions: (1) Films of pure [70]PCBM are approximately five times more compliant than films of pure [60]PCBM; BHJ films with [70]PCBM are also more compliant than those with [60]PCBM. (2) Bulk heterojunction films comprising technical grades of [60]PCBM and [70]PCBM are approximately two to four times more compliant than are films made using 99% grades. Tensile modulus is found to be an excellent predictor of brittleness: BHJs produced with technical grade methanofullerene accommodate strains 1.4 to 2.2 times greater than those produced with 99% grades. The smallest range of stretchability was found for BHJs with 99% [60]PCBM (fracture at 3.5% strain), while the greatest

is found for technical grade [70]PCBM (11.5% strain). Mechanical properties are correlated to the microstructures of the blended films informed from analyses of UV-vis spectra using the weakly interacting H-aggregate model. Photovoltaic measurements show that solar cells made with technical grade [70]PCBM have similar efficiencies to those made with higher-grade material, but with decreased cost, and increased mechanical robustness.

1.1 Introduction and Background

1.1.1 Methanofullerenes in organic solar cells.

Increasing the mechanical compliance of organic semiconductors in a way that does not sacrifice electronic performance will accomplish two goals. The first goal is to improve the lifetime against mechanical failure for printed, flexible devices.[1] The second goal is to enable a new class of ultra-flexible and intrinsically stretchable devices for portable, lightweight power sources,[2] wearable and implantable health monitors,[3] and fracture-proof consumer electronics.[4] One important application of organic semiconductors is the organic solar cell, in which fullerenes and their derivatives are present in all of the most efficient devices produced to date.[5] The high electron mobilities of fullerenes,[6] the solubility of methanofullerenes (e.g., [60]PCBM and [70]PCBM, **Figure 1.1**), high rates of charge transfer,[7] and their spherical (or quasi-spherical) shape, which permits transfer of an electron from any direction, suggest that fullerenes will continue to be the material of choice for a variety of applications. These materials, however, have high embodied energy in their purest form,[8,9] and polymer:methanofullerene bulk heterojunction films are stiffer, more brittle, and have lower cohesive energy in comparison to films of the pure polymer.[10–12] Additionally, the high energies of production (because of the resources needed to separate them by chromatography) are correlated with the high cost of methanofullerenes (compared to

conjugated polymers and small molecules, such as copper phthalocyanine).[9] We hypothesized that disorder introduced into BHJ films in the form of isomers or mixed sizes within the PCBM phases would affect the mechanical properties of polymer:methanofullerene bulk heterojunction blends, which will influence the yield of working devices during roll-to-roll coating[13] and the lifetime against mechanical failure in outdoor or portable environments, or in stretchable and ultra-flexible applications.[1,14] Using "technical grades" of PCBM,[15–17] in which the C_{60} and C_{70} derivatives are incompletely separated but otherwise pure, it might be possible to address two problems at the same time: reducing the cost and production energy of organic solar cells, and simultaneously increasing the mechanical resilience. While our group and others have examined the role of the polymer in determining the deformability of the active components in ultra-compliant systems, the role of small molecule semiconductors—of which methanofullerenes may be the most prominent class—has not been explored.

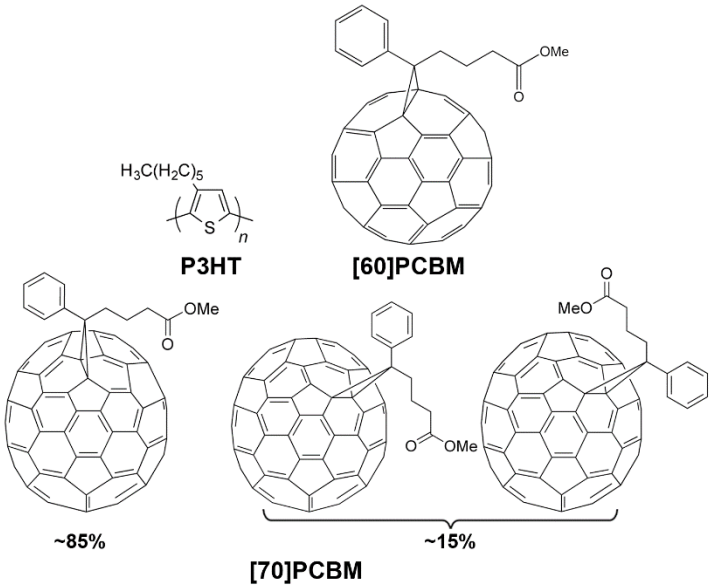

Figure 1.1. Chemical structures of P3HT and the methanofullerenes studied. Isomers of [70]PCBM depicting the structures of the chiral α-type isomer (left) and the two possible β-type isomers (right). The α-type isomer is present in 85% and the two β-type isomers are present in approximately equal amounts. More isomers exists in theory (not in figure), but at most in very small amounts (from HPLC and ^{1}H NMR) (see also ref. [18]).

1.1.2 Embodied energy of methanofullerenes.

Fullerenes have high energies of production, in part, because they need to be separated from the carbon soot produced by the two common methods of production: pyrolysis (of toluene or tetralin) or arc plasma with graphite as a feedstock.[9] According to the analysis by Anctil et al., pyrolysis requires 146 kg tetralin to produce 1 kg of C_{60} and 0.78 kg of C_{70}.[9] C_{70} has a greater production energy than does C_{60} largely because C_{70} is more difficult to separate from higher-order fullerenes than is C_{60}; the purification steps (from 95% to 99.9% purity) increase the embodied energy of C_{60} by a factor of two and of C_{70} by a factor of three.[9] The net result is that the embodied energies of [60]PCBM and [70]PCBM (after functionalization of the fullerene core) at 99.9% purity are 65 GJ kg^{-1} and 90 GJ kg^{-1}, respectively.[9] (While these values are nearly an order of magnitude higher than those of polysilicon,[19] methanofullerenes are present in much smaller absolute amounts in organic solar cells than polysilicon is present in conventional cells.) The contribution of methanofullerenes to the cumulative energy demand of an entire module, however, is substantial: from 19% to 31%, depending on the choices of other materials in devices in which the electron donor is a polymer.[20] Substantial savings in embodied energy (which correlates well with cost for manufactured products)[9] are thus possible if one can use mixtures of methanofullerenes. The use of these mixed methanofullerene derivatives (technical grades) will produce different morphologies in bulk heterojunction films than will highly purified samples. For example, Andersson et al. showed a drastic change in the morphology of a polymer:[60]PCBM blend with the addition of <10% [70]PCBM to the methanofullerene component.[15] One expects these different morphologies to affect not only the electronic performance of the blend, but also its compliance and mechanical stability,[15,21] through the effect of increased free volume in mixtures of molecules of different sizes or isomers.

1.1.3 Mechanical properties and morphology of the bulk heterojunction.

Organic semiconductors exhibit a wide range of tensile moduli, ranging from 30 MPa to 16 GPa,[11] and propensity to fracture, from <2.5% strain to greater than 150% strain on elastic substrates.[22] This disparity suggests that modules composed of different organic semiconductors may have unequal yields during mechanically rigorous roll-to-roll manufacturing processes, unequal lifetimes in the environment, and unequal amenabilities to stretchable and ultra-flexible applications.[23] One key determinant of the variation in mechanical properties in the active layer of an organic solar cell is the morphology of the donor-acceptor bulk heterojunction. Morphology refers to the details of molecular mixing, the texture and degree of crystallinity of the phases, and the extent of phase separation.[24] These key parameters have a large influence on the power conversion efficiencies of organic solar cells, given materials with good charge-transport properties, complementary absorption, and favorable relative positions of their frontier molecular orbitals. It has been shown that the mechanical properties of bulk heterojunction systems comprising conjugated polymers and small molecules are influenced by many aspects of the chemical structure (e.g., the presence of the fused or isolated rings in the main chain,[25,26] length and the composition of pendant groups,[10,27] size and intermolecular forces within crystallites)[22] and microstructural order (e.g., the addition of methanofullerene,[10,11,21,25–27] intercalation of methanofullerenes between side chains of polymers,[28,29] effect of processing conditions,[21] presence of plasticizing additives).[10,30] One aspect of the makeup of the bulk heterojunction whose effects on the mechanical properties have not been explored is the makeup (i.e., size and purity) of the methanofullerene phase.

We thus investigated two methanofullerene derivatives—[60]PCBM and [70]PCBM—at two different grades—99% grade, and technical grades (≥90% either [60]PCBM or [70]PCBM,

and the remainder the other) along with their blends with regioregular poly(3-hexylthiophene) (P3HT). The hypothesis that guided our experiments was that the use of methanofullerene samples with technical grades of [60]PCBM and [70]PCBM (i.e., incomplete separation of C_{60} and C_{70} derivatives) would form BHJ films with greater compliance than films in which the methanofullerene sample was of 99% grade. We measured two mechanical properties, the tensile modulus and the ductility (as manifested in the crack on-set strain), of P3HT:methanofullerene films before thermal annealing (as-cast, AC) and after thermal annealing (annealed, AN), as well as pure methanofullerene films. The tensile moduli were measured using the mechanical buckling technique.[31,32] The crack on-set strains were used to measure the ductility of the film on a stretchable substrate. We observed trends in the mechanical properties that were correlated with the microstructures of the blended films informed from analyses of UV-vis spectra using the weakly interacting H-aggregate model. Our results led us to conclude that it is possible to increase the mechanical compliance of a bulk heterojunction film by using technical grade methanofullerenes (thereby lowering the cost and embodied energy), which produce statistically similar photovoltaic efficiencies.

1.2 Results and Discussion

1.2.1 Mechanical properties of pure methanofullerene and bulk heterojunction films.

We measured the tensile moduli of films using the buckling technique.[11,31] Briefly, the film of interest was spin-coated onto passivated glass slide, then transferred to an elastomeric substrate bearing a small tensile pre-strain. The pre-strain was then released, and the resulting compression forced the film to adopt buckles. For the bulk heterojunction films, the tensile modulus of each film, E_f, was calculated from the measured buckling wavelength, λ_b, the thickness of the film, d_f,

the tensile modulus of the substrate, E_s, and the Poisson's ratios of the film and the substrate, v_f and v_s, using equation 1:

$$E_f = 3E_s\left(\frac{1-v_f^2}{1-v_s^2}\right)\left(\frac{\lambda_b}{2\pi d_f}\right)^3 \quad (\mathbf{1})$$

However, the high stiffness and brittleness of the pure methanofullerenes caused the films to fracture when the pre-strain was released; this damage precluded accurate measurements.[10,33] To avoid this problem, we performed the measurement on a bilayer system comprising a PEDOT:PSS film and the pure methanofullerene film. We chose the layer of PEDOT:PSS as the second layer to behave as a substrate with favorable surface energy and allow for a uniform film of pure methanofullerene. Studies on the interface mixing of PEDOT:PSS and the layer of P3HT:PCBM by Huang et al.[34] and Dupont et al.[35] have shown that very little methanofullerene diffuses into PEDOT:PSS at room temperature, and thus we assumed the presence of a distinct interface. We then used equation 2 to calculate the modulus of the methanofullerene film ($E_{f,2}$) (**Figure 1.2a**, dark grey bars) from the effective modulus of the bilayer (E_{eff}) and the modulus of the PEDOT:PSS film ($E_{f,1}$);[32] both E_{eff} and $E_{f,1}$ are obtained separately via the typical buckling method. (A detailed explanation of the calculation is provided in the Supporting Information.)

$$E_{eff} = \frac{1+m^2n^4+2mn(2n^2+3n+2)}{(1+n)^3(1+mn)}E_{f,1};\ \text{where } m=\frac{E_{f,2}}{E_{f,1}},\ n=\frac{d_{f,2}}{d_{f,1}} \quad (\mathbf{2})$$

From the results summarized in **Figure 1.2a** and **Table 1.1**, the moduli of the pure [60]PCBM films were higher than the pure [70]PCBM films for both technical grade (Tech. Gr.) and 99% samples. We attributed this observation to the greater tendency of [60]PCBM to pack efficiently and to crystallize.[36,37] The difference in behavior is consistent with the presence of isomers in [70]PCBM, which hinder efficient packing. Importantly, we observed that technical grade [60]PCBM had a lower modulus than 99% [60]PCBM. The average value for technical grade

[70]PCBM was somewhat lower than for 99% [70]PCBM, but within experimental error. In addition, we observed that value of the 1:1 mixture of [60]PCBM and [70]PCBM sat between the values of the technical grades of [60]PCBM and [70]PCBM.

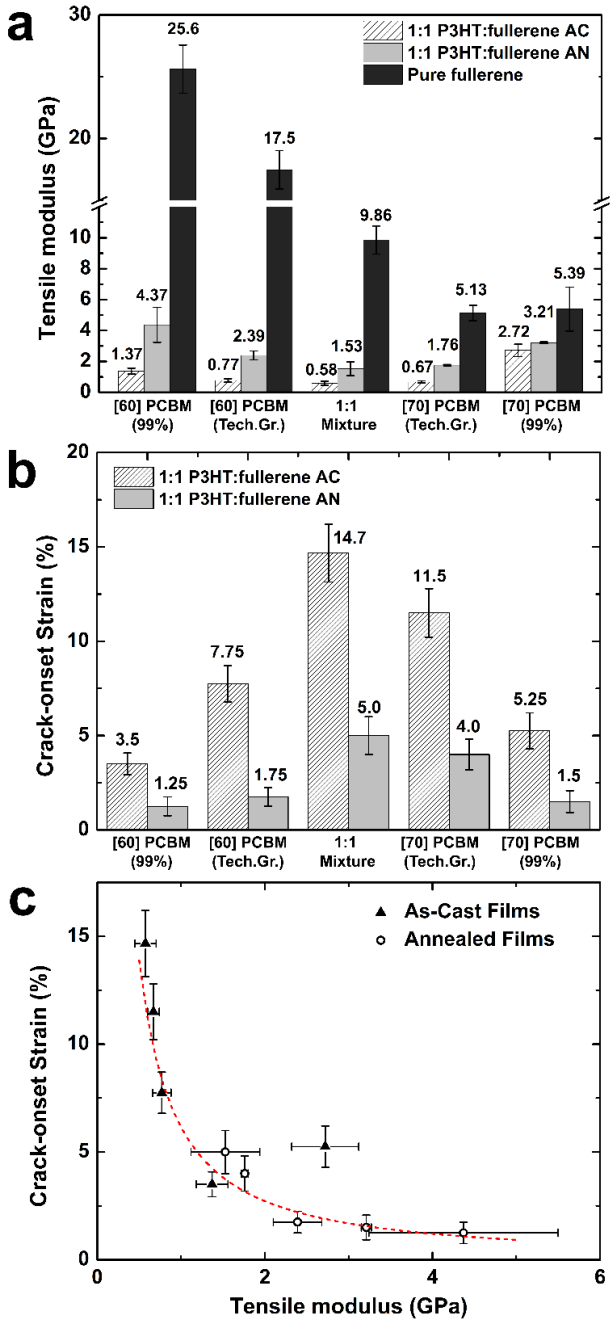

Figure 1.2. Mechanical properties of the bulk heterojunction and pure methanofullerene films, arranged from left to right in order of increasing content of [70]PCBM. (a) Tensile moduli of films tested in this work. The dark gray bars represent the tensile moduli of pure methanofullerene films as obtained from the bilayer method. The bilayer systems consisted of PEDOT:PSS/methanofullerene. The light gray bars and gray bars represent the moduli of blends of P3HT:methanofullerene (1:1 ratio) spin-coated from chloroform solution for both as-cast and annealed films. The value of the tensile modulus of the pure P3HT film measured in parallel to these experiments was 0.55 ± 0.09 GPa. (b) Uniaxial crack-onset strains of the thin films transferred onto PDMS substrate. All pure methanofullerene films cracked at strains below 0.5%. (c) Plot of the correlation between crack-onset strains and tensile moduli of all the films tested.

Table 1.1. Summary of tensile moduli of the methanofullerene films tested in this work from measurement with the buckling-based method and the bilayer technique.[†] The value of the pure as-cast P3HT used in this experiment, obtained in parallel, was 0.55 ± 0.09 GPa.

Materials	Tensile modulus (GPa)				
	[60]PCBM (99%)	[60]PCBM (Tech. Gr.)	1:1 Mixture	[70]PCBM (Tech. Gr.)	[70]PCBM (99%)
Pure methanofullerene[§]	25.6 ± 1.95	17.5 ± 1.55	9.86 ± 0.91	5.13 ± 0.50	5.39 ± 1.42
P3HT:methanofullerene (1:1, As-cast)[‡]	1.37 ± 0.19	0.77 ± 0.11	0.58 ± 0.13	0.67 ± 0.07	2.72 ± 0.40
P3HT:methanofullerene (1:1, Annealed)[‡]	4.37 ± 1.13	2.39 ± 0.29	1.53 ± 0.44	1.76 ± 0.04	3.21 ± 0.06

[†] The bilayer technique uses the buckling-based method to obtain the effective modulus of the bilayer system comprising a layer of PEDOT:PSS film (modulus obtained separately) and pure methanofullerene film, and then backs out the modulus of the pure methanofullerene film. [§] Obtained from the modified bilayer technique. [‡] Obtained from conventional buckling-based method.

Table 1.2. Summary of crack-onset strains of the thin films when transferred onto PDMS substrate.

Materials	Crack-onset strain (%)				
	[60]PCBM (99%)	[60]PCBM (Tech.Gr.)	1:1 Mixture	[70]PCBM (Tech. Gr.)	[70]PCBM (99%)
Pure methanofullerene	< 0.5	< 0.5	< 0.5	< 0.5	< 0.5
P3HT:methanofullerene (1:1, As-cast)	3.5 ± 0.58	7.75 ± 0.98	14.7 ± 1.53	11.5 ± 1.29	5.25 ± 0.96
P3HT:methanofullerene (1:1, Annealed)	1.25 ± 0.5	1.75 ± 0.5	5.0 ± 1.0	4.0 ± 0.82	1.5 ± 0.58

We then characterized the mechanical properties of the P3HT:methanofullerene blends. We used a single polymer (regioregular P3HT) to isolate the effects of the methanofullerene. We selected regioregular P3HT because it is the most widely studied material in the literature for bulk heterojunction OPV devices.[38] While it has not produced state-of-the-art values of *PCE* in several years[39] (though some recent reports have been favorable),[40] it seems to be especially amenable to scale-up by roll-to-roll coating[41] because it works well in relatively thick films, and it has a low cost due to its short synthetic route.[8,42] Moreoever, the morphology of P3HT when mixed with [60]PCBM is the basis for many studies in the field,[38] and the mechanical properties of pure P3HT and P3HT:[60]PCBM films have been well characterized.[10,11,21,25] In previous publications by our group, we reported the tensile modulus of pure P3HT to be 1.09 ± 0.15 GPa.[10] This value was in

the range of those reported by various groups, or 0.22 to 1.33 GPa.[11,21,25] The modulus of the batch of pure P3HT used in this study was 0.55 ± 0.09 GPa, approximately half the value we obtained in our previous study.[10] We attribute the differences in moduli commonly obtained for P3HT (and generally not other materials) primarily to the closeness of its glass transition temperature (T_g = 12–25 °C)[43,44] to ambient temperature, and possibly to the sensitivity of its T_g to batch-to-batch variability. Our principal concern, however, was not with the absolute values of the tensile moduli, but with the effects of the methanofullerene component.

Figure 1.2a shows the tensile modulus of the BHJ films, and **Table 1.1** summarizes the tensile moduli of the films tested in this work. The crack-onset strains (**Figure 1.2b**) correlate well with the measured tensile moduli: films with higher modulus are more brittle (**Figure 1.2c**). While we note that the crack-onset strains provide a measurement of the apparent brittleness of the active layer films, the mechanical properties of complete solar cell devices will be dependent not only on the P3HT:methanofullerene actively layer, but also on all other components of the device (e.g. the substrate and the electrode). However, in the case that the substrate and the electrode are more compliant than the active layer,[30] the active layer will be the limiting factor in the mechanical compliance and robustness of solar cell devices. In stretchable devices for wearable or biologically integrated applications, all components must accommodate tensile strain in a specified range.

The data in **Figure 1.2** reveal four salient features: (1) all BHJ films were stiffer than films of the pure polymer (consistent with previous results[10,11,21,25]); (2) thermal annealing increased the stiffness of all BHJ films;[22,27] (3) technical grade methanofullerenes and 1:1 mixture of [60]PCBM and [70]PCBM produced lower moduli in the BHJ films; (4) films containing principally [70]PCBM were more compliant than films containing principally [60]PCBM given the same thermal history in three of four cases. The following discussion attempts to explain these key

observations using spectroscopic and photovoltaic measurements, and arguments from the literature.

1.2.2 Stiffening effect of methanofullerenes on the pure polymers.

The current model of the bulk heterojunction, which has been derived principally from blends of poly(3-alkylthiophene) (P3AT) and [60]PCBM, comprises a three-phase system: an aggregated polymer-rich phase, a methanofullerene-rich phase, and a well-mixed amorphous phase.[38] The mixed phase forms as a consequence of the miscibility of methanofullerene molecules within the amorphous domains of the polymer,[45,46] and thus the current model predicts the absence of pure amorphous polymer domains in P3HT:PCBM films. In a compelling visualization of the evolution in morphology of the BHJ, Roehling et al. used electron-tomographic three-dimensional reconstructions of a blend before and after annealing (using an endohedral methanofullerene for phase contrast), and showed a clear reduction of the fraction of the mixed phase.[47] The ratio of phases within the ternary system went from (P3HT:methanofullerene:mixed) 28:28:44 (as-cast) to 50:37:13 (annealed), or "mostly mixed" to "mostly crystalline P3HT."[47]

The crystalline phases of methanofullerenes have been characterized in detail.[48] In particular, Zheng et al. observed a striking evolution in crystalline morphology in pure [60]PCBM films from needle-like, to axialite, to faceted crystalline slices.[49] A similar transformation was observed in crystallites grown in the interface between a solvent and a non-solvent.[50] In blended films of P3HT:[60]PCBM, Verploegen et al. used grazing incidence X-ray scattering (GIXS) to measure the evolution in crystallization of the two components during thermal annealing, and observed diffraction peaks consistent with crystalline [60]PCBM.[36] Indeed [60]PCBM is known to form crystals upon extended annealing that are large enough to be visible by optical

microscopy.[51] Thus, the current model predicts that the [60]PCBM-enriched phase in the bulk heterojunction is at least partially crystalline.[38] Due to the presence of isomers in [70]PCBM, however, has not been observed to crystallize in neat films or in blends. The disorder in [70]PCBM was the basis of our hypothesis that the larger methanofullerene might produce films with reduced stiffness.

In every instance in which the moduli of pure conjugated polymers and their blends with fullerenes are reported in the same paper, the blends are stiffer than the pure polymer.[10,11,21] The mechanical properties of pure P3ATs are influenced, among other factors, by the degree of crystallinity and the T_g of the amorphous domains relative to ambient temperature. The proximity of T_g to ambient temperature suggests that the temperature at which experiments are carried out is near the high end of the range in which P3HT is in the glassy state. While the ordered domains of P3HT are generally unaffected by the presence of methanofullerenes in BHJ films,[52] the pure amorphous phase of the polymer is consumed by methanofullerene to form the mixed phase. Methanofullerene molecules not dispersed in the mixed phase form a third, methanofullerene-enriched phase that is either amorphous or partially ordered (in the case of [60]PCBM, which can pack efficiently because it is a single isomer). Differences in mechanical properties between the pure polymer and the BHJ can thus be attributed to the effects of the mixed phase and the methanofullerene-enriched phase. Because the pure methanofullerene films are stiffer than either pure P3HT or the corresponding BHJ, we predicted that the methanofullerene-enriched domains behave as stiff inclusions within the BHJ film. We also suspect that the mixed phase in a BHJ film is stiffer than the amorphous phase in pure P3HT. This behavior is consistent with the observation by Hopkinson et al., and confirmed by us, that the addition of [60]PCBM increases T_g of P3HT—i.e., [60]PCBM is an anti-plasticizer.[53] The high modulus of the P3HT:[60]PCBM blend relative

to the pure polymer is also predicted on the basis of the composite theory applied to BHJ films by Tahk et al.,[11] but the agreement may be serendipitous because it does not take into account the presence of pure, unmixed phases. In a separate study, our group has shown that the ratio of the polymer to methanofullerene also strongly influenced the mechanical properties of the resulting BHJ films; the tensile modulus increased when the weight percentage of methanofullerene was increased from 0% to 50%.[54]

1.2.3 Stiffening effect of thermal annealing.

A trade-off between electronic and mechanical properties has been observed in the context of thermal history of organic semiconductors.[21] Generally, post-processing treatment such as thermal annealing increases the crystallinity of the materials, which usually improves the electrical properties while in some cases increases the stiffness. For example, films of PBTTT doubled in tensile modulus after thermal annealing,[22] while pure P3HT films exhibited a minimal change in modulus.[21,25] The effect of thermal annealing of pure polymer films on the mechanical properties is thus not generalizable. Polymer:methanofullerene blends, however, have been consistently shown to increase in tensile modulus with thermal treatment.[27] The origin of the increase in modulus is the thermally evolved microstructure of the ternary blend. As-cast P3HT:PCBM films are characterized by low order and a large percentage of mixed phase.

An increasing volume fraction of ordered polymer and methanofullerene-enriched phases should be correlated with an increase in modulus of the blended film. Order in P3HT can be determined using a widely practiced method, based on the work of Spano and coworkers, who showed that the UV-vis spectra of the polymer can be deconvoluted into contributions from the aggregated (i.e., ordered) and amorphous phases utilizing the weakly interacting H-aggregate

model.[55] The ratio of these contributions, after taking into account the unequal absorption coefficients of the ordered and the amorphous domains, can be used to determine the percent aggregated polymer. To analyze the order of different P3HT:methanofullerene blends, we first obtained the UV-vis spectra of the blend and then subtracted the absorption of the pure methanofullerene. **Figures 1.3a** and **1.3b** show the evolution in the ultraviolet-visible (UV-vis) spectra of the P3HT component of the P3HT:methanofullerene blends. The absorption due to the methanofullerenes was approximated as the absorption of thin films of the methanofullerenes (prepared in the same manner as the blends) and subtracted from the spectra of the blends.[21,56] (Before subtraction, the methanofullerene absorption spectra were normalized to the peaks at 335 nm for [60]PCBM and 379 nm for [70]PCBM.) Though this method of subtraction overestimates the methanofullerene contribution to the absorption spectra, it has a minimal effect on the strongly absorbing regions of P3HT. (While we note that [70]PCBM is more strongly absorbing in the visible region than [60]PCBM, the absorbance is still dominated by the P3HT component of the blend in the visible region.) The absence of vibronic peaks (longer-wavelength shoulders) in the as-cast films suggests the absence of ordered aggregates of pure polymer. A clear increase in order upon thermal annealing is observed from the differences in the UV-vis spectra. To obtain the percent of the polymer in the aggregated phase of the annealed films, we used a MATLAB program to perform a least-squares fit of the weakly interacting H-aggregate model to the experimental data. This method was introduced by Clark et al. and later used by Awartani et al. to correlate microstructure to mechanical properties,[21,57] and produces consistent fits that are relatively insensitive to the range of bounds for the fit (as long as it is performed in the strongly absorbing region for aggregated polymer).[56] The morphology as assayed by UV-vis was not dependent on the substrate: spin-coating the BHJ films on glass treated with oxygen plasma, passivated with a

fluorinated silane monolayer, or on glass bearing a film of PEDOT:PSS produced indistinguishable UV-vis spectra (**Figure C.1**, Supporting Information).

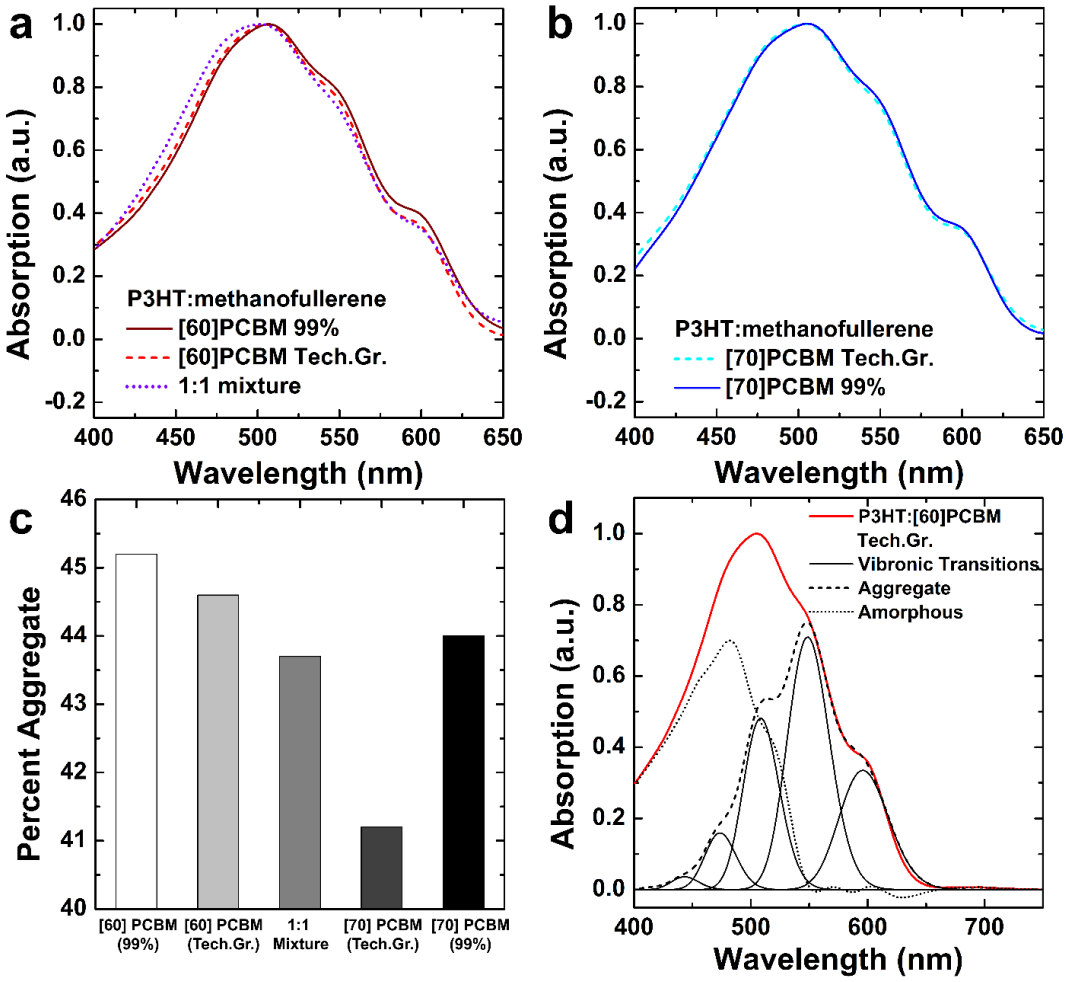

Figure 1.3. Absorption of P3HT:methanofullerene thin films after annealing treatment with the methanofullerene signal subtracted. (a) P3HT with [60]PCBM for 99% grade and technical grade (Tech. Gr.) along with the 1:1 mixture of [60]PCBM and [70]PCBM. (b) P3HT with [70]PCBM for technical grade (Tech. Gr.) and 99% grade. (c) Percent aggregate of the P3HT:methanofullerene films as calculated via the weakly interacting H-aggregate analysis. (d) Example of deconvolution of the absorption spectra using the weakly interacting H-aggregate analysis.

1.2.4 Effect of incomplete separation of [60]PCBM and [70]PCBM in technical grades.

Enrichment of [60]PCBM and [70]PCBM from technical grade to 99% increased the tensile modulus of the resulting films. We attributed this effect to two factors. The first factor is that neat films of the technical grade methanofullerenes had lower tensile moduli (though the

moduli of neat films of technical grade [70]PCBM and 99% [70]PCBM were within error, those of the corresponding BHJ films were not). If the packing structures of the methanofullerene-enriched phases in the BHJ films resemble those of the neat methanofullerene films, then it stands to reason that the stiffening effect of the methanofullerene-rich inclusions would be reduced for technical grade samples in the BHJ films. One possible reason for decreased stiffness of the technical grade samples may be a consequence of less efficient packing of methanofullerenes in the presence of molecules of the "wrong" size. There may be a differential stiffening effect between [60]PCBM and [70]PCBM on the mixed phase of the BHJ, which may account for the fact that the moduli of the BHJ comprising technical grade [70]PCBM were less stiff than the one comprising 99% [70]PCBM, even though the moduli of the neat [70]PCBM films of both grades were similar. We admit to some uncertainty in rationalizing the greater modulus (though also greater ductility) of the as-cast P3HT:methanofullerene blend comprising 99% [70]PCBM compared to that of the as-cast blend comprising 99% [60]PCBM, especially in light of the significantly lower modulus of unblended 99% [70]PCBM compared to 99% [60]PCBM. We note however, that the mechanical properties will not necessarily be proportional to the modulus of the pure methanofullerene component, because differences observed between blended films comprising [60] and [70]PCBM are dependent on at least four factors: (1) unequal miscibility of [60]PCBM and [70]PCBM in amorphous P3HT; (2) unequal anti-plasticization even given the same miscibility; (3) unequal influence on the aggregation behavior of the polymer; and (4) packing structures—and thus mechanical properties—within the methanofullerene-enriched phases that do not necessarily resemble those in the neat methanofullerene films. Ultimately, the expected behavior was recovered upon annealing. That is, the annealed blend comprising 99%

[70]PCBM had a lower modulus and greater ductility than the annealed blend comprising 99% [60]PCBM.

Another factor that may account for increased modulus of the BHJ film for 99% grade methanofullerenes is the increase in the order within the polymer phase induced by the higher-grade methanofullerene. Analysis of the spectra shown in **Figures 1.3a** and **1.3b** by the weakly interacting H-aggregate model[21,27,55] reveal that the percent aggregate of the polymer increases from 44.6% to 45.2% (for technical grade [60]PCBM to 99% [60]PCBM) and from 41.2% to 44.0% (for [70]PCBM technical grade to [70]PCBM 99%) (**Figure 1.3c**). The reason that the ordered polymer phase increased with increasing purity of the methanofullerene is not immediately clear. We tentatively assigned this effect, nevertheless, to the expectation that efficient packing of methanofullerene-enriched phases might remove methanofullerenes from the mixed phase, and thus permit additional polymer chains to form aggregates, which are correlated with stiffer films.

1.2.5 Effect of methanofullerene size and isomerism.

Increasing the size of the fullerene core, from [60]PCBM to [70]PCBM, decreased the tensile moduli of the resulting blended films. While holding the grade and the post-treatment of the film constant, the moduli of the P3HT:methanofullerene films were lower in [70]PCBM samples compared to [60]PCBM samples (with one exception out of four pairs, the as-cast BHJ film made with 99% grade [60]PCBM was more compliant than the as-cast BHJ film made with 99% grade [70]PCBM, though the relationship was reversed after annealing). We attributed the lower compliance of BHJs comprising [70]PCBM compared to [60]PCBM principally to the presence of isomers of [70]PCBM, which impede crystallization. As shown in **Figure 1.1**, [70]PCBM exists as isomers because C_{70} has D5 symmetry.

1.2.6 Photovoltaic properties.

We then measured the photovoltaic properties of the four BHJ blends for which we obtained mechanical data. We fabricated the devices by mixing the methanofullerenes in a 1:1 ratio with P3HT, using *o*-dichlorobenzene (ODCB) as the solvent. Given our ultimate interest in systems in which every component is stretchable, we chose PEDOT:PSS, doped with DMSO and Zonyl,[27] as the transparent anode, and eutectic gallium-indium (EGaIn) as the cathode. **Figure 1.4a** shows the current density vs. voltage (*J*-*V*) plots and **Table 1.3** summarizes the figures of merit. We observed increases in the short-circuit current (J_{sc}) in devices comprising [70]PCBM when compared to those with [60]PCBM. The observation agreed well with previously published results.[15–17] The effect of purity on J_{sc} and V_{oc} between the same methanofullerene size were minimal—similar values were obtained from [60]PCBM with technical grade and 99% grade as well as [70]PCBM with technical grade and 99% grade. However, in this study, the 99% [60]PCBM produced an increase in the fill factor (*FF*) and therefore the power conversion efficiency (*PCE*), compared to technical grade [60]PCBM. The difference in performance between technical grade [70]PCBM and 99% [70]PCBM was within experimental error. The only methanofullerene sample of the four measured with statistically lower *PCE* than the other three was technical grade [60]PCBM.

External quantum efficiency (*EQE*) of the devices are shown in **Figure 1.4b**. The effect of the size of the methanofullerenes were observed to be similar to that on the J_{sc}. High *EQE* values were observed in devices prepared from both technical grade and 99% [70]PCBM, suggesting that the photon-electron conversion processes are efficient. The purity of the methanofullerene increased the *EQE* values slightly, however the trend in the *EQE* values generally corresponded

with the *PCE* values obtained in the solar cells. We calculated the expected short-circuit current ($J_{SC,Calc}$), shown in **Table 1.3**, using the following equation:

$$J_{SC,Calc} = \int e\, EQE(\lambda)\, N_p(\lambda)\, d\lambda \qquad (3)$$

Where e is the elemental charge, λ is the wavelength, $EQE(\lambda)$ is external quantum efficiency, and $N_p(\lambda)$ is the total number of incident photons per second per square centimeter, obtained from the reference solar spectral irradiance AM 1.5G. The differences in the calculated J_{SC} between technical grade and higher purity samples were small, 8% for [60]PCBM and 5% for [70]PCBM. We also observed that our measured J_{SC} are lower than the calculated values, though within the 20% error margins outlined by Zimmermann et al.[58]

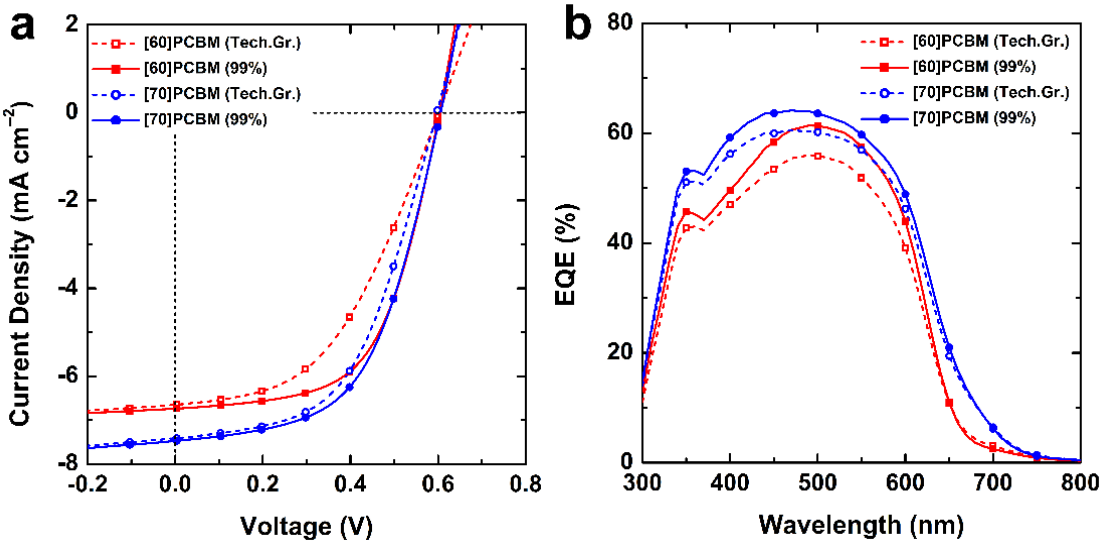

Figure 1.4. (a) Photovoltaic characteristic of averaged devices (N ≥ 8) with an active layer of 1:1 blend of P3HT and respective methanofullerenes. The architecture of the devices was PEDOT:PSS/P3HT:methanofullerene/EGaIn. (b) External quantum efficiencies of the devices with the same composition.

Table 1.3. Summary of the photovoltaic figures of merit for P3HT:methanofullerene solar cells fabricated in this work ($N \geq 8$) [†]

Device	V_{OC} (mV)	J_{SC} (mA cm^{-2})	*FF* (%)	*PCE* (%)	J_{SC}, calc from *EQE* (mA cm^{-2})
P3HT:[60]PCBM (99%)	602 ± 5.5	6.74 ± 0.2	59 ± 3.0	2.36 ± 0.2	8.27
P3HT:[60]PCBM (Tech.Gr.)	602 ± 3.7	6.60 ± 0.4	48 ± 4.8	1.89 ± 0.2	7.58
P3HT:[70]PCBM (Tech.Gr.)	598 ± 11.2	7.41 ± 0.3	53 ± 1.7	2.35 ± 0.1	8.92
P3HT:[70]PCBM (99%)	606 ± 7.5	7.47 ± 0.4	55 ± 1.3	2.48 ± 0.1	9.40

[†]The solar cell device architecture was PEDOT:PSS/P3HT:methanofullerene/EGaIn. PEDOT:PSS, doped with 7% DMSO and 0.1% Zonyl, was spin-coated to create a layer of ~150 nm thick. The active layer was spin-coated from a solution of 1:1 P3HT:methanofullerene in ODCB (40 mg mL^{-1}) and thermally annealed at 125 °C in an inert atmosphere. EGaIn droplets were extruded to create the active area of ~0.02 cm^{-2}.

1.3 Conclusion

Organic solar cells are in principal capable of producing substantial amounts of renewable energy at low cost, but only if they can be made in high yield using techniques for high-speed (e.g., roll-to-roll) manufacturing. Furthermore, organic solar cells have the potential to occupy niches in ultra-flexible, stretchable, wearable, collapsible, and portable applications, which would not be amenable to conventional—or even other thin-film—technologies. Mechanical compliance is often assumed for organic optoelectronic devices because of the ability to bend thin films to small radii of curvature. The mechanical properties, however, are not favorable for every organic semiconductor; it is important to understand these properties to mitigate potential routes of mechanical failure during fabrication and use in the outdoor environment (due to the forces of thermal expansion, wind, and precipitation, for example) and to enable stretchable and ultra-flexible applications. All applications demanding moderate to extreme mechanical deformation, however, require elucidation of the interplay between molecular structure and microstructure, and their influence on the mechanical properties of organic semiconductors.

This paper explored the effect of the size and the extent of mixing of two ubiquitous methanofullerene materials on the mechanical properties of organic solar cells. Our analysis,

summarized in **Figure 1.5**, illustrates the effect of the extent of mixing on the mechanical properties of polymer:methanofullerene bulk heterojunction blends. In particular, use of technical grade [70]PCBM instead of 99% [60]PCBM increased the stretchability by a factor of three (from a crack-onset strain of 3.5% to 11.5%). This increase in compliance would, for example, substantially increase the range of tensile strains available in a wearable or portable device. The influence on flexibility is also significant: the less compliant film on the surface of a substrate with a thickness of 200 μm could be wrapped around a cylinder with a diameter of approximately 6 mm without fracture, while the more compliant film could be wrapped around a cylinder with a diameter of approximately 2 mm. Increased deformability should also increase the lifetime against damage during repeated loading.

While an earlier study found no statistically significant influence of the ratio between [60]PCBM and [70]PCBM of several methanofullerene derivatives on the power conversion efficiency of the P3HT:methanofullerene OPV devices,[15–17] the photovoltaic measurements in this study suggest that devices made using [70]PCBM of lower grade may be slightly but not substantially less efficient than those made using materials of higher grade. We note however, in contrast to earlier studies, that we used ITO-free anodes and EGaIn cathodes because of our underlying interest in stretchable and ultra-flexible applications. These substitutions could in principle lead to small differences observed between this study and earlier ones. Lowered efficiency could be tolerated if counterbalanced by decreased cost and increased yield and lifetime, as appears to be possible in principle, based on our observations.

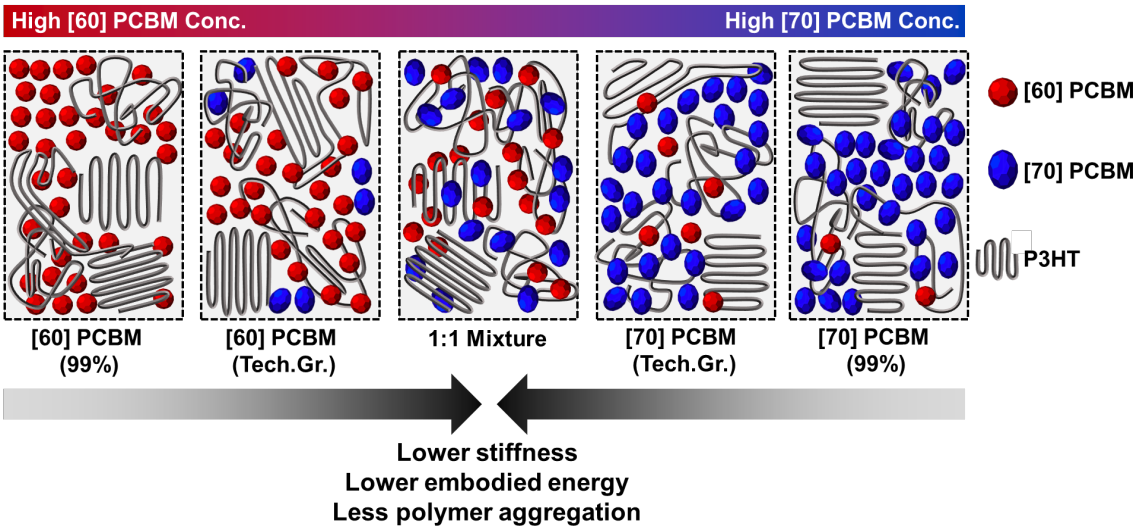

Figure 1.5. Schematic summary of the effect of mixed grades of methanofullerenes on the mechanical properties of P3HT:methanofullerene blends.

1.4. Experimental Methods

1.4.1 Materials.

Methanofullerene derivatives were synthesized by Solenne BV, Groningen, The Netherlands. We conducted our experiments using four different methanofullerene samples: [60]PCBM (99% and technical grade, which was 90% [60]PCBM with the remainder [70]PCBM), and [70]PCBM (99% and technical grade, which was 93.5% [70]PCBM with the remainder [60]PCBM). Mixtures with a 1:1 ratio were prepared by mixing 99% grades of [60]PCBM and [70]PCBM by weight. Regioregular poly(3-hexylthiophene) (P3HT, M_n = 44 kDa, PDI = 2.0) was purchased from Sigma-Aldrich and used as received. PDMS, Sylgard 184, Dow Corning, was prepared according to the manufacturer's instruction at a ratio of 10:1 (base:crosslinker) and cured at room temperature for 36 to 48 h when it was used for buckling experiments. (Tridecafluoro-1,1,2,2-tetrahydrooctyl)-1-trichlorosilane (FOTS) was obtained from Gelest. PEDOT:PSS (Clevios PH1000) was purchased from Heraeus. DMSO was purchased from BDH with purity of

99.9%. Zonyl (FS-300) fluorosurfactant, chloroform, ODCB, acetone, isopropanol, and eutectic gallium-indium (EGaIn) were purchased from Alfa Aesar.

1.4.2 Preparation of films.

For the buckling-based method and crack-onset experiments, hydrophobic glass slides were prepared as the initial substrate for the thin films. Glass slides (2.5 cm × 2.5 cm) were cleaned by bath sonication in detergent, deionized water, acetone, and isopropanol for 15 min each and dried under a stream of compressed air. The surface was then activated with an air plasma (30 W, 200 mTorr, 3 min) before enclosing in a vacuum desiccator with FOTS. The desiccator was left under dynamic vacuum for 12 h. The glass slides were rinsed with deionized water and isopropanol and dried under a stream of compressed air before use. For buckling-based method, P3HT:methanofullerene films were spin-coated onto FOTS treated glass slides using three different spin speeds to achieve three thicknesses. For the crack-onset experiments, all films were spin-coated at the parameters to obtain similar thicknesses. The as-cast (AC) films were then placed under vacuum for 1 h to remove any residual solvent. The annealed (AN) films were placed on the hot plate under inert atmosphere at 125 °C for 30 min before use. The films were spin-coated on plasma cleaned glass slides for UV-vis absorption experiments. We observed minimal differences in the UV-vis absorption when the films were spin-coated onto plasma-treated, FOTS-treated, and PEDOT:PSS glass slides (**Figure C.1,** Supporting Information).

1.4.3 Buckling-based methodology and crack-onset experiment.

The elastomer poly(dimethylsiloxane) (PDMS) was chosen as the substrate for all mechanical measurements. The mixed and degassed prepolymer was allowed to cure at room

temperature for 36 to 48 h before it was used in an experiment. The PDMS was then cut into rectangular pieces (l = 8 cm, w = 1 cm, h = 0.3 cm) and stretched to strains of 2% using a computer-controlled stage, which applied strain to samples using a linear actuator. While the PDMS rectangles were under strain, microscope slides (5 cm × 2.5 cm activated using oxygen plasma and treated with FOTS to later facilitate separation of the PDMS) were clipped onto the back of each rectangle using binder clips to maintain the strain. Transferring the P3HT:methanofullerene films to the pre-strained PDMS substrate was performed by initially scoring the films along the edges with a razor and placing the films against the PDMS. After applying a minimum amount of pressure to create a conformal seal between the PDMS and the P3HT:methanofullerene films, we separated the glass/stretched PDMS from the glass/conjugated polymer film in one fast motion. In most cases, the areas in which the films were in contact with the PDMS were successfully transferred to the pre-strained PDMS rectangles. The binder clips were then removed and the PDMS allowed to relax to the equilibrium length. Buckles formed in the P3HT:methanofullerene films upon relaxation of the PDMS. Buckling wavelengths were obtained from the optical micrographs. Due to the inherent brittleness of the pure methanofullerene films, we employed the bilayer technique to obtain the tensile moduli. In these sets of experiments, a layer of PEDOT:PSS film of known tensile modulus is used as interfacial layer. The PEDOT:PSS films were spin-coated onto the FOTS glass slides before spin-coating the desirable layers of the pure methanofullerene films. The PEDOT:PSS layer assisted in modifying the surface energy such that the methanofullerene solutions can be easily deposited and facilitate the buckling-based experiment by lowering the effective modulus of the bilayer system. From the known modulus of the PEDOT:PSS and the measured thickness ratio between the PEDOT:PSS and the methanofullerene layer, the modulus of the methanofullerene layers were calculated using equation 2.

For crack-onset experiments, the PDMS substrates were cut into rectangular pieces (l = 8 cm, w = 1 cm, h = 0.15 cm). The P3HT:methanofullerene films were transferred onto the PDMS substrates baring no pre-strain in the same manner as described above. The P3HT:methanofullerene films/PDMS was then subjected to incremental increase in uniaxial strain with a step size of 0.5%. At each step, an optical micrograph was taken and the strain at which the first crack formed was recorded.

1.4.4 Fabrication of organic solar cells.

We deposited a layer of PEDOT:PSS from an aqueous solution containing 92.9 wt % Clevios PH 1000 (~0.9−1.2 wt % PEDOT:PSS), 7.0 wt % DMSO, and 0.1 wt % Zonyl fluorosurfactant on plasma treated glass slides as the transparent anode. The solution was filtered and spin-coated at a speed of 500 rpm for 120 s, followed by 2000 rpm for 30 s. The films were then dried at 150 °C for 30 min. The photoactive layers were subsequently spin-coated on the PEDOT:PSS layer at a speed of 500 rpm for 240 s, followed by 2000 rpm for 60 s. A thin strip of the PEDOT:PSS anode was exposed by wiping away a section of the photoactive layer with chloroform for electrical contact. The samples were then immediately placed in a nitrogen-filled glovebox and annealed at 125 °C for 30 min. EGaIn was used as the top contact.

1.4.5 Characterization of films.

The photovoltaic properties were measured in a nitrogen-filled glovebox using a solar simulator with a 100 mW cm^{-2} flux under AM 1.5G condition (ABET Technologies 11016-U up-facing using calibrated with a reference cell with a KG5 filter). The current density versus voltage was measured using a Keithley 2400 SourceMeter. The absorbance of the materials was measured

using a PerkinElmer Lambda 1050 UV-vis-NIR spectrophotometer. The wavelength range measured was 300-850 nm with a step size of 1 nm. The films were prepared in the same manner as described in the above section of preparation of films. *EQE* measurement were measured in air. The photocurrent as a function of wavelength were recorded by a multifunction optical power meter (Newport Model 2936-R) using 300 W xenon lamp and Cornerstone monochromator (Newport Model 74004) illumination.

1.4.6 Weakly interacting H-aggregate model.

In the aggregated state (i.e., crystallites in solid films), the coupled electron-vibrational (vibronic) transitions determine the absorption of weakly interactive H-aggregates and can be modeled as Gaussian fits by:[21,55–57]

$$A(E) \propto \sum_{m=0} \left(\frac{S^m}{m!}\right) \times \left(1 - \frac{We^{-S}}{2E_\mathrm{p}} \sum_{n \neq m} \frac{S^n}{n!\,(n-m)}\right)^2 \times exp\left(\frac{-\left(E - E_{00} - mE_\mathrm{p} - \frac{1}{2}WS^m e^{-S}\right)^2}{2\,\sigma^2}\right) \quad (\mathbf{4})$$

In the above equation, A is the absorption by an aggregate as a function of the photon energy (E). E_{00} is the energy of the 0→0 vibronic transition, which is allowed assuming some disorder in the aggregates.[55] S is the Huang-Rhys factor, which is calculated from absorption and emission spectra, and is set to 1 for P3HTs.[55,57] E_p is the intermolecular vibration energy, which (in the case where S = 1) is set to 0.179 eV as determined by Raman spectroscopy.[59] W is the free exciton bandwidth, which is related to the nearest neighbor interchain excitonic coupling. Upon coupling, a dispersion of the energies occurs, the width of which is equal to W (which is four times the nearest neighbor coupling). The terms m and n are the ground- and excited state vibrational levels and σ is the Gaussian linewidth. The Gaussian linewidth, σ, E_p, W, and the scaling factor for the calculated absorption were found by a least squares fit to the experimental absorption in the region

of 1.93 to 2.25 eV.[21,56,60] This region was selected because the absorption is dominated by the polymer aggregates. Above 2.30 eV, the amorphous polymer dominates absorption.[57,60]

Acknowledgements

This work was supported by the Air Force Office of Scientific Research (AFOSR) Young Investigator Program, grant number FA9550-13-1-0156. Additional support was provided by the laboratory startup funds from the University of California, San Diego. S.S. acknowledges support provided by the National Science Foundation Graduate Research Fellowship under Grant No. DGE-1144086. D. R. acknowledges support from the Initiative for Maximizing Student Development at UCSD.

Chapter 1, in full, is a reprint of the material as it appears in *Chemistry of Materials*, 2015, 27, 3902-3911. American Chemical Society, 2015. Suchol Savagatrup, Daniel Rodriquez, Adam D. Printz, Alexander B. Sieval, Jan C. Hummelen, and Darren J. Lipomi. Suchol Savagatrup was the primary investigator and author of this paper.

References

(1) Savagatrup, S.; Printz, A. D.; O'Connor, T. F.; Zaretski, A. V.; Rodriquez, D.; Sawyer, E. J.; Rajan, K. M.; Acosta, R. I.; Root, S. E.; Lipomi, D. J. Mechanical Degradation and Stability of Organic Solar Cells: Molecular and Microstructural Determinants. *Energy Environ. Sci.* **2015**, *8*, 55–80.

(2) Kaltenbrunner, M.; White, M. S.; Głowacki, E. D.; Sekitani, T.; Someya, T.; Sariciftci, N. S.; Bauer, S. Ultrathin and Lightweight Organic Solar Cells with High Flexibility. *Nat. Commun.* **2012**, *3*, 770.

(3) O'Connor, T. F.; Rajan, K. M.; Printz, A. D.; Lipomi, D. J. Toward Organic Electronics with Properties Inspired by Biological Tissue. *J. Mater. Chem. B* **2015**, *3*, 4947.

(4) Savagatrup, S.; Printz, A. D.; O'Connor, T. F.; Zaretski, A. V.; Lipomi, D. J. Molecularly Stretchable Electronics. *Chem. Mater.* **2014**, *26*, 3028–3041.

(5) Dou, L.; You, J.; Hong, Z.; Xu, Z.; Li, G.; Street, R. A.; Yang, Y. 25th Anniversary Article: A Decade of Organic/Polymeric Photovoltaic Research. *Adv. Mater.* **2013**, *25*, 6642.

(6) Li, H.; Tee, B. C.-K.; Giri, G.; Chung, J. W.; Lee, S. Y.; Bao, Z. High-Performance Transistors and Complementary Inverters Based on Solution-Grown Aligned Organic Single-Crystals. *Adv. Mater.* **2012**, *24*, 2588.

(7) Liu, T.; Troisi, A. What Makes Fullerene Acceptors Special as Electron Acceptors in Organic Solar Cells and How to Replace Them. *Adv. Mater.* **2013**, *25*, 1038.

(8) Burke, D. J.; Lipomi, D. J. Green Chemistry for Organic Solar Cells. *Energy Environ. Sci.* **2013**, *6*, 2053–2066.

(9) Anctil, A.; Babbitt, C. W.; Raffaelle, R. P.; Landi, B. J. Material and Energy Intensity of Fullerene Production. *Environ. Sci. Technol.* **2011**, *45*, 2353.

(10) Savagatrup, S.; Makaram, A. S.; Burke, D. J.; Lipomi, D. J. Mechanical Properties of Conjugated Polymers and Polymer-Fullerene Composites as a Function of Molecular Structure. *Adv. Funct. Mater.* **2014**, *24*, 1169–1181.

(11) Tahk, D.; Lee, H. H.; Khang, D.-Y. Elastic Moduli of Organic Electronic Materials by the Buckling Method. *Macromolecules* **2009**, *42*, 7079–7083.

(12) Brand, V.; Bruner, C.; Dauskardt, R. H. Cohesion and Device Reliability in Organic Bulk Heterojunction Photovoltaic Cells. *Sol. Energ. Mat. Sol. Cells* **2012**, *99*, 182.

(13) Dupont, S. R.; Voroshazi, E.; Heremans, P.; Dauskardt, R. H. Adhesion Properties of Inverted Polymer Solarcells: Processing and Film Structure Parameters. *Org. Electron.* **2013**, *14*, 1262.

(14) Jørgensen, M.; Norrman, K.; Gevorgyan, S. A.; Tromholt, T.; Andreasen, B.; Krebs, F. C. Stability of Polymer Solar Cells. *Adv. Mater.* **2012**, *24*, 580.

(15) Andersson, L. M.; Hsu, Y.-T.; Vandewal, K.; Sieval, A. B.; Andersson, M. R.; Inganäs, O. Mixed C60/C70 Based Fullerene Acceptors in Polymer Bulk-Heterojunction Solar Cells. *Org. Electron.* **2012**, *13*, 2856.

(16) Popescu, L. M. Fullerene Based Organic Solar Cells, University of Groningen, 2008.

(17) Kronholm, D. F.; Hummelen, J. C.; Sieval, A. B.; Van't Hof, P. Patent US2013/8435716, 2013.

(18) Wienk, M. M.; Kroon, J. M.; Verhees, W. J. H.; Knol, J.; Hummelen, J. C.; van Hal, P. A.; Janssen, R. A. J. Efficient Methano[70]fullerene/MDMO-PPV Bulk Heterojunction Photovoltaic Cells. *Angew. Chem.* **2003**, *115*, 3493.

(19) Williams, E. D.; Ayres, R. U.; Heller, M. The 1.7 Kilogram Microchip: Energy and Material Use in the Production of Semiconductor Devices. *Environ. Sci. Technol.* **2002**, *36*, 5504.

(20) Anctil, A.; Babbitt, C. W.; Raffaelle, R. P.; Landi, B. J. Cumulative Energy Demand for Small Molecule and Polymer Photovoltaics. *Prog. Photovolt Res. Appl.* **2013**, *21*, 1541.

(21) Awartani, O.; Lemanski, B. I.; Ro, H. W.; Richter, L. J.; DeLongchamp, D. M.; O'Connor, B. T. Correlating Stiffness, Ductility, and Morphology of Polymer:Fullerene Films for Solar Cell Applications. *Adv. Energy. Mater.* **2013**, *3*, 399–406.

(22) O'Connor, B.; Chan, E. P.; Chan, C.; Conrad, B. R.; Richter, L. J.; Kline, R. J.; Heeney, M.; McCulloch, I.; Soles, C. L.; DeLongchamp, D. M. Correlations between Mechanical and Electrical Properties of Polythiophenes. *ACS Nano* **2010**, *4*, 7538–7544.

(23) Dupont, S. R.; Oliver, M.; Krebs, F. C.; Dauskardt, R. H. Interlayer Adhesion in Roll-to-Roll Processed Flexible Inverted Polymer Solar Cells. *Sol. Energ. Mat. Sol. Cells* **2012**, *97*, 171–175.

(24) Liu, F.; Gu, Y.; Jung, J. W.; Jo, W. H.; Russell, T. P. On the Morphology of Polymer-Based Photovoltaics. *J. Polym. Sci. Part B Polym. Phys.* **2012**, *50*, 1018.

(25) Lipomi, D.; Chong, H.; Vosgueritchian, M.; Mei, J.; Bao, Z. Toward Mechanically Robust and Intrinsically Stretchable Organic Solar Cells: Evolution of Photovoltaic Properties with Tensile Strain. *Sol. Energ. Mat. Sol. Cells* **2012**, *107*, 355–365.

(26) Printz, A.; Savagatrup, S.; Burke, D.; Purdy, T.; Lipomi, D. Increased Elasticity of a Low-Bandgap Conjugated Copolymer by Random Segmentation for Mechanically Robust Solar Cells. *RSC Adv.* **2014**, *4*, 13635–13643.

(27) Savagatrup, S.; Printz, A. D.; Rodriquez, D.; Lipomi, D. J. Best of Both Worlds: Conjugated Polymers Exhibiting Good Photovoltaic Behavior and High Tensile Elasticity. *Macromolecules* **2014**, *47*, 1981.

(28) Printz, A. D.; Savagatrup, S.; Rodriquez, D.; Lipomi, D. J. Role of Molecular Mixing on the Stiffness of Polymer:fullerene Bulk Heterojunction Films. *Sol. Energy Mater. Sol. Cells* **2015**, *134*, 64–72.

(29) Brand, V.; Levi, K.; McGehee, M. D.; Dauskardt, R. H. Film Stresses and Electrode Buckling in Organic Solar Cells. *Sol. Energ. Mat. Sol. Cells* **2012**, *103*, 80.

(30) Savagatrup, S.; Chan, E.; Renteria-Garcia, S. M.; Printz, A. D.; Zaretski, A. V.; O'Connor, T. F.; Rodriquez, D.; Valle, E.; Lipomi, D. J. Plasticization of PEDOT:PSS by Common Additives for Mechanically Robust Organic Solar Cells and Wearable Sensors. *Adv. Funct. Mater.* **2015**, *25*, 427.

(31) Stafford, C. M.; Harrison, C.; Beers, K. L.; Karim, A.; Amis, E. J.; VanLandingham, M. R.; Kim, H.-C.; Volksen, W.; Miller, R. D.; Simonyi, E. E. A Buckling-Based Metrology for Measuring the Elastic Moduli of Polymeric Thin Films. *Nat. Mater.* **2004**, *3*, 545–550.

(32) Stafford, C. M.; Guo, S.; Harrison, C.; Chiang, M. Y. M. Combinatorial and High-Throughput Measurements of the Modulus of Thin Polymer Films. *Rev. Sci. Instrum.* **2005**,

76, 062207.

(33) Wilder, E. A.; Guo, S.; Lin-Gibson, S.; Fasolka, M. J.; Stafford, C. M. Measuring the Modulus of Soft Polymer Networks via a Buckling-Based Metrology. *Macromolecules* **2006**, *39*, 4138.

(34) Huang, D. M.; Mauger, S. A.; Friedrich, S.; George, S. J.; Dumitriu-LaGrange, D.; Yoon, S.; Moule, A. J. The Consequences of Interface Mixing on Organic Photovoltaic Device Characteristics. *Adv. Funct. Mater.* **2011**, *21*, 1657.

(35) Dupont, S. R.; Voroshazi, E.; Nordlund, D.; Vandewal, K.; Dauskardt, R. H. Controlling Interdiffusion, Interfacial Composition, and Adhesion in Polymer Solar Cells. *Adv. Mater. Interfaces* **2014**, 1400135.

(36) Verploegen, E.; Mondal, R.; Bettinger, C. J.; Sok, S.; Toney, M. F.; Bao, Z. Effects of Thermal Annealing Upon the Morphology of Polymer-Fullerene Blends. *Adv. Funct. Mater* **2010**, *20*, 3519.

(37) Miller, N. C.; Gysel, R.; Miller, C. E.; Verploegen, E.; Beiley, Z.; Heeney, M.; McCulloch, I.; Bao, Z.; Toney, M. F.; McGehee, M. D. The Phase Behavior of a Polymer-Fullerene Bulk Heterojunction System That Contains Bimolecular Crystals. *J. Polym. Sci. Part B Polym. Phys.* **2011**, *49*, 499.

(38) Brady, M. M. A.; Su, G. G. M.; Chabinyc, M. M. L. Recent Progress in the Morphology of Bulk Heterojunction Photovoltaics. *Soft Matter* **2011**, *7*, 11065.

(39) Dang, M. T.; Hirsch, L.; Wantz, G. P3HT:PCBM, Best Seller in Polymer Photovoltaic Research. *Adv. Mater.* **2011**, *23*, 3597–3602.

(40) Liao, S.-H.; Li, Y.-L.; Jen, T.-H.; Cheng, Y.-S.; Chen, S.-A. Multiple Functionalities of Polyfluorene Grafted with Metal Ion-Intercalated Crown Ether as an Electron Transport Layer for Bulk-Heterojunction Polymer Solar Cells: Optical Interference, Hole Blocking, Interfacial Dipole, and Electron Conduction. *J. Am. Chem. Soc.* **2012**, *134*, 14271.

(41) Krebs, F. C.; Espinosa, N.; Hösel, M.; Søndergaard, R. R.; Jørgensen, M. 25th Anniversary Article : Rise to Power – OPV-Based Solar Parks. *Adv. Mater.* **2014**, *26*, 29–39.

(42) Osedach, T. P.; Andrew, T. L.; Bulović, V. Effect of Synthetic Accessibility on the Commercial Viability of Organic Photovoltaics. *Energy Environ. Sci.* **2013**, *6*, 711.

(43) Kim, J. Y.; Frisbie, C. D. Correlation of Phase Behavior and Charge Transport in Conjugated Polymer/Fullerene Blends. *J. Phys. Chem. C* **2008**, *112*, 17726.

(44) Zhao, J.; Swinnen, A.; Van Assche, G.; Manca, J.; Vanderzande, D.; Van Mele, B. Phase Diagram of P3HT/PCBM Blends and Its Implication for the Stability of Morphology. *J. Phys. Chem. B* **2009**, *113*, 1587.

(45) Treat, N. D.; Brady, M. A.; Smith, G.; Toney, M. F.; Kramer, E. J.; Hawker, C. J.; Chabinyc,

M. L. Interdiffusion of PCBM and P3HT Reveals Miscibility in a Photovoltaically Active Blend. *Adv. Energy Mater.* **2011**, *1*, 82.

(46) Treat, N. D.; Varotto, A.; Takacs, C. J.; Batara, N.; Al-Hashimi, M.; Heeney, M. J.; Heeger, A. J.; Wudl, F.; Hawker, C. J.; Chabinyc, M. L. Polymer-Fullerene Miscibility: A Metric for Screening New Materials for High-Performance Organic Solar Cells. *J. Am. Chem. Soc.* **2012**, *134*, 15869.

(47) Roehling, J. D.; Batenburg, K. J.; Swain, F. B.; Moulé, A. J.; Arslan, I. Three-Dimensional Concentration Mapping of Organic Blends. *Adv. Funct. Mater.* **2013**, *23*, 2115.

(48) Choi, S. H.; Liman, C. D.; Krämer, S.; Chabinyc, M. L.; Kramer, E. J. Crystalline Polymorphs of [6,6]-Phenyl-C61-Butyric Acid N -Butyl Ester (PCBNB). *J. Phys. Chem. B* **2012**, *116*, 13568.

(49) Zheng, L.; Liu, J.; Ding, Y.; Han, Y. Morphology Evolution and Structural Transformation of Solution-Processed Methanofullerene Thin Film under Thermal Annealing. *J. Phys. Chem. B* **2011**, *115*, 8071.

(50) Zheng, L.; Han, Y. Solvated Crystals Based on [6,6]-Phenyl-C61-Butyric Acid Methyl Ester (PCBM) with the Hexagonal Structure and Their Phase Transformation. *J. Phys. Chem. B* **2012**, *116*, 1598.

(51) Müller, C.; Ferenczi, T. a. M.; Campoy-Quiles, M.; Frost, J. M.; Bradley, D. D. C.; Smith, P.; Stingelin-Stutzmann, N.; Nelson, J. Binary Organic Photovoltaic Blends: A Simple Rationale for Optimum Compositions. *Adv. Mater.* **2008**, *20*, 3510.

(52) Treat, N. D.; Chabinyc, M. L. Phase Separation in Bulk Heterojunctions of Semiconducting Polymers and Fullerenes for Photovoltaics. *Annu. Rev. Phys. Chem.* **2014**, *65*, 59.

(53) Hopkinson, P. E.; Staniec, P. A.; Pearson, A. J.; Dunbar, A. D. F.; Wang, T.; Ryan, A. J.; Jones, R. A. L.; Lidzey, D. G.; Donald, A. M. A Phase Diagram of the P3HT: PCBM Organic Photovoltaic System: Implications for Device Processing and Performance. *Macromolecules* **2011**, *44*, 2908.

(54) Savagatrup, S.; Printz, A. D.; Wu, H.; Rajan, K. M.; Sawyer, E. J.; Zaretski, A. V.; Bettinger, C. J.; Lipomi, D. J. Viability of Stretchable poly(3-Heptylthiophene) (P3HpT) for Organic Solar Cells and Field-Effect Transistors. *Synth. Met.* **2015**, *203*, 208.

(55) Spano, F. C. Modeling Disorder in Polymer Aggregates: The Optical Spectroscopy of Regioregular poly(3-Hexylthiophene) Thin Films. *J. Chem. Phys.* **2005**, *122*, 234701.

(56) Turner, S. T.; Pingel, P.; Steyrleuthner, R.; Crossland, E. J. W.; Ludwigs, S.; Neher, D. Quantitative Analysis of Bulk Heterojunction Films Using Linear Absorption Spectroscopy and Solar Cell Performance. *Adv. Funct. Mater.* **2011**, *21*, 4640.

(57) Clark, J.; Chang, J.-F.; Spano, F. C.; Friend, R. H.; Silva, C. Determining Exciton Bandwidth and Film Microstructure in Polythiophene Films Using Linear Absorption

Spectroscopy. *Appl. Phys. Lett.* **2009**, *94*, 163306.

(58) Zimmermann, E.; Ehrenreich, P.; Pfadler, T.; Dorman, J. A.; Weickert, J.; Schmidt-Mende, L. Erroneous Efficiency Reports Harm Organic Solar Cell Research. *Nat. Photonics* **2014**, *8*, 669.

(59) Louarn, G.; Trznadel, M. Raman Spectroscopic Studies of Regioregular Poly (3-Alkylthiophenes). *J. Phys. Chem.* **1996**, *3654*, 12532.

(60) Pingel, P.; Zen, A.; Abellon, R. D.; Grozema, F. C.; Siebbeles, L. D. A.; Neher, D. Temperature Resolved Local and Macroscopic Charge Carrier Transport in Thin P3HT Layers. *Adv. Funct. Mater.* **2010**, *20*, 2286.

Chapter 2

Mechanical Properties of Solution-Processed Small-Molecule Semiconductor Films

Daniel Rodriquez,[1] Suchol Savagatrup,[1] Eduardo Valle,[1] Christopher M. Proctor[2], Caitlin McDowell,[2] Guillermo C. Bazan,[2] Thuc-Quyen Nguyen,[2] and Darren J. Lipomi[1]*

[1]*Department of NanoEngineering, University of California, San Diego*

9500 Gilman Drive, Mail Code 0448, La Jolla, CA 92093-0448

[2]*Center for Polymers and Organic Solids, Department of Chemistry and Biochemistry,*

University of California Santa Barbara, CA 93106-9510

Abstract

Advantages of semiconducting small molecules—as opposed to semiconducting polymers—include synthetic simplicity, monodispersity, low cost, and ease of purification. One purported disadvantage of small-molecule films is reduced mechanical robustness. This paper measures the tensile modulus and crack-onset strain for pure films of the high-performance solution-processable small-molecule donors 7,7′-[4,4-bis(2-ethylhexyl)-4H-silolo[3,2-b:4,5-b′]dithiophene-2,6-diyl]bis[6-fluoro-4-(5′-hexyl-[2,2′-bithiophen]-5-yl)benzo[c][1,2,5]thiadiazole] (DTS(FBTTh$_2$)$_2$), 2,5-di-(2-ethylhexyl)-3,6-bis-(5″-n-hexyl-[2,2′,5′,2″]terthiophen-5-yl)-pyrrolo[3,4-c]pyrrole-1,4-dione (SMDPPEH), and 6,13-bis(triisopropylsilylethynyl)pentacene (TIPS-pentacene), the acceptor 5,5′-(2,1,3-benzothiadiazole-4,7-diyldi-2,1-ethenediyl)bis[2-hexyl-1H-isoindole-1,3(2H)-dione] (HPI-BT), blends of DTS(FBTTh$_2$)$_2$ and SMDPPEH with [6,6]-phenyl C$_{71}$ butyric acid methyl ester (PC$_{71}$BM) and with HPI-BT, and bulk heterojunction films processed with the additives 1,8-diiodooctane (DIO) and polystyrene (PS). The most deformable films of solution-processed organic semiconductors are found to exhibit tensile moduli and crack-onset strains comparable to those measured for conjugated polymers. For example, the tensile modulus of as-cast DTS(FBTTh$_2$)$_2$ is 0.68 GPa (i.e., comparable to poly(3-hexylthiophene) (P3HT), the common polymer), while it exhibits no cracks when stretched on an elastomeric substrate until strains of 14%. While this high degree of stretchability is lost upon the addition of PC$_{71}$BM (4.2 GPa, 1.42%), it can be partially recovered using processing additives. Tensile modulus and crack-onset strain are highly correlated, which is typical of van der Waals solids. Increased surface roughness was correlated to increased modulus and brittleness within films of similar composition. Increased elasticity can be rationalized by the presence of alkyl side chains, which decrease the van der Waals

attraction between molecules in the crystalline grains. These measurements and observations could have important consequences for the stability of devices based on molecular semiconductors, especially those destined for stretchable or ultra-flexible applications, or those demanding mechanical robustness during roll-to-roll fabrication or use in the outdoor environment.

2.1 Introduction

Organic semiconductors fall into two categories: polymers and small molecules. While both classes of materials have achieved similar levels of performance in thin-film transistors (i.e., charge-carrier mobility) and solar cells (i.e., efficiency), each class of materials has its own set of advantages and disadvantages.[1] For example, polymers can be easier to coat from solution than are small molecules.[2] Small molecules on the other hand are by definition monodisperse and thus less subject to batch-to-batch variability.[3] One advantage typically posited for polymers is superior mechanical resilience compared to small molecules, because small molecules are van der Waals solids that do not have entanglements and thus increased strength and toughness, which are characteristic of polymeric materials.[4] However, we have observed that the deformability of small-molecule thin films can be improved by additives (such as high molecular weight polystyrene) and that small molecules comprising alkyl side chains tend to be more compliant than those lacking side chains. Nevertheless, it is granted that the total energy that can be absorbed by conjugated polymers in either the elastic or plastic regimes of deformation—as manifested in the resilience, tensile strength, and toughness—will almost certainly surpass those of small-molecule semiconductors. The ability to store or dissipate significant mechanical energy, however, may be irrelevant in an encapsulated module, where the resistance to deformation is provided by the substrate. Thus, low tensile modulus (to reduce interfacial stresses upon bending or tensile

deformations) and high strains at which the first cracks appear may be the most relevant predictors of the lifetime of organic electronic devices, at least for bending and stretching deformations. Despite the importance of mechanical properties in determining the lifetime and range of application of flexible (or even stretchable) organic electronic devices, tensile modulus and crack-onset strain have never been reported for solution-processed small-molecule semiconductors. This paper reports these quantities for the first time for four of the five materials ($PC_{71}BM$ has been reported previously)[5]—three electron donors and one acceptor (**Figure 2.1**)—which are promising for thin-film transistors when used alone, or for solar cells when mixed with $PC_{71}BM$ or other acceptors.

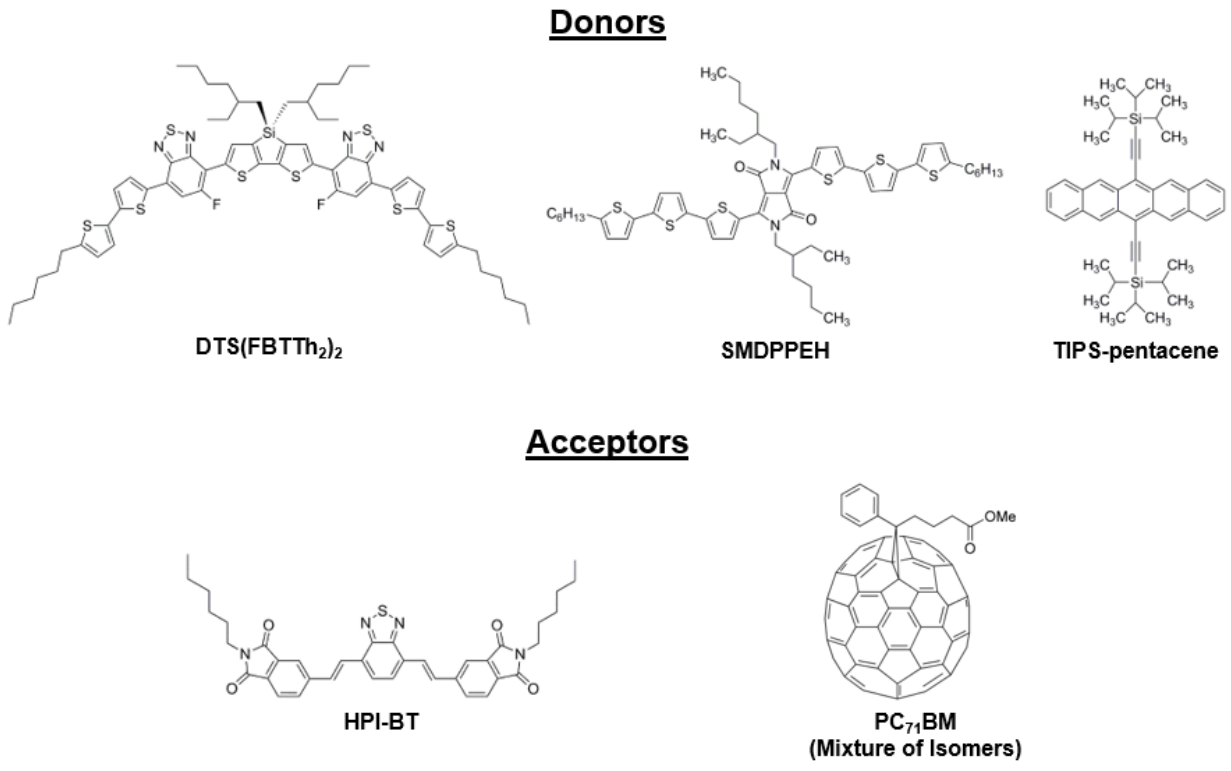

Figure 2.1. Chemical structures of the small molecules whose mechanical properties were measured in this work. Mechanical properties of $DTS(FBTTh_2)_2$, SMDPPEH, TIPS-pentacene and HPI-BT were measured for the first time, while those of $PC_{71}BM$ were first reported in ref.[5]

Devices based on organic semiconductors—e.g., solar cells, thin-film transistors, light-emitting devices, and RFID tags—have the potential to be fabricated by gravure, screen, slot-die, and inkjet printing in roll-to-roll modalities, and thus may have advantages to traditional devices based on silicon for applications demanding low-cost.[6] These low-cost (and sometimes short-lived) devices for which organic materials are regarded as the ideal solutions (e.g., for portable and disposable applications) are often made on flexible foils and must survive mechanical forces during both fabrication and use.[7] Despite mechanically demanding form factors for thin-film organic electronic devices, the electronic properties of such devices are nearly always optimized on glass or silicon substrates, and thus the mechanical properties that will affect the lifetime in the real world are not known and seldom tested. The absence of mechanical information of these compounds is salient because the cohesive fracture energies of these materials, generally within the range of 1–10 J m^{-2}, are a few orders of magnitude smaller than those of conventional semiconductors and engineering plastics.[8] While the deformability of one class of solution-processed organic semiconductor—conjugated polymers—is generally regarded as favorable, our work and that of others has revealed that these materials occupy a wide range of mechanical behavior that depends crucially on molecular and solid-state packing structure.[9–13] In contrast, the deformability of small-molecule semiconductors is generally purported to be unfavorable.

We reasoned that the payoff in the event that our experiments were to reveal unexpectedly high deformability in small-molecule films would be significant. At the outset, however, we had reason to doubt such a favorable outcome, as pentacene—albeit without an alkyl chain—was found by Tahk and coworkers to have a tensile modulus of 16 GPa (an order of magnitude stiffer than P3HT) and crack at compressive strains (probably significantly) less than 4% on elastomeric substrates (tensile strains were not tested, but it is expected to fracture at small strains).[14] Moreover,

our laboratory previously found that films of $PC_{61}BM$ and $PC_{71}BM$ crack at <0.5% tensile strains on elastomeric substrates.[5] Unsubstituted small molecules deposited by vacuum deposition (e.g., pentacene) and those containing a low fraction of aliphatic carbon atoms compared to π-conjugated atoms (e.g., methanofullerenes), however, are not representative of state-of-the-art soluble small-molecule semiconductors, which contain relatively long or branched alkyl chains.[15]

2.1.1 Mechanical properties of van der Waals solids.

In considering the mechanical properties of small-molecule organic semiconductors, it is worth considering the mechanical response of polymeric semiconductors, about which more is known. For a semicrystalline conjugated polymer, tensile deformation in the elastic regime is accommodated principally by straightening of the chains in the amorphous domains; the loss in entropy produces a restoring force. To the extent that the crystalline domains deform elastically, strain energy is stored in the van der Waals bonds being shifted from equilibrium; compressive strains are resisted by steric repulsive forces and tensile strains are resisted by attractive van der Waals forces between the molecules in the solids. For conjugated polymers, structures that form highly crystalline microstructures due to fused rings in the backbone, interdigitation of the side chains, or both, exhibit increased stiffness.[16,17] When the semicrystalline polymer plastically deforms—i.e., when the yield point is surpassed—the strain energy is absorbed by crystallization of aligned chains in the amorphous domains, rearrangement of the van der Waals bonds in the crystalline domains, and the formation of crystallites that are partially aligned along the stretched axis, and which exhibit birefringence.[18] Finally, decohesion and fracture occurs by pullout of chains and by scission of covalent bonds.[8]

For small-molecule semiconductors, most of the modes by which strain energy is stored or absorbed that are characteristic of polymers are absent. Solution-processed small-molecule semiconductors can be glassy, polycrystalline, or semicrystalline, and thermal annealing tends to increase the average size of the crystallites if the molecules can crystallize.[19] In the case of glassy semiconductors such as di(4-methylphenyl)methano-C_{60} bis-adduct (DMPCBA), the film remains amorphous upon deposition and (up to 20 h) after thermal annealing.[20] The glassy nature and thermal stability of this material is a result of its chemical structure which sterically prevents the C_{60} cores from close packing, rendering it soluble but amorphous in the solid state.[20] Thus, the energy of elastic deformation is stored solely by perturbation of the molecules in the glass, and the elastic modulus is determined by the strength of the van der Waals bonds. The strength of these bonds is lowered by the presence of side chains (which push the polarizable cores of the molecules farther from each other) and branching in the side chains. The sizes of core structures that have similar rigidities have a relatively small stiffening effect on the solid material, as solid anthracene is only slightly stiffer than naphthalene (8.4 vs. 8.1 GPa).[21] The presence of a flexible group in the core reduces the stiffness however, as the modulus of solid diphenylethane is 6.3 GPa.[21] Possible mechanisms of plastic deformation include deformation of the crystallites that retain the same lattice structure, or hypothetically by the formation of strained crystalline polymorphs.[22]

2.2 Experimental Design

2.2.1 Selection of materials.

The overall goal of this study was to correlate the chemical structures of small molecules to their thin film mechanical properties and to elucidate the necessary features for mechanical deformability. To this end, we measured the properties of four different molecular semiconductors:

$DTS(FBTTh_2)_2$, SMDPPEH, and TIPS-pentacene (donors), and HPI-BT (an acceptor), whose structures are shown in **Figure 2.1**. To measure the properties of films relevant to organic solar cells, we also measured the mechanical properties of $DTS(FBTTh_2)_2$ and SMDPPEH in bulk heterojunctions with HPI-BT, and with the standard electron acceptor, $PC_{71}BM$. $DTS(FBTTh_2)_2$ is an example of a high-performance organic semiconductor that has achieved power conversion efficiency (*PCE*) of up to 7%, when mixed with $PC_{71}BM$ and 0.4% DIO in the active layer.[23] This performance exceeds that of the highest performing solar cells comprising active layers of P3HT and $PC_{61}BM$. TIPS-pentacene was selected because the mechanical properties of the core structure, pentacene, were measured by Tahk et al.,[14] and thus this material provides a comparison between an unsubstituted core structure, and a structure bearing side chains. $DTS(FBTTh_2)_2$ is a high-performance donor for organic solar cells.[23] The crystal structure of $DTS(FBTTh_2)_2$ is triclinic with two molecules assigned to a unit cell, and exhibits alkyl stacking, hexyl stacking and π-π overlap.[3] Upon thermal annealing, crystallites in the as-cast film grow into large fibrils and form highly ordered regions that exhibit lamellar stacking. SMDPPEH was selected for its relatively simple chemical structure, and the ubiquity of the DPP group as an electron-deficient unit in low-bandgap molecular and polymeric semiconductors. SMDPPEH has achieved *PCE* values of up to 3% with $PC_{71}BM$ as the acceptor.[24] $PC_{71}BM$ is the standard acceptor in high-performance organic solar cells. We have measured its modulus and crack-onset strain in a previous publication and found that "technical grades" of $PC_{71}BM$ —which comprise a mixture of incompletely separated but otherwise pure derivatives of C_{60} and C_{70} in which ≥90% of the blend is $PC_{71}BM$ —are more elastic and ductile than pure films of either $PC_{61}BM$ or $PC_{71}BM$.[5] Moreover, compared to $PC_{61}BM$, $PC_{71}BM$ has the greater deformability, most likely because of its existence as a mixture of isomers and therefore decreased tendency to form well packed

structures in the solid state.[5] Because of the high cost and production energy of fullerene derivatives,[25] the community has been seeking non-fullerene electron acceptors.[26] One such example is HPI-BT, whose mechanical properties we also tested in this work.

2.2.2 Selection of processing additives.

Processing additives are ubiquitous in high-performance organic solar cells.[27] For example, the presence of 1,8-diiodooctane (DIO) significantly increases the *PCE* of cells based on DTS(FBTTh$_2$)$_2$:PC$_{71}$BM bulk heterojunctions: from 5.8% to 7.1% when mixed with a solution containing 0.4% DIO by volume.[3] Another class of additives is polymeric. For example, high molecular weight polystyrene (PS) has been shown to increase *PCE* values further, from 7.1% to 8.2% by adding 2.5 wt % (M_n = 20 MDa).[2] Addition of PS improves wetting, increases thickness and absorbance, and leads to a morphology consisting of large interpenetrated fibrils, as seen in bright-field TEM images.[2] We hypothesized that both DIO and PS (M_n = 900 KDa and 20 MDa) might increase the mechanical compliance and ductility of devices based on small-molecule semiconductors, in particular DTS(FBTTh$_2$)$_2$:PC$_{71}$BM bulk heterojunction films.

2.2.3 Mechanical characterization: tensile modulus.

The tensile modulus of a solid is the slope of a plot of stress vs. strain in the elastic (linear, low-strain) regime of deformation. It describes the ability of a solid to store potential energy due to a load, or its tendency to resist elastic deformation. It is one of many manifestations of the strength of the intermolecular forces in a van der Waals solid. We measured the tensile modulus using the well-known buckling-based metrology (i.e., surface wrinkling).[28] This method is a well-established quantitative and rapid method of analyzing the mechanical properties of thin film

systems such as organic semiconductors, polymer brushes, and nanoscale structured materials whose mechanical properties can be otherwise difficult to measure.[28] Measurements produced from this method agree well with those obtained from traditional pull testing—when sufficient quantities of the material are available for conventional measurements—and dynamic mechanical analysis.[29] We suggest that low tensile modulus is possibly desirable for mechanically robust thin films because it reduces interfacial stresses with load-bearing substrates and encapsulants. Moreover, for semiconducting polymers with relatively low molecular weight tested in the literature so far, low tensile modulus is often correlated with high ductility (crack-onset strain).[5]

2.2.4 Mechanical characterization: crack-onset strain.

The crack-onset strain of a thin film on an elastic substrate is an indirect measurement of the strain at fracture, which is—like the buckling technique for measuring the tensile modulus—useful if not enough material is available for conventional tensile testing. The method is indirect because it is dependent on the adhesion between the film and the substrate (poor adhesion localizes strain to thin areas and defects in the film, and thus leads to increased effective brittleness).[29] Nevertheless, it is a useful metric for comparison between similar materials of their respective abilities to accommodate strain without fracture. Two different methods of determining the crack-onset strain were employed: stretch tests (high-strain regime, **Figure 2.2a**) and bending tests (low-strain regime, **Figure 2.2b**). Stretch tests were employed as a quick and effective means of determining the crack-onset of films that can be strained > 5% (high-strain regime). The strain (ε) induced in the stretch test was calculated using $\Delta L/L_0$, where L_0 is the original length and ΔL is the change in length. We used bending tests to access lower strains of especially brittle materials, for which stretch tests could not resolve the crack-onset strain.[30] The bending test offers precise

control over the applied strain, either by varying the thickness t or the radius of curvature R, $\varepsilon = t/R$, and could be used to access strains of 0.5% to 15%, but was most useful for materials that fractured at small strains, 0.5% to 2%.

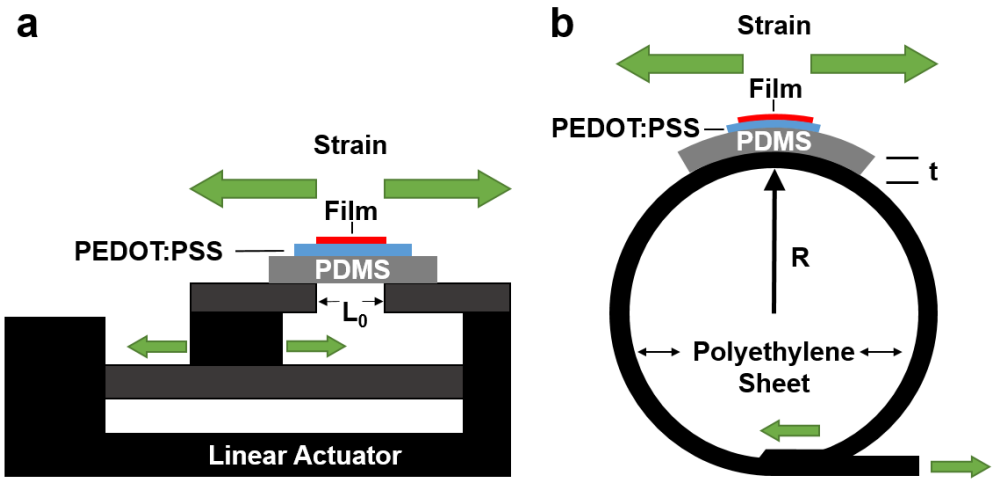

Figure 2.2. Schematic diagram of the two methods of determining crack-onset strain. (a) Stretch test (high-strain regime). (b) Bending test (low-strain regime).

2.3 Results and Discussion

2.3.1 General observations.

Values of tensile modulus (top row, blue) and crack-onset strain (bottom row, red) are shown in **Figure 2.3**. The strong correlation between these quantities is shown in **Figure 2.4**. Six key observations can be made. (I) The non-fullerene small-molecules DTS(FBTTh$_2$)$_2$, SMDPPEH, TIPS-pentacene, and HPI-BT are substantially more compliant (modulus <1.5 GPa) and stretchable (crack-onset strain >5%) compared to the modulus and brittleness measured previously for other small molecular semiconductors, including methanofullerenes[5] or unsubstituted pentacene.[14] In particular, DTS(FBTTh$_2$)$_2$ had the lowest tensile modulus of the pure small-molecule films (0.79 GPa) and could absorb the greatest strain before failure, up to 14%. (II) The bulk heterojunction films comprising DTS(FBTTh$_2$)$_2$ or SMDPPEH and PC$_{71}$BM were

significantly stiffer and more brittle than pure films of the small molecular donors. This observation is consistent with the stiffening effect of methanofullerenes on conjugated polymers in general: for poly(3-alkylthiophene)s (P3ATs), $PC_{61}BM$ behaves as an anti-plasticizer.[5,31] (III) Annealing bulk heterojunction films of $DTS(FBTTh_2)_2$:$PC_{71}BM$ increases the tensile modulus from 4.2 GPa to 17.6 GPa and decreases the crack-onset strain from 1.4% to 1.1%. (IV) The effect of the additives DIO and PS on bulk heterojunction films of $DTS(FBTTh_2)_2$:$PC_{71}BM$ is to decrease the tensile modulus and increase the crack-onset strain. (V) Bulk heterojunction films of the two molecular donors with the acceptor HPI-BT are significantly more deformable than the same donors mixed with $PC_{71}BM$. Observations current-voltage (I–V) will be examined in detail below.

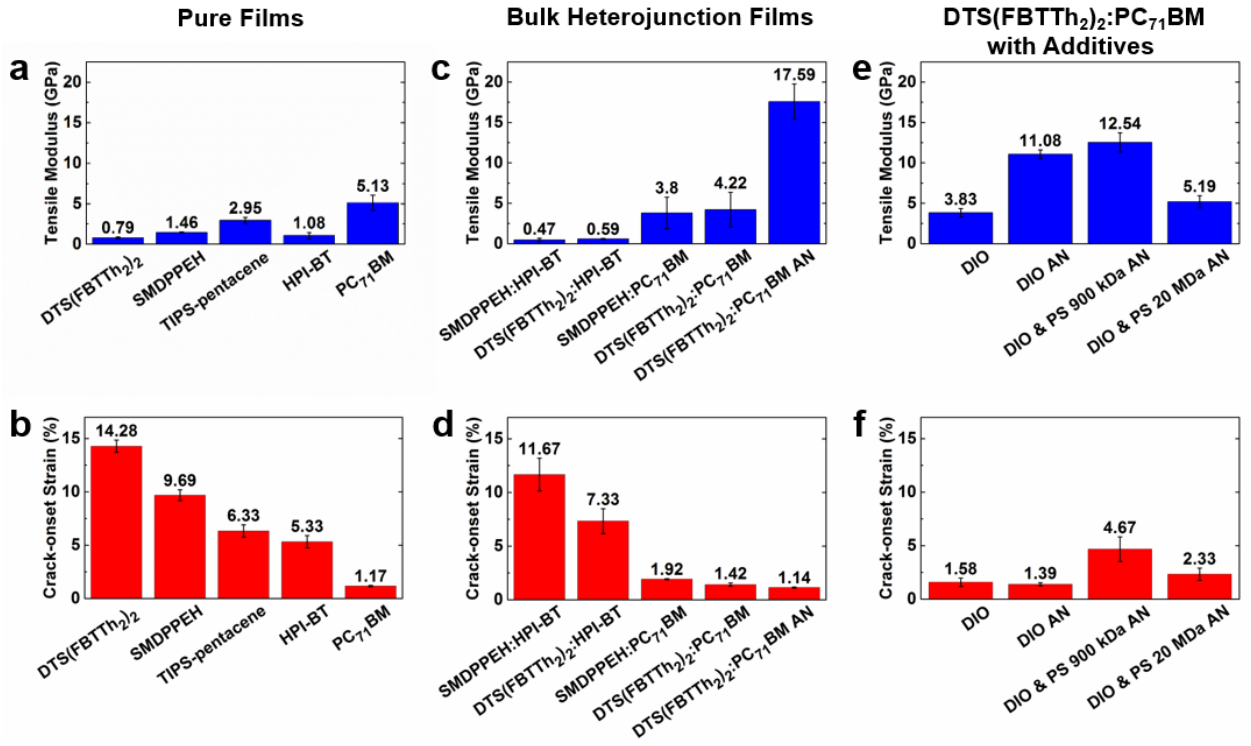

Figure 2.3. Tensile modulus of pure small-molecule thin films (a) mixed bulk heterojunction thin films (b) and films containing additives (c). Crack-onset of pure small-molecule thin films (d) mixed bulk heterojunction thin films (e) and films containing additives (f).

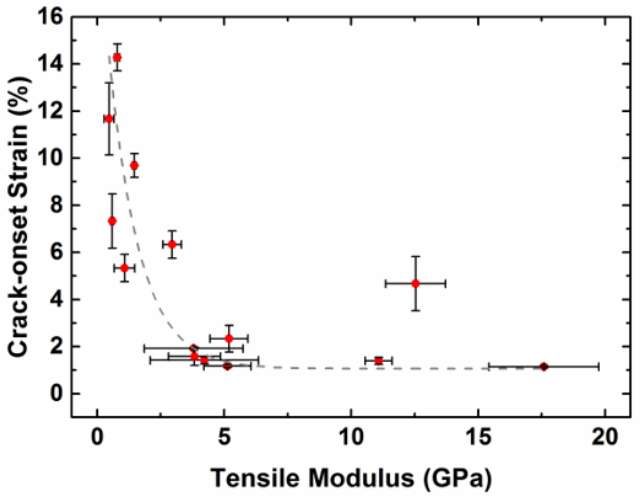

Figure 2.4. Correlation between tensile moduli and crack-onset strains for all the films tested.

2.3.2 I. Softening effect of side chains.

The effect of side chains on comb-like polymers is, in general, to reduce the glass transition temperature, modulus, brittleness, and tensile strength.[32] This effect is well known in P3AT semi-conducting polymers (the rationale for the softening effect of side chains in polymers is that side chains reduce the density of load-bearing covalent bonds along the strained axis and reduce the density of noncovalent interactions between main chains).[29] To find the glass transition temperature, T_g, of the small molecules under study we conducted differential scanning calorimetry (DSC) measurements, however, no clear T_g was observed in any of the materials (**Figure B.2**). The lack of an observable T_g from DSC thermograms of similar materials has been reported by others and complimentary measurements such as modulated-temperature DSC (MTDSC) are usually required to observe the glass transition.[33] To elucidate the affect of side chains in small-molecule semiconductors, we compared the tensile modulus of TIPS-pentacene, 2.95 ± 0.36 GPa, to the modulus of unsubstituted pentacene films measured by Tahk et al. using the buckling technique, 16.09 ± 2.83 GPa.[14] The softening effect of side chains was investigated

in molecular monolayers by Cun et al. in a study of N,N′-dihexadecyl-quinacridone (QA16C). This molecule posesses two alkyl side chains that are each 16 carbon atoms long but has a core that is isosteric with pentacene.[34] The authors used both STM measurements and density functional theory (DFT) calculations, which predicted a tensile modulus of 0.92 ± 0.08 GPa.[34] The analysis of the authors suggested that the origin of the elastic properties of QA16C arose due to conformational changes in the side chains under mechanical strain.[34]

2.3.3 II. Stiffening and embrittling effect of $PC_{71}BM$.

Similar to its effect on the mechanical properties of conjugated polymers, $PC_{71}BM$ was observed to stiffen and embrittle bulk heterojunction films in which the donor is a small molecule (**Figure 2.3c** and **2.3d**). For example, the tensile modulus of $DTS(FBTTh_2)_2$ was increased by a factor of 5 in the bulk heterojunction, and its crack-onset strain was decreased by a factor of 10. For P3AT:methanofullerene bulk heterojunction films comprising a crystalline P3AT phase, a fullerene-rich phase, and an amorphous mixed phase, the fullerene increased the glass transition temperature of the mixed phase.[5] Moreover, the mechanical properties of the fullerene-rich phase were thus dominated by the properties of the fullerene, which was stiff and brittle.[5] For small-molecule:fullerene bulk heterojunction films, we postulate similar effects. The microstructure of as-cast SMDPPEH:$PC_{71}BM$ does not exhibit large phase separation, but consists of fiberlike structures, SMDPPEH rich domains, and oval shaped features attributed to $PC_{71}BM$-rich domains.[24] Morphological features in the films were differentiated by decreasing the donor to acceptor ratio and observing that the oval features grew in size with increasing $PC_{71}BM$ concentration.[24] A structural analog, $DPP(TBFu)_2$—in which the terminal alkylated bithiophene units of SMDPPEH are replaced with benzofuran units—has also been reported.

DPP(TBFu)$_2$:PC$_{71}$BM is well mixed and amorphous when as cast with no thermal treatment. Upon annealing, DPP(TBFu)$_2$ nuclei were found to grow and expel PC$_{71}$BM; separation of phases was found to create a DPP(TBFu)$_2$ rich phase consisting mainly of crystallites, along with a PC$_{71}$BM-rich phase.[35]

2.3.4 III. Increased stiffness and brittleness by thermal annealing.

Thermal annealing had a profound increase on the modulus of DTS(FBTTh$_2$)$_2$:PC$_{71}$BM films, blended in a weight ratio of 3:2, (from 4.2 to 17.6 GPa) and increase in brittleness (crack-onset strain from 1.42% as-cast to 1.14% annealed). We chose this system for thermal annealing because this treatment was included in the procedure that produced the best solar cells from these materials,[23] but in all polymers, small-molecules, and bulk heterojunction films we have ever measured, we have never observed an organic semiconductor film to soften when thermally annealed.[36] The stiffening effect can be correlated to microstructural features observed previously: when mixed with PC$_{71}$BM, the as-cast DTS(FBTTh$_2$)$_2$:PC$_{71}$BM bulk heterojunction film was found to be largely well mixed and amorphous.[3] As the film is annealed DTS(FBTTh$_2$)$_2$ crystallizes into wire like structures and PC$_{71}$BM rich domains.[3] A similar stiffening effect has been observed in polymeric systems after thermal annealing, for example PBTTT.[17] O'Connor et al. measured the tensile modulus of as-cast and annealed PBTTT thin films and reported moduli of 0.88 ± 0.24 and 1.8 ± 0.35 GPa, respectively, an order of magnitude stiffer.[17] They attributed the large increase in modulus to changes in microstructural features: an increase in overall crystallinity and an increase in the size of the crystallites.[17]

2.3.5 IV. Effect of additives.

Processing additives offer a means of improving device functionality without the need for extra processing steps, such as thermal or solvent annealing.[37] Their function can vary, but under favorable circumstances they help to achieve a solid-state microstructure that augments charge separation compared to an unmodified bulk heterojunction film.[37] In a previous paper, we reported a plasticizing effect of both DIO and low-molecular-weigth PDMS on P3HT:$PC_{61}BM$ bulk heterojunction films.[29] A similar plasticizing effect of both DIO and polystyrene of 900 kDa and 20 MDa molecular weight on the mechanical properties of DTS$(FBTTh_2)_2$:$PC_{71}BM$ is shown in **Figure 2.3e** and **2.3f**. The microstructure of DTS$(FBTTh_2)_2$:$PC_{71}BM$:DIO has been found to have more phase separation compared with DTS$(FBTTh_2)_2$:$PC_{71}BM$ and also exhibits larger grains.[38] When PS was added to the bulk heterojunction, the microstructure of DTS$(FBTTh_2)_2$:$PC_{71}BM$:DIO:PS evolved into one with long DTS$(FBTTh_2)_2$ fibrils, well mixed domains, and PS rich domains.[38] The DTS$(FBTTh_2)_2$ fibrils crossed PS rich domains that were well disperesed throughout the film. It may be possible that the PS rich domains serve to accommodate strain when the film is under tension, which would be consistent with the observed increase in crack-onset, from 1.58% to 4.67%, with the addition of PS. All of these additives produced significant reductions in the tensile modulus and increase in the crack-onset strain. Given that these additives can also increase the *PCE* of organic solar cells, it seems that the use of additives might be one approach to achieving the "best of both worlds" of electronic performance and mechanical deformability.

2.3.6 V. Mechanical properties of bulk heterojunctions with HPI-BT as the acceptor.

Given the well-known stiffening effect of fullerenes on bulk heterojunctions comprising either a conjugated polymer or small molecule as the donor, a substitute for the fullerene with greater deformability would be beneficial. We observed that the small-molecule HPI-BT was a factor of 5 more compliant than $PC_{71}BM$, and also a factor of 5 more ductile (**Figure 2.3a** and **2.3b**). Moreover, bulk heterojunctions comprising $DTS(FBTTh_2)_2$:HPI-BT and SMDPPEH:HPI-BT were both significantly more deformable than bulk heterojunctions in which the acceptor was $PC_{71}BM$ (**Figure 2.3c** and **2.3d**). Since the bulk heterojunction consisted of only non-fullerene small molecules and exhibited a relatively large degree of stretchability, we fabricated organic solar cells comprising only stretchable components, including an anode containing highly plasticized poly(3,4-ethylenedioxythiophene):poly(styrenesulfonate) (PEDOT:PSS) and a cathode of liquid eutectic gallium indium, though the efficiencies were very low for this pair of materials (**Figure B.1**).

2.3.7 Mode of fracture.

The way in which organic thin films fracture under strain has important technological consequences. For ductile fracture, in which cracks open but do not span the entire width of the film perpendicular to the strained axis, it should still be possible to use these materials in devices requiring lateral charge transport (i.e., thin-film transistors). For materials exhibiting brittle fracture, in which cracks easily propagate across the entire dimension perpendicular to the strained axis, devices with lateral charge transport will likely be inoperable. The type of fracture observed was qualitatively related to the crack-onset strain (**Figure 2.5**). That is, materials with small crack-onset strains exhibited brittle fracture.

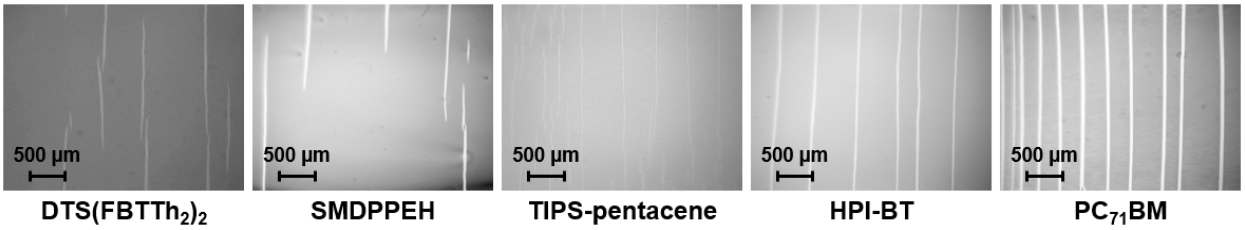

Figure 2.5. Optical micrographs of cracking behavior of four pure organic semiconductors at 15% strain, from partially ductile behavior (left) to completely brittle behavior (right).

2.3.8 Correlation of surface morphology with mechanical properties.

For small-molecule films, we found that the surface roughness was a strong predictor of the stiffness within films of the same composition, but not between films of different compositions (**Figure 2.6**). For example, in the case of DTS(FBTTh$_2$)$_2$, pure films are rough (RMS roughness 3.53 nm) compared with SMDPPEH (0.62 nm), but DTS(FBTTh$_2$)$_2$ exhibits a lower modulus. Thermal annealing of DTS(FBTTh$_2$)$_2$ doubled the RMS roughness to 6.92 nm; this increase was consistent with the growth of crystals in the film. However, addition of PC$_{71}$BM produced a smoother film (RMS roughness of 0.55 nm), but the modulus increased substantially, as PC$_{71}$BM may interrupt some of the ordering seen in the pure film. Upon thermal annealing, the RMS roughness doubled to 1.04 nm; this increase in roughness was accompanied by a large increase in tensile modulus from 4.22 GPa to 17.59 GPa. Our results were consistent with those observed in P3ATs, which exhibited an increase in surface roughness that correlated to an increase in tensile moduli as the alkyl side chains became shorter.[29] This trend was attributed to an increased degree of crystallinity within films containing shorter alkyl chains for P3ATs, and thus increased tensile modulus.[29]

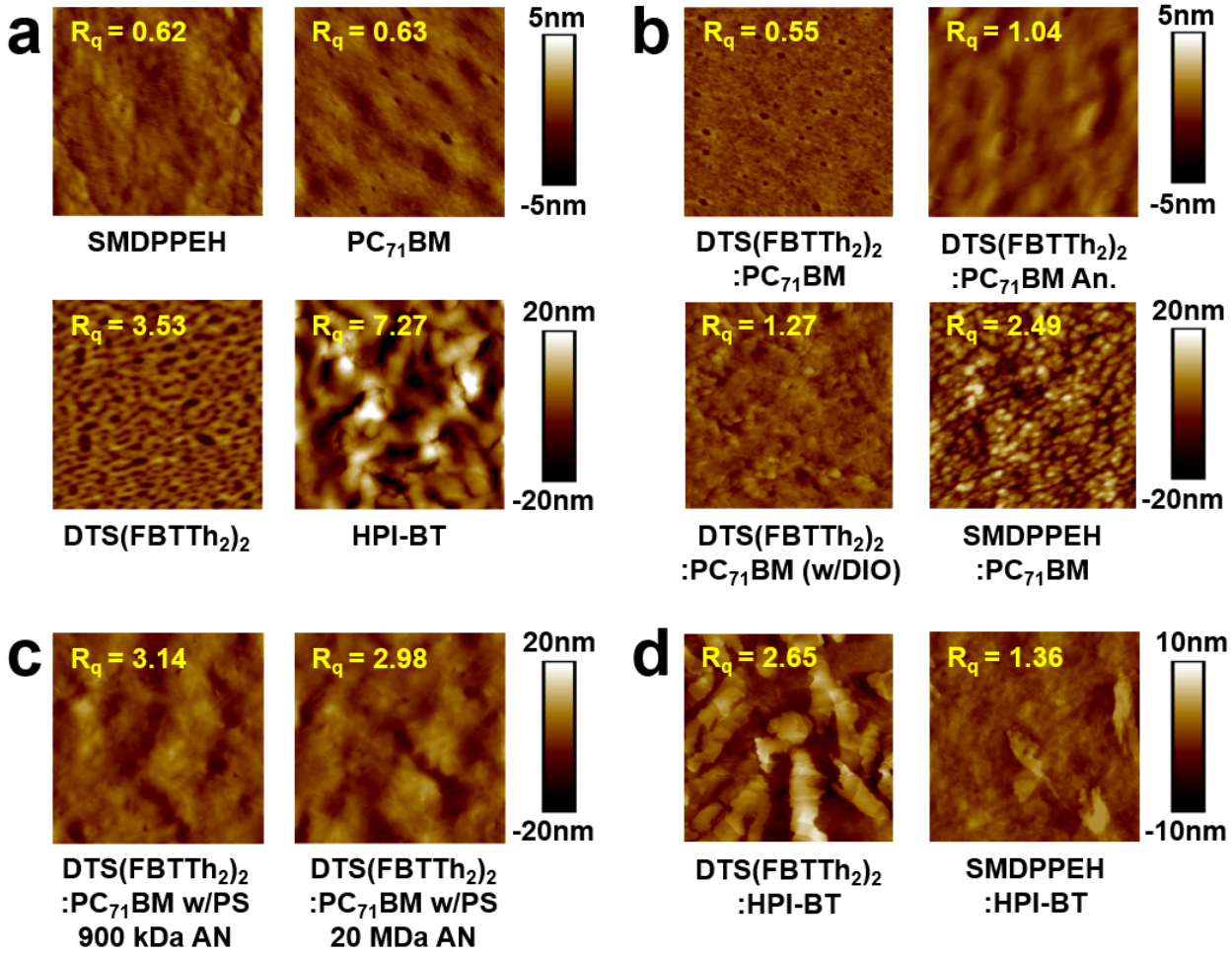

Figure 2.6. Surface morphology of thin film bulk heterojunction solar cells. (a) Pure small-molecule donor and acceptor thin films. (b) Small-molecule bulk heterojunction thin films mixed with $PC_{71}BM$. (c) $DTS(FBTTh_2)_2$:$PC_{71}BM$ bulk heterojunction films with 900 kDa and 20 MDa polystyrene additives, after thermal annealing. (d) Small-molecule bulk heterojunction thin films mixed with HPI-BT.

2.3.9 Mechanism of strain accommodation in small-molecule films.

As we hypothesized at the outset, alkyl-substituted, solution-processable small molecules indeed possess greater deformability than unsubstituted π-conjugated small molecules (e.g., acenes). Alkyl solubilizing groups separate the conjugated core units from each other, and thus reduce the van der Waals cohesive energy. Accordingly, the interplanar distance in SMDPPEH was found to be 1.47 nm by grazing-incidence X-ray diffraction.[19] In contrast, the spacing in $DTS(FBTTh_2)_2$ was 2.2 nm in the (001) direction, which describes the stacking of ethyl hexyl side

chains of the dithienosilole unit spaced between conjugated backbones, and 1.6 nm in the (011) plane which corresponds to the end capped hexyl stacking.[3] In either direction the spacing in SMDPPEH was found to be smaller than in DTS(FBTTh$_2$)$_2$, suggesting stronger intermolecular forces and possibly higher tensile modulus (although the mechanical trends were uncorrelated to melting transitions observed by DSC, **Figure B.2**). The crack-onset strains of DTS(FBTTh$_2$)$_2$ and SMDPPEH in particular were greater than or approximately equal to 10%. This surprisingly (to us) high degree of stretchability could be accommodated by plastic deformation of the crystalline grains themselves, though ultraviolet-visible spectroscopy (**Figure B.3**) revealed only minor differences in absorption between pristine films and those stretched to 10%, and thus did not indicate significant evolution in the microstructure, except for a broadening and red-shifted onset of the absorption for SMDPPEH. Molecular modeling and in situ X-ray diffraction during the process of deformation could yield insights regarding the mechanism of plastic deformation in these and similar materials.

2.4 Conclusions

Our examination of the mechanical properties of high-performance organic semiconductors revealed unexpected deformability—low tensile modulus and high crack-onset strain—of solution-processable small molecules. These findings suggest that devices employing pure films of organic semiconductors, e.g., for thin-film transistors, could be subjected to significant deformations without mechanical failure. For solar cells, in which the pure donors must be mixed with an electron acceptor such as the methanofullerene PC$_{71}$BM, the composite films exhibited significant stiffness and brittleness. Use of processing additives such as DIO and PS, which can increase the efficiency of these devices, however, recovered some of the deformability.

Substitution of $PC_{71}BM$ with the small-molecule acceptor HPI-BT produced highly deformable films. While deformation in the elastic regime was easily rationalized by the presence of alkyl solubilizing groups, which are likely to decrease the van der Waals attraction between adjacent molecules in the crystalline lattice, the mechanism of plastic deformation requires additional insights—perhaps in the form of molecular modeling and in situ X-ray diffraction—to understand. Regardless of the mechanism of deformation, however, it appears that the purported disadvantage of small-molecule semiconductors of mechanical fragility may not be as problematic as believed, especially because these films will be fabricated on and encapsulated in flexible foils that bear the load.

2.5 Experimental Methods

2.5.1 Materials.

2,5-Di-(2-ethylhexyl)-3,6-bis-(5″-n-hexyl-[2,2′,5′,2″]terthiophen-5-yl)-pyrrolo[3,4-c]pyrrole-1,4-dione (SMDPPEH), 7,7′-[4,4-Bis(2-ethylhexyl)-4H-silolo[3,2-b:4,5-b′]dithiophene-2,6-diyl]bis[6-fluoro-4-(5′-hexyl-[2,2′-bithiophen]-5-yl)benzo[c][1,2,5]thiadiazole] ($DTS(FBTTh_2)_2$), 6,13-Bis(triisopropylsilylethynyl)pentacene (TIPS-Pentacene), and 5,5′-(2,1,3-Benzothiadiazole-4,7-diyldi-2,1-ethenediyl)bis[2-hexyl-1H-isoindole-1,3(2H)-dione] (HPI-BT) were purchased from Sigma-Aldrich and used as received. 1,8-Diiodooctane (DIO) was purchased from Sigma-Aldrich with 98% purity. [6,6]-Phenyl C_{71} butyric acid methyl ester ($PC_{71}BM$) technical grade was purchased from Solenne BV, Groningen, The Netherlands and used as received. Polystyrene samples of M_n = 900 KDa and 20 MDa were obtained from Alfa Aesar (Cat# 41943), Haverhill, MA and Pressure Chemical Co., Pittsburgh, PA., respectively. PDMS, Sylgard 184, Dow Corning, was prepared as stated in the manufacturer's instructions at a ratio of 10:1

(base:crosslinker) and cured at room temperature for 36-48 h when used for buckling and crack-onset experiments. (Tridecafluoro-1,1,2,2-tetrahydrooctyl)-1-tri- chlorosilane (FOTS) was obtained from Gelest. Poly(3,4-ethylenedioxythiophene) polystyrene sulfonate (PEDOT:PSS) (Clevios PH1000) was purchased from Heraeus. Dimethyl sulfoxide (DMSO) was purchased from BDH with purity of 99.9%. Zonyl (FS-300) fluorosurfactant, chloroform, acetone, and isopropanol were purchased from Alfa Aesar.

2.5.2 Preparation of substrates.

Glass slides used as substrates were cut into 2.5 cm squares with a diamond-tipped scribe. The slides were then successively cleaned with Alconox solution (2 mg mL^{-1}), deionized water, acetone, and isopropyl alcohol (IPA) in an ultrasonic bath for 10 min each and rinsed and dried with compressed air. After sonication, the glass was plasma treated at ~30W for 3 min at a base pressure of 200 mTorr in ambient air to remove residual organic material and activate the surface. Silicon substrates used for AFM measurements were cut into 1-cm^2 pieces. To remove debris from the surface, the silicon substrates were cleaned and plasma treated in the same manner as described above.

PEDOT:PSS substrates were prepared from an aqueous solution containing 99 wt % Clevios PH 1000 and 1 wt % Zonyl fluorosurfactant. The solution was filtered with a 1μm glass microfiber (GMF) syringe before being spin coated onto glass for buckling measurements and PDMS for crack-onset measurements. For buckling experiments PEDOT:PSS was annealed at 150 °C for 30 min in ambient air and allowed to naturally cool to room temperature. For crack-onset experiments PDMS was UV-ozone treated for 15 min prior to the spin-coating of PEDOT:PSS. After spin-coating the films were dried under vacuum for 30 min, no thermal treatment.

2.5.3 Bilayer film buckling.

The bilayer buckling technique is a modified version of the single-layer buckling test that has been employed by our group to determine the tensile moduli of especially brittle films that would otherwise fracture upon the release of pre-strain in the single-layer buckling test. This method can also measure the tensile moduli of organic semiconductors that do not adhere to hydrophobic substrates. Bilayer buckling uses an interfacial layer of PEDOT:PSS, with a favorable surface energy, to permit the spin-coating and mechanical transfer of thin-films on hydrophobic substrates. The effective tensile modulus of each bilayer film was calculated using the same method as single layer buckling, eq 1.

$$E_{\mathrm{f}} = 3E_{\mathrm{s}}\left(\frac{1-\upsilon_{\mathrm{f}}^2}{1-\upsilon_{\mathrm{s}}^2}\right)\left(\frac{\lambda_{\mathrm{b}}}{2\pi d_{\mathrm{f}}}\right)^3 \qquad (\mathbf{1})$$

After obtaining the effective modulus of the bilayer film, E_{eff}, and measuring the tensile modulus of PEDOT:PSS in a separate buckle test, E_2, we used eq 2. to extract the modulus of the small-molecule films, E_1. Below, m is the modulus ratio, E_2/E_1, and n is the thickness ratio, h_2/h_1.

$$E_{\mathrm{eff}} = \left(\frac{1+m^2n^4+2mn(2n^2+3n+2)}{(1+n)^3(1+mn)}\right)E_1 \qquad (\mathbf{2})$$

2.5.4 Preparation of small-molecule solutions.

Solutions of SMDPPEH, DTS(FBTTh$_2$)$_2$, TIPS-pentacene, HPI-BT, PC$_{71}$BM, and their physical blends were prepared in $CHCl_3$ (10mg mL^{-1}) for the buckling technique, crack-onset tests, and AFM images. All solutions were stirred overnight at ambient temperature and for 2 hours at 70 °C prior to spin-coating. The solutions were then filtered with a 1-µm GMF syringe filter immediately before being spin-coated onto glass, silicon, or PEDOT:PSS substrates.

2.5.5 Characterization of materials.

Atomic force microscopy (AFM) micrographs were taken using a Veeco Scanning Probe Microscope in tapping mode. Data was analyzed with Nanoscope Analysis v1.40 software (Bruker Corp.). The small-molecule solutions were spin-coated onto the silicon slides at a spin speed of 1000 rpm (500 rpm s^{-1} ramp) for 120 s followed by 2000 rpm (1000 rpm s^{-1} ramp) for 30 s. After spin-coating annealed samples were immediately placed in a nitrogen-filled glovebox and annealed at 70 °C for 10 min. After 10 min the annealed samples were allowed to cool for 30 min on the hot plate.

Acknowledgements

This research was supported by the Air Force Office of Scientific Research (AFOSR) Young Investigator Program awarded to D. L., grant number FA9550-13-1-0156. D. R. and S. S. acknowledge support provided by the National Science Foundation Graduate Research Fellowship Program under Grant No. DGE-1144086 and the Kaplan Dissertation Year Fellowship, awarded to S.S.. C.M.P and T.-Q.N thank the Office of Naval Research (Award # N000141410076). TQN thanks the Camille Dreyfus Teacher-Scholar Awards Program.

Chapter 2, in full, is a reprint of the material as it appears in *ACS Applied Materials & Interfaces*, 2016, 8, 11649-11657. American Chemical Society, 2016. Daniel Rodriquez, Suchol Savagatrup, Eduardo Valle, Christopher M. Proctor, Caitlin McDowell, Guillermo C. Bazan, Thuc-Quyen Nguyen, and Darren J. Lipomi. The dissertation author was the primary investigator and author of this paper.

References

(1) Li, Y.; Sonar, P.; Murphy, L.; Hong, W. High Mobility Diketopyrrolopyrrole (DPP)-Based Organic Semiconductor Materials for Organic Thin Film Transistors and Photovoltaics. *Energy Environ. Sci.* **2013**, *6*, 1684–1710.

(2) Huang, Y.; Wen, W.; Mukherjee, S.; Ade, H.; Kramer, E. J.; Bazan, G. C. High-Molecular-Weight Insulating Polymers Can Improve the Performance of Molecular Solar Cells. *Adv. Mater.* **2014**, *26*, 4168–4172.

(3) Love, J. A.; Proctor, C. M.; Liu, J.; Takacs, C. J.; Sharenko, A.; van der Poll, T. S.; Heeger, A. J.; Bazan, G. C.; Nguyen, T. Q. Film Morphology of High Efficiency Solution-Processed Small-Molecule Solar Cells. *Adv. Funct. Mater.* **2013**, *23*, 5019–5026.

(4) Li, G.; Zhu, R.; Yang, Y. Polymer Solar Cells. *Nat. Photonics* **2012**, *6*, 153–161.

(5) Savagatrup, S.; Rodriquez, D.; Printz, A. D.; Sieval, A. B.; Hummelen, J. C.; Lipomi, D. J. [70]PCBM and Incompletely Separated Grades of Methanofullerenes Produce Bulk Heterojunctions with Increased Robustness for Ultra-Flexible and Stretchable Electronics. *Chem. Mater.* **2015**, *27*, 3902–3911.

(6) Carle, J. E.; Andersen, T. R.; Helgesen, M.; Bundgaard, E.; Jorgensen, M.; Krebs, F. C. A Laboratory Scale Approach to Polymer Solar Cells Using One Coating/Printing Machine, Flexible Substrates, No ITO, No Vacuum and No Spincoating. *Sol. Energy Mater. Sol. Cells* **2013**, *108*, 126–128.

(7) Dupont, S. R.; Oliver, M.; Krebs, F. C.; Dauskardt, R. H. Interlayer Adhesion in Roll-to-Roll Processed Flexible Inverted Polymer Solar Cells. *Sol. Energy Mater. Sol. Cells* **2012**, *97*, 171–175.

(8) Bruner, C.; Miller, N. C.; McGehee, M. D.; Dauskardt, R. H. Molecular Intercalation and Cohesion of Organic Bulk Heterojunction Photovoltaic Devices. *Adv. Funct. Mater.* **2013**, *23*, 2863–2871.

(9) Savagatrup, S.; Printz, A. D.; Rodriquez, D.; Lipomi, D. J. Best of Both Worlds: Conjugated Polymers Exhibiting Good Photovoltaic Behavior and High Tensile Elasticity. *Macromolecules* **2014**, *47*, 1981–1992.

(10) Awartani, O.; Lemanski, B. I.; Ro, H. W.; Richter, L. J.; DeLongchamp, D. M.; O'Connor, B. T. Correlating Stiffness, Ductility, and Morphology of Polymer:Fullerene Films for Solar Cell Applications. *Adv. Energy Mater.* **2013**, *3*, 399–406.

(11) Kim, T.; Kim, J.-H.; Kang, T. E.; Lee, C.; Kang, H.; Shin, M.; Wang, C.; Ma, B.; Jeong, U.; Kim, T.-S.; Kim, B. J. Flexible, Highly Efficient All-Polymer Solar Cells. *Nat. Commun.* **2015**, *6*, 8547.

(12) Wu, H.-C.; Benight, S. J.; Chortos, A.; Lee, W.-Y.; Mei, J.; To, J. W. F.; Lu, C.; He, M.; Tok, J. B.-H.; Chen, W.-C.; Bao, Z. A Rapid and Facile Soft Contact Lamination Method:

Evaluation of Polymer Semiconductors for Stretchable Transistors. *Chem. Mater.* **2014**, *26*, 4544–4551.

(13) Liang, J.; Li, L.; Chen, D.; Hajagos, T.; Ren, Z.; Chou, S.-Y.; Hu, W.; Pei, Q. Intrinsically Stretchable and Transparent Thin-Film Transistors Based on Printable Silver Nanowires, Carbon Nanotubes and an Elastomeric Dielectric. *Nat. Commun.* **2015**, *6*, 7647.

(14) Tahk, D.; Lee, H. H.; Khang, D.-Y. Elastic Moduli of Organic Electronic Materials by the Buckling Method. *Macromolecules* **2009**, *42*, 7079–7083.

(15) Lin, Y.; Li, Y.; Zhan, X. Small Molecule Semiconductors for High-Efficiency Organic Photovoltaics. *Chem. Soc. Rev.* **2012**, *41*, 4245–4272.

(16) Printz, A. D.; Savagatrup, S.; Rodriquez, D.; Lipomi, D. J. Role of Molecular Mixing on the Stiffness of Polymer:fullerene Bulk Heterojunction Films. *Sol. Energy Mater. Sol. Cells* **2015**, *134*, 64–72.

(17) O'Connor, B.; Chan, E. P.; Chan, C.; Conrad, B. R.; Richter, L. J.; Kline, R. J.; Heeney, M.; McCulloch, I.; Soles, C. L.; DeLongchamp, D. M. Correlations between Mechanical and Electrical Properties of Polythiophenes. *ACS Nano* **2010**, *4*, 7538–7544.

(18) Printz, A. D.; Zaretski, A. V.; Savagatrup, S.; Chiang, A. S.-C.; Lipomi, D. J. Yield Point of Semiconducting Polymer Films on Stretchable Substrates Determined by Onset of Buckling. *ACS Appl. Mater. Interfaces* **2015**, *7*, 23257–23264.

(19) Tamayo, A.; Kent, T.; Tantitiwat, M.; Dante, M. a.; Rogers, J.; Nguyen, T.-Q. Influence of Alkyl Substituents and Thermal Annealing on the Film Morphology and Performance of Solution Processed, Diketopyrrolopyrrole-Based Bulk Heterojunction Solar Cells. *Energy Environ. Sci.* **2009**, *2*, 1180–1186.

(20) Cheng, Y. J.; Liao, M. H.; Chang, C. Y.; Kao, W. S.; Wu, C. E.; Hsu, C. S. Di(4-Methylphenyl)methano-C60 Bis-Adduct for Efficient and Stable Organic Photovoltaics with Enhanced Open-Circuit Voltage. *Chem. Mater.* **2011**, *23*, 4056–4062.

(21) Simmons, G. W. H. *Single Crystal Elastic Constants and Calculated Aggregate Properties: A Handbook*; The MIT Press: Cambridge, 1971.

(22) Giri, G.; Verploegen, E.; Mannsfeld, S. C. B.; Atahan-Evrenk, S.; Kim, D. H.; Lee, S. Y.; Becerril, H. a.; Aspuru-Guzik, A.; Toney, M. F.; Bao, Z. Tuning Charge Transport in Solution-Sheared Organic Semiconductors Using Lattice Strain. *Nature* **2011**, *480*, 504–508.

(23) van der Poll, T. S.; Love, J. a.; Nguyen, T.-Q.; Bazan, G. C. Non-Basic High-Performance Molecules for Solution-Processed Organic Solar Cells. *Adv. Mater.* **2012**, *24*, 3646–3649.

(24) Tamayo, A. B.; Dang, X. D.; Walker, B.; Seo, J.; Kent, T.; Nguyen, T.-Q. A Low Band Gap, Solution Processable Oligothiophene with a Dialkylated Diketopyrrolopyrrole Chromophore for Use in Bulk Heterojunction Solar Cells. *Appl. Phys. Lett.* **2009**, *94*, 1–3.

(25) Anctil, A.; Babbitt, C. W.; Raffaelle, R. P.; Landi, B. J. Material and Energy Intensity of Fullerene Production. *Environ. Sci. Technol.* **2011**, *45*, 2353–2359.

(26) Nielsen, C. B.; Holliday, S.; Chen, H.; Cryer, S. J.; Mcculloch, I. Non-Fullerene Electron Acceptors for Use in Organic Solar Cells. *Acc. Chem. Res.* **2015**, *48*, 2803–2812.

(27) Peet, J.; Kim, J. Y.; Coates, N. E.; Ma, W. L.; Moses, D.; Heeger, A. J.; Bazan, G. C. Efficiency Enhancement in Low-Bandgap Polymer Solar Cells by Processing with Alkane Dithiols. *Nat. Mater.* **2007**, *6*, 497–500.

(28) Chung, J. Y.; Nolte, A. J.; Stafford, C. M. Surface Wrinkling: A Versatile Platform for Measuring Thin-Film Properties. *Adv. Mater.* **2011**, *23*, 349–368.

(29) Savagatrup, S.; Makaram, A. S.; Burke, D. J.; Lipomi, D. J. Mechanical Properties of Conjugated Polymers and Polymer-Fullerene Composites as a Function of Molecular Structure. *Adv. Funct. Mater.* **2014**, *24*, 1169–1181.

(30) Park, B. S.-I.; Ahn, J.; Feng, X.; Wang, S.; Huang, Y.; Rogers, J. A. Theoretical and Experimental Studies of Bending of Inorganic Electronic Materials on Plastic Substrates **. *Adv. Funct. Mater.* **2008**, *18*, 2673–2684.

(31) Hopkinson, P. E.; Staniec, P. A.; Pearson, A. J.; Dunbar, A. D. F.; Wang, T.; Ryan, A. J.; Jones, R. A. L.; Lidzey, D. G.; Donald, A. M. A Phase Diagram of the P3HT:PCBM Organic Photovoltaic System: Implications for Device Processing and Performance. *Macromolecules* **2011**, *44*, 2908–2917.

(32) Postema, A. R.; Liou, K.; Wudl, F.; Smith, P. Highly Oriented, Low-Modulus Materials from Liquid Crystalline Polymers: The Ultimate Penalty for Solubilizing Alkyl Side Chains. *Macromolecules* **1990**, *23*, 1842–1845.

(33) Zhao, J.; Swinnen, A.; Van Assche, G.; Manca, J.; Vanderzande, D.; Van Mele, B. Phase Diagram of P3HT/PCBM Blends and Its Implication for the Stability of Morphology. *J. Phys. Chem. B* **2009**, *113*, 1587–1591.

(34) Cun, H.; Wang, Y.; Du, S.; Zhang, L.; Zhang, L.; Yang, B.; He, X.; Wang, Y.; Zhu, X.; Yuan, Q.; Zhao, Y.-P.; Ouyang, M.; Hofer, W. A.; Pennycook, S. J.; Gao, H. Tuning Structural and Mechanical Properties of Two-Dimensional Molecular Crystals: The Roles of Carbon Side Chains. *Nano Lett.* **2012**, *12*, 1229–1234.

(35) Sharenko, A.; Kuik, M.; Toney, M. F.; Nguyen, T.-Q. Crystallization-Induced Phase Separation in Solution-Processed Small Molecule Bulk Heterojunction Organic Solar Cells. *Adv. Funct. Mater.* **2014**, *24*, 3543–3550.

(36) Savagatrup, S.; Printz, A. D.; O'Connor, T. F.; Zaretski, A. V.; Rodriquez, D.; Sawyer, E. J.; Rajan, K. M.; Acosta, R. I.; Root, S. E.; Lipomi, D. J. Mechanical Degradation and Stability of Organic Solar Cells: Molecular and Microstructural Determinants. *Energy Environ. Sci.* **2014**, *8*, 55–80.

(37) Perez, L. A.; Chou, K. W.; Love, J. A.; van der Poll, T. S.; Smilgies, D. M.; Nguyen, T.-Q.; Kramer, E. J.; Amassian, A.; Bazan, G. C. Solvent Additive Effects on Small Molecule Crystallization in Bulk Heterojunction Solar Cells Probed during Spin Casting. *Adv. Mater.* **2013**, *25*, 6380–6384.

(38) McDowell, C.; Abdelsamie, M.; Zhao, K.; Smilgies, D.-M.; Bazan, G. C.; Amassian, A. Synergistic Impact of Solvent and Polymer Additives on the Film Formation of Small Molecule Blend Films for Bulk Heterojunction Solar Cells. *Adv. Energy Mater.* **2015**, *5*, 1–9.

Chapter 3

Comparison of Methods for Determining the Mechanical Properties of Semiconducting Polymer Films for Stretchable Electronics

Daniel Rodriquez,[1†] Jae-Han Kim,[2†] Samuel E. Root,[1] Zhuping Fei,[3] Pierre Boufflet,[3] Martin Heeney,[3] Taek-Soo Kim,*[,2] and Darren J. Lipomi*[,1]

(†These authors contributed equally.)

[1]*Department of NanoEngineering, University of California, San Diego*

9500 Gilman Drive, Mail Code 0448, La Jolla, CA 92093-0448

[2]*Department of Mechanical Engineering, Korea Advanced Institute of Science and Technology (KAIST), Yuseong-gu, Daejeon 34141, Korea.*

[3]*Department of Chemistry and Centre for Plastic Electronics, Imperial College London, Exhibition Rd, London, SW7 2AZ, UK*

Abstract

This paper describes a comparison of two characterization techniques for determining the mechanical properties of thin-film organic semiconductors for applications in soft electronics. In the first method, the film is supported by water (film-on-water, FOW), and a stress-strain curve is obtained using a direct tensile test. In the second method, the film is supported by an elastomer (film-on-elastomer, FOE), and is subjected to three tests to reconstruct the key features of the stress-strain curve: the buckling test (tensile modulus), the onset of buckling (yield point), and the crack-onset strain (strain at fracture). The specimens used for the comparison are four poly(3-hexylthiophene) (P3HT) samples of increasing molecular weight (M_n = 15, 40, 63, and 80 kDa). The methods produced qualitatively similar results for mechanical properties including the tensile modulus, the yield point, and the strain at fracture. The agreement was not quantitative because of differences in mode of loading (tension vs. compression), strain rate, and processing between the two methods. Experimental results are corroborated by coarse-grained molecular dynamics simulations, which lead to the conclusion that in low molecular weight samples (M_n = 15 kDa), fracture occurs by chain pullout. Conversely, in high molecular weight samples (M_n > 25kDa), entanglements concentrate the stress to few chains; this concentration is consistent with chain scission as the dominant mode of fracture. Our results provide a basis for comparing mechanical properties that have been measured by these two techniques, and provide mechanistic insight into fracture modes in this class of materials.

3.1 Introduction

The mechanical properties of thin-film organic semiconductors play an important role in the durability of organic electronic devices such as organic solar cells, thin-film transistors, light-

emitting devices, and biosensors.[1–4] For example, low tensile moduli reduce interfacial stresses and are necessary to achieve "mechanical invisibility" in wearable patch-like devices.[5] High ductility and toughness, on the other hand, will increase the lifetimes of devices against fracture and enable stretching and bonding of devices to curve surfaces of buildings, vehicles, and body parts.[6] Recently, stretchability in organic semiconductors has been achieved by modification of the molecular structure to include chemical crosslinking groups or by surface embedding in an elastomer.[7,8] Since organic semiconductors are usually cast into films as thin as a few tens of nanometers thick, it is challenging to obtain mechanical information using conventional methods, such as pull testing of freestanding samples.[9] Moreover, the mechanical properties of thin films are not necessarily the same as those of bulk samples.[10] This challenge has led to the development of methods for determining the mechanical properties of thin films of semiconducting polymers that do not require preparation of bulk samples (laboratory-scale syntheses of new materials usually do not produce a large enough yield).[11–13]

The purpose of this paper is to compare two of these experimental methods (**Figure 3.1**), and to compare the results with a simulated stress-strain curve produced by a coarse-grained molecular dynamics simulation.[14] The first method, which we refer to as "film-on-water" (FOW), is similar to a conventional pull test, except that the thin-film sample is suspended on water.[1,12] This method produces a stress-strain curve like that of a conventional pull test. The second method, which we refer to as "film-on-elastomer" (FOE), combines three measurements that together can be used to approximate the stress-strain curve.[15] The three measurements used in the FOE method are (1) the buckling method to obtain the tensile modulus, (2) the onset of surface wrinkles to approximate the yield point, and (3) the crack-onset strain to approximate the strain at fracture.[15–17] We chose the widely studied regioregular poly(3-hexylthiophene) (P3HT) of four different

molecular weights to serve as the subject of our comparison of the two methods. While we found good qualitative agreement between the two methods in showing increasing resistance to fracture with increasing molecular weight, the agreement in tensile modulus was poor. Differences in the values of mechanical properties produced by these methods are attributed to the ways in which the films are deformed and the extent to which defects and heterogeneity in the films influence the force required to deform them. The results we report may interest researchers concerned with metrology of thin-film polymers and increasing the lifetimes of devices for stretchable, ultra-flexible, and mechanically robust applications.

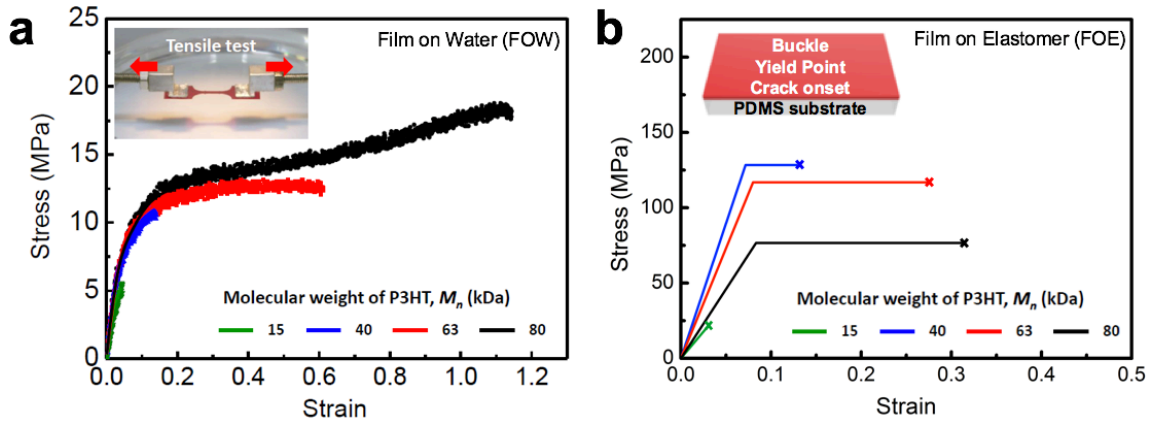

Figure 3.1. Comparison of stress-strain behavior measured for film-on-water and film-on-elastomer methods. (a) Engineering stress-strain curves of P3HT thin films with increasing molecular weight (15, 41, 64, 80 kDa) determined by FOW methods. (b) Approximated stress-strain curves for the same P3HT thin films determined by FOE methods.

3.2 Experimental Section

3.2.2 Molecular weight of poly(3-hexylthiophene) (P3HT).

We selected P3HT for this study because of its well-known microstructure, thermal transitions, and optoelectronic properties in thin-film transistors, solar cells, and biosensors.[18] Of particular importance for this study is its quasi-living synthetic mechanism using the Grignard metathesis polymerization, which affords excellent control over molecular weight and dispersity.[19]

The molecular weight, in turn, has a profound effect on microstructure and optoelectronic properties. For example, an early study by Kline et al. showed an increase in field-effect mobility with molecular weight from a value of 1.7×10^{-6} $cm^2\ V^{-1}\ s^{-1}$ at 3.2 kDa to 9.4×10^{-6} $cm^2\ V^{-1}\ s^{-1}$ at 36.5 kDa.[20] This change in mobility was correlated to significant changes in the morphology of the system, from rod-like structures in the 3.2 kDa sample to isotropic nodule structures in the 36.5 kDa film, as seen in AFM images.[20] X-ray diffraction measurements revealed that the 3.2 kDa sample had a greater signal intensity for the <100> peak than the 36.5 kDa sample, which indicated a higher degree of crystallinity, albeit lower mobility.[20] However, the mobility of the low molecular weight sample could be increased by manipulating the morphology through annealing or using a solvent with a high boiling point.[21] Recent studies have shown that the mobility of P3HT continues to increase with molecular weight until it saturates at a critical value.[22] This critical point occurs once the molecular weight is high enough such that the lattice disorder becomes independent of polymer chain length.[22] We note that values of molecular weight obtained from gel-permeation chromatography (GPC) using polystyrene standards overestimate the weight obtained by MALDI-TOF-MS or NMR by a value of approximately 1.67.[23]

3.2.3 Effect of molecular weight on the mechanical properties of P3HT.

While the mechanical properties of P3HT as a function of molecular weight have been measured before, the results were obtained using bulk samples,[9] or nano-dynamic mechanical analysis,[24] as opposed to measurement on thin films. In general, increasing the molecular weight of P3HT increases the ductility (strain at fracture) and toughness (total energy density absorbed by the material at the point of fracture).[9] The most important microstructural characteristic that influences the mechanical properties of polymers with increasing molecular weight is the density

of entanglements.[25] An entanglement is a physical linking of polymer chains, and a consequence of the fact that two chains can slide past but not cross one another.[25] Another effect is that at higher molecular weights, stiff crystallites are connected by tie molecules.[22] Using traditional pull testing, Koch et al. measured the mechanical properties of bulk samples of P3HT tapes prepared by melt casting in a uniaxial tensile test. The authors reported that the stress at failure increased from 8 MPa to 24 MPa and the elongation improved from ~10% to ~300% in the 20 and 110 kDa samples, respectively.[9] The role of entanglements was established by measuring the specific viscosity of each solution. The authors determined the critical molecular weight at which the chains become entangled to be ~35 kDa, as indicated by a sharp increase in viscosity.[9] Moreover, the melting temperature and enthalpy of fusion saturated after ~30 kDa, which further provides evidence for the onset of chain entanglement at this molecular weight.[9] The resistance to fracture of thin films of high molecular weight P3HT has also been measured using a four-point bend test. For example, Bruner et al. showed that as the molecular weight of P3HT increased, the cohesive energy of composites of P3HT with the fullerene derivative phenyl-C_{61}-butyric acid methyl ester ([60]PCBM) exhibited an increase from ~1-2 J m^{-2} at 28 kDa to nearly ~17 J m^{-2} at 100 kDa.[26]

3.2.4 Film-on-water (FOW) measurements.

The FOW technique is a pseudo free-standing tensile test that exploits the high surface tension of water, 73 mN m^{-1}, to suspend thin films on the water surface.[12] The low viscosity of water allows for unimpeded sliding of the films on the water surface; this scenario is ideal for replicating a free-standing tensile test.[12] Once the film is floated on the water surface, it is attached to the load grips using small PDMS slabs that make van der Waals adhesion with the load cell and the thin film. The film is then strained at a strain rate of ~0.3×10^{-3} s^{-1} until failure of the film to

produce a stress-strain curve. This method combines the advantages of free-standing tensile tests with those of substrate-supported tests. That is, it provides a direct measurement of the mechanical properties while providing a means of manipulating ultra-thin films which would otherwise collapse upon themselves in air.

3.2.5 Film-on-elastomer (FOE) measurements.

FOE methods comprise three separate measurements that collectively approximate a stress-strain curve of a thin film and allow the rough estimation of the energies of deformation, i.e., resilience and toughness. The three tests are mechanical buckling to measure the tensile modulus, onset of buckling to measure the yield point, and stretching until failure to determine the crack-onset strain.[15–17] Mechanical buckling, also known as surface wrinkling, is a well-documented method of measuring the tensile modulus of otherwise difficult-to-measure thin film systems such as organic semiconductors, polymer brushes, and nanostructured materials supported by an elastomeric substrate.[10] This technique is useful over a wide range of film thicknesses (20 to 500 nm) and tensile moduli and is sufficiently sensitive to detect modulus anisotropy in polymer thin films.[27–30] The tensile moduli of materials obtained from this method agree well with those reported from traditional methods and dynamic mechanical analysis.[31–33] Onset of buckling is an FOE method that detects the formation of surface wrinkles to determine the yield point of the film. The method is performed by cyclically, and incrementally, straining and relaxing a thin film on an elastomeric substrate (i.e., 0%→1% →0%→2%→0%→ 3% → 0%, etc.). Once the yield point is reached, the film is plastically deformed and upon relaxation the film is compressed and buckles form on the surface. The onset of buckles in the film manifests as a diffraction pattern obtained using a laser, or can be visibly seen in a microscope under favorable conditions.[34] Crack-onset

strain measurements in the FOE method are used to determine the strain at which the material begins to fail. Briefly, a thin-film material is transferred to an elastomeric substrate and is incrementally strained until the formation of pinholes or cracks appear in the film. While the FOE methods were introduced as an alternative to nanoindentation and tensile tests of free-standing samples, the FOE methods are time consuming and use significantly more material than FOW methods.

3.2.6 Molecular dynamics (MD).

MD simulations can be used to predict the nanoscale structural and mechanical properties of polymeric materials.[35] They probe mechanical phenomena on a level of detail that is impossible to characterize experimentally. Although high molecular weight polymers are exceedingly time-consuming to simulate using atomistic models, detailed coarse-grained models can be used to simulate highly entangled polymeric systems.[36–38] To complement our experimental study, we employed a three-site model for P3HT developed by Huang and coworkers to simulate the effect of molecular weight on structure, entanglement and response to uniaxial tensile loading. We have previously demonstrated that this model predicts the mechanical properties of P3HT accurately.[38]

3.3 Results and Discussion

3.3.1 Tensile modulus.

We measured the tensile modulus of each film using two different methods, FOW and FOE, and compared the results (**Figure 3.2a,b**). We can see that the FOE method produced values for tensile moduli that were 3-7 times higher than those produced by FOW. However, both sets of values were in the range of values reported in literature, 0.22 to 1.33 GPa.[16,39–43] In the FOW tests,

the modulus was constant for samples ≥40 kDa. Similar tendencies for the modulus of P3HT to saturate with increasing molecular weight have been reported using a molecular dynamics simulation.[35] Tummala et al. showed that the modulus does not change significantly above the entanglement chain length since the modulus is the stress response in the initially elastic regime.[35] In the FOE method, the moduli increased as the molecular weight increased from 15 kDa to 40 kDa, and decreased for samples >40 kDa. We hypothesize that the polymer chains are well packed and confined up to 40 kDa (just above the entanglement chain length). However, above the entanglement length, polymer chains exhibit slower reptation dynamics and cannot pack as efficiently. This phenomenon results in increased free volume of the amorphous domains and softer behavior in compression tests. For both the FOW and FOE method, the 15 kDa sample exhibited the lowest modulus and greatest brittleness. The brittleness observed for 15 kDa is consistent with the fact that the molecular weight is smaller than the previously determined entanglement molecular weight for P3HT of 25 kDa, as determined by GPC.[9]

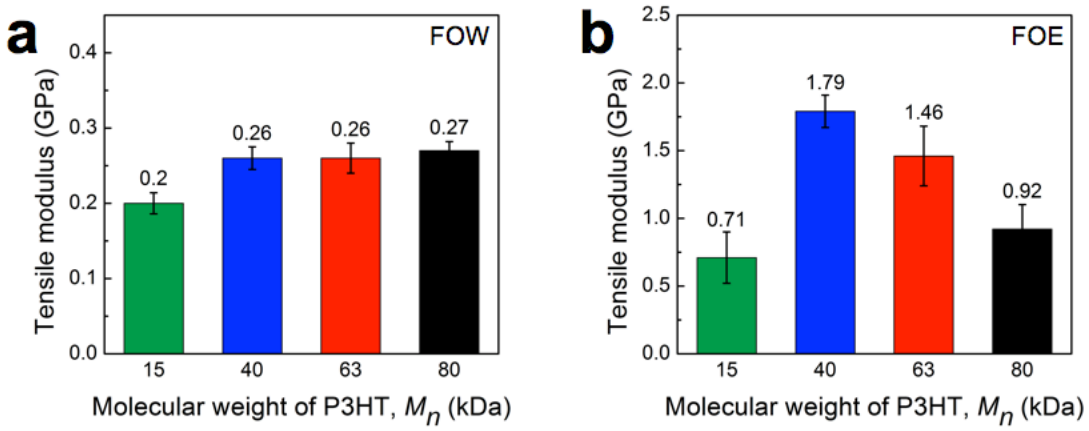

Figure 3.2. Tensile moduli of P3HT thin films with a range of molecular weight. (a) As measured by FOW methods. (b) As measured by FOE methods.

We attribute the difference in values for tensile modulus obtained using the FOW and FOE methods to three factors: (1) voids in the film which create a different stress response under tension

vs. compression, (2) inhomogeneities in thickness (surface roughness), and (3) strain rate. It is often found that materials measured in compression exhibit higher moduli than those measured in tension.[44] For example, a study by Johnston et al. reported the tensile modulus of PDMS cured at room temperature to be 1.32 ± 0.07 MPa, the same sample exhibited a compressive modulus of 186.9 ± 5.39 MPa.[45] Similar results have been reported for polyethylene and epoxy resins.[46,47] In the FOW method, the films experience tensile stress, whereas the buckling technique used in the FOE method produces compressive stress. Variation in the stress response of the materials under these two modes of deformation can occur for two reasons. The first is the presence of imperfections, voids, and pinholes arising from free volume in the polymer network or processing of the films. Under tension, these imperfections will grow or elongate and can manifest as a reduction in the modulus, whereas in compression voids and pinholes will be closed; closing of the pinholes minimizes their effects and leads to a higher modulus (**Figure 3.3**).[44]

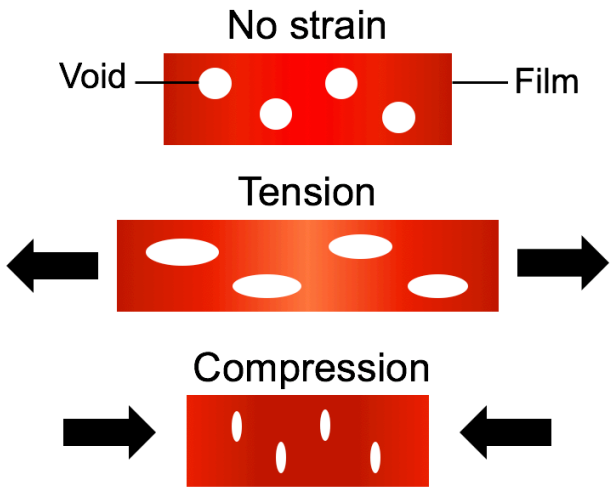

Figure 3.3. Illustration depicting the effect of tensile and compressive stresses on voids, pinholes, and imperfections in a thin film. Under tension defects will grow and become larger, in compression this effect is reversed and the defects shrink.

The second factor that may contribute to lower values for modulus in the FOW method is surface roughness and imperfections. That is, in a thin film, the roughness may be a significant

fraction of the total thickness of the film. We used atomic force microscopy (AFM) to quantify the degree of surface roughness (**Figure 3.4**). Overall, it shows similar surface morphology in all the samples. The peak-to-valley roughness, R_{pv}, was around 25-34 nm, which is 13-17% of total films thickness (~200 nm). The inhohogeneities of film thickness from the high peak-to-valley distances can cause the stress concentration in the thinnest regions of the film under tension, and the concentration of the stress would thus produce lower values for modulus and premature failure. In compression this effect is mitigated because the valleys at the film surface will be closed.

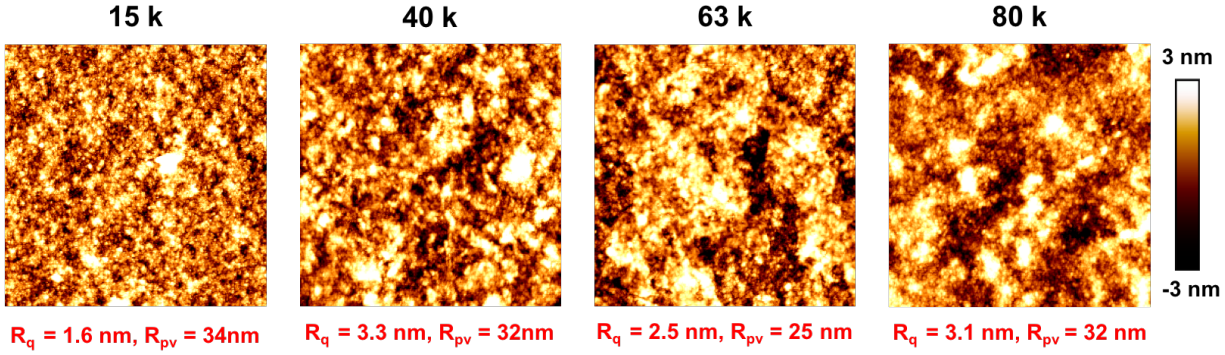

Figure 3.4. AFM images showing the surface morphology of P3HT with increasing molecular weight. Scan area was 5 × 5 μm.

In any stress-strain measurement, the strain rate effects the apparent modulus. Generally, higher strain rates lead to higher moduli.[44] To illustrate this effect, we tested a 63 kDa P3HT sample at a fast and slow strain rate in the FOW setup (**Figure 3.5**). The FOW tensile test conducted at a relatively slow strain rate of 0.3×10^{-3} s^{-1} produced a modulus value of 0.261 GPa. The fast FOW test had a strain rate of 3.0×10^{-3} s^{-1} and the modulus obtained was 0.438 GPa, which is almost 2× larger than the value obtained using the slow test. A similar experiment was performed using the FOE method where a sample was compressed at a relatively slow rate of 0.3×10^{-1} s^{-1} on a linear actuator and a fast rate by releasing the strain instantaneously, but there was no significant change in the buckling wavelength with varying strain rate. We hypothesize the

strain rate effects in tensile loading are largely responsible for the differences in the moduli reported by the two methods, FOW and FOE. In the FOW test the strain rate was slow at 0.3×10^{-3} s^{-1} however, a faster strain rate would have produced a larger tensile modulus. Collectively the effects from varying strain rate, inhomogenieties in film thickness, and void space in the films behaving differently in tension versus compression lead to a larger tensile modulus being reported in compressive FOE buckling measurements then those reported in free-standing FOW tensile tests.

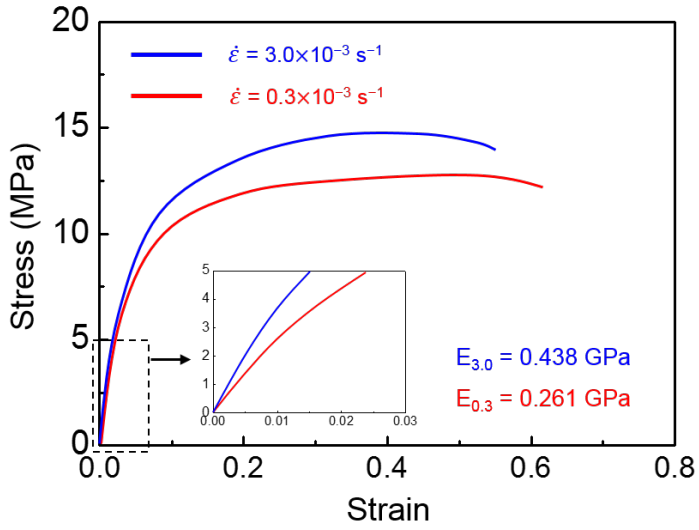

Figure 3.5. Stress-strain curves of 63 kDa P3HT tested using two different strain rates. The FOW pull test conducted using the faster strain rate produced a 2× larger apparent tensile modulus.

3.3.2 Ductility.

Both methods show good qualitative agreement in the increase of ductility of the films with increasing molecular weight (**Table 3.1**). The differences in the absolute values of the strain at failure arise from the labeling of the failure point in FOE methods. In the FOW method, the strain at failure is the point at which the film is completely ruptured; in the FOE method, the strain at failure is labeled as the onset of cracks or pinholes in the film. The strain at which the film

completely ruptures (bifurcates) in the FOE method would be much higher than in the FOW method. The great extent to which a film on an elastomeric substrate can be stretched is not a true represenation of the strain at which a freestanding film would fail. This difference is due to the film being supported by an elastomeric substrate which redistributes stress to the film (as opposed to in the FOW method, where stress is concentrated to the defects and thin areas). The mechanical behavior of the elastomeric substrate also plays an important role in the crack behavior observed in the thin films. A stiff substrate with an elastic modulus closer to that of the P3HT thin film lead to the onset of cracks at a higher strain, compared to a softer elastomer which cracked at relatively lower strains due to the greater mismatch in the elastic modulus. (**Figure C.1**). To mitigate this effect, it is best to select a substrate that is close to the modulus of the thin film to help reduce interfacial stresses while maintaining sufficient adhesion for the transfer of the film to the substrate. It was expected that the ductility of the films would increase with molecular weight for two reasons: (1) at higher molecular weight there is an increase in the degree of interchain π-stacking in the crystalline regions of the film which increases the number of van-der-Waals bonds needed to be broken for chain pullout to occur and (2) in the amorphous regime there is an increase in the number of intrachain folds and physical linking of the polymer chains which makes disentanglement of chains increasingly difficult.[26] We hypothesize that at low molecular weight the polymer film has a low density of entanglements and cracking occurs by chain pullout. At high molecular weight there is a high density of entanglements and cracking occurs by chain scission.

Table 3.1. Tabulated values of the mechanical properties of P3HT films as a function of molecular weight.

FOW Methods				
M_n (kDa)	**Tensile modulus (GPa)**	**Strain at fracture (%)**	**Toughness (kJ/m^3)**	**Tensile strength (MPa)**
15	0.203 ± 0.014	4.5 ± 0.3	0.14 ± 0.01	4.5 ± 0.3
40	0.263 ± 0.015	13.0 ± 1.2	0.99 ± 0.08	10.5 ± 0.5
63	0.261 ± 0.020	58.7 ± 6.5	6.80 ± 0.78	12.6 ± 0.2
80	0.270 ± 0.012	95.6 ± 7.7	13.17 ± 0.97	17.1 ± 0.6
FOE Methods				
M_n (kDa)	**Tensile modulus (GPa)**	**Crack onset strain (%)**	**Estimated toughness (kJ/m^3)**	**Tensile strength (MPa)**
15	0.71 ± 0.19	2.83 ± 0.41	0.85 ± 0.21	----
40	1.79 ± 0.12	12.83 ± 1.72	11.87 ± 3.77	----
63	1.46 ± 0.22	27.33 ± 4.37	27.25 ± 7.62	----
80	0.92 ± 0.18	31.17 ± 11.67	20.69 ± 9.89	----

3.3.3 Aggregation behavior.

Ultraviolet/visible (UV-vis) spectroscopy measurements were used to measure how the optoelectronic properties changed with molecular weight (**Figure 3.6a**). In particular we sought to analyze the degree of aggregation present in the semi-crystalline P3HT thin films. The absorption of weakly interacting H-aggregates is determined by coupled electronic-vibrational (vibronic) energy transitions. Two effects were observed: (1) there was a small red shift with increasing molecular weight and (2) the peaks associated with the vibronic progression are the most pronounced for the 80 kDa sample. Similar results have been reported previously by Kline and Zen et al.[21,48] Analysis using the weakly interacting H-aggregate model revealed an increase in the conjugation length of P3HT with increasing molecular weight, as manifested in a decrease in the exciton bandwidth extracted using the weakly interacting H-aggregate model of Spano and

coworkers **(Figure 3.6b)**.[49–52] These results correlate well with the observed feature changes in the UV-vis spectra, that is, longer conjugation length leads to absorption at lower energy.[53] We hypothesize that increased conjugation in a P3HT thin film leads to more resistance to deformation and therefore a higher tensile modulus as observed in **Figure 3.2a**. H-aggregate analysis also showed that the 15 kDa sample had the highest fraction of aggregates which is due to the ability of low molecular weight P3HT to form chain extended crystals and distinct lamellae.[9] As the polymer chains become longer the lamellar structures become intermixed in an amorphous network of polymer which decreases the overall fraction of aggregates. However, once the polymer chains become sufficiently long the degree of self-folding grows which is manifested as an increase in the fraction of aggregates as seen in **Figure 3.6b** (data points indicated in blue).

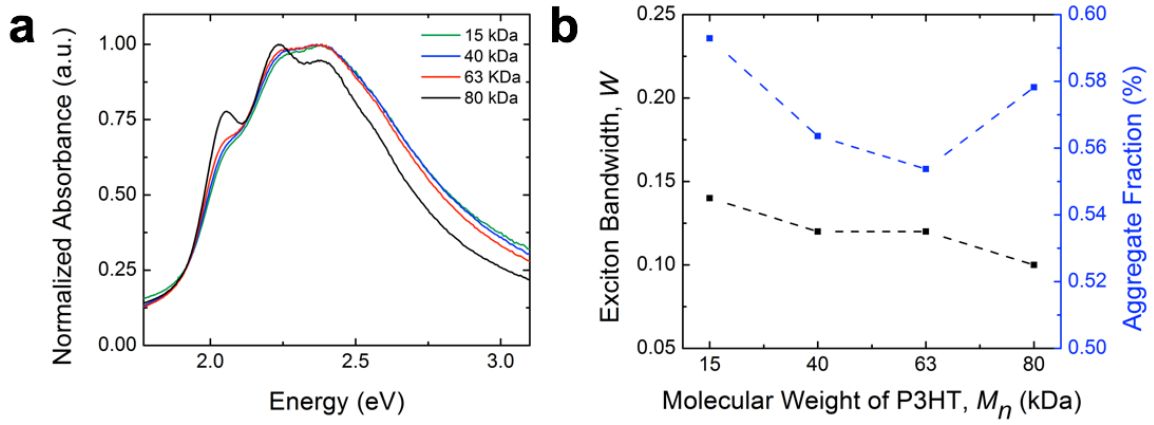

Figure 3.6. (a) UV-vis spectra showing the normalized absorbance of P3HT thin films with increasing M_n. (b) Exciton bandwidth, *W*, of the P3HT thin films as determined by the weakly interacting H-aggregate model. *W* is inversely correlated with conjugation length.

3.3.4 Molecular dynamics simulations.

Coarse-grained molecular dynamics simulations were used to demonstrate the microscopic effects of entanglements on the tensile response. A description of the models and simulation protocols used can be found in our previous publication.[38] We prepared two systems: one with chain lengths equal to the entanglement length, $N_e \approx 50$ repeat units, and one with high molecular

weight chains of 300 repeat units ($\approx 6N_e$). The morphology was prepared to represent a polymer film that was spin coated from a good solvent such as chloroform; it was homogenous and did not contain voids. To quantify entanglements, a primitive path analysis was performed using the Z1 algorithm of Kröger and coworkers.[54–57] As expected, we found that the low molecular weight system was barely entangled with ≈ 2 interior kinks per chain while the high molecular weight system was highly entangled with ≈ 8 interior kinks per chain. The low molecular weight system (50-mers) was observed to fracture via chain pullout (**Figure 3.7**). The high molecular weight system (300-mers) did not crack in the simulations, instead, we observed that the stress was concentrated to relatively few entangled chains (**Figure 3.7**). Although the model employed in these simulations did not include the potential for bonds to break, this observation provided evidence that fracture in entangled samples is in fact due to chain scission. The order of magnitude obtained for the tensile modulus (~1 GPa) was in closer agreement with the FOE method than with the FOW method. We attribute this finding to the fast strain rate employed in the simulations, as well as the absence of macroscopic heterogeneities, voids, and thin-film confinement effects.

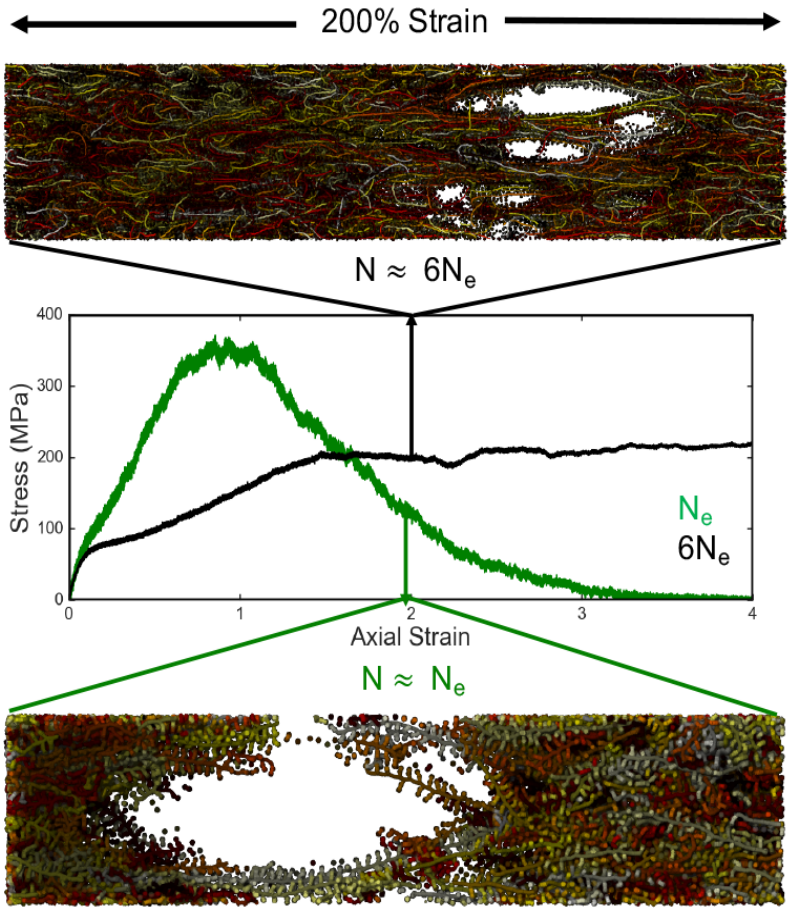

Figure 3.7. Comparison of uniaxial tensile response between disentangled ($N \approx N_e$) and highly entangled ($N \approx 6N_e$) systems, as computed by coarse-grained MD. Snapshots illustrate a 5-nm slice of the simulation trajectory at 200% strain. Polymers are colored by chain number to make them distinguishable.

3.4 Conclusions

In conclusion, we compared the results from two different methods (FOW and FOE) of determining the mechanical properties of P3HT thin films as a function of molecular weight. The FOE method produced higher values of the tensile modulus than the FOW method. These results can be attributed to various differences between the two metrological techniques including mode of loading (tension vs. compression), strain rate, and substrate effects. Complementary coarse-grained MD simulations demonstrate that fracture occurs via chain-pullout in the low molecular

weight samples, and provides evidence to support the hypothesis that entangled systems exhibit chain scission as the dominant fracture mechanism. All three methods produced good qualitative agreement in finding the strain at which the films failed and showed an increase in ductility with increasing molecular weight of P3HT. This work revealed that mechanical analysis of thin films is not independent of the method used to study them and offers a point of reference for comparing the mechanical properties of materials measured using a pull test and those using methods involving thin films bonded to elastomers. Furthermore, the results presented here make a strong case for employing pull tests, such as FOW, over FOE based experiments to save time, preserve material, and to obtain the most facile, reliable, and precise measurements of mechanical properties.

Acknowledgements

This research was supported by the Air Force Office of Scientific Research (AFOSR), grant number FA9550-16-1-0220. D. R. acknowledges support provided by the National Science Foundation Graduate Research Fellowship Program under Grant No. DGE-1144086. This work was performed in part at the San Diego Nanotechnology Infrastructure (SDNI), a member of the National Nanotechnology Coordinated Infrastructure, which is supported by the National Science Foundation (Grant ECCS-1542148). Computational resources to support this work were provided by the Extreme Science and Engineering Discovery Environment (XSEDE) Program through the National Science Foundation grant number ACI-1053575.

Chapter 3, in full, is a reprint of the material as it appears in *ACS Applied Materials & Interfaces*, 2017, 9, 8855-8862. American Chemical Society, 2017. Daniel Rodriquez, Jae-Han

Kim, Samuel E. Root, Zhuping Fei, Pierre Boufflet, Martin Heeney, Taek-Soo Kim, and Darren J. Lipomi. The dissertation author was the primary investigator and author of this paper.

References

(1) Kim, T.; Kim, J.-H.; Kang, T. E.; Lee, C.; Kang, H.; Shin, M.; Wang, C.; Ma, B.; Jeong, U.; Kim, T.-S.; Kim, B. J. Flexible, Highly Efficient All-Polymer Solar Cells. *Nat. Commun.* **2015**, *6* (May), 8547.

(2) Fukuda, K.; Takeda, Y.; Mizukami, M.; Kumaki, D.; Tokito, S. Fully Solution-Processed Flexible Organic Thin Film Transistor Arrays with High Mobility and Exceptional Uniformity. *Sci. Rep.* **2014**, *4*, 3947.

(3) Jin Young, O.; Kim, S.; Baik, H. K.; Jeong, U. Deformable Electronics: Conducting Polymer Dough for Deformable Electronics (Adv. Mater. 22/2016). *Adv. Mater.* **2016**, *28* (22), 4564.

(4) Khan, H. U.; Roberts, M. E.; Johnson, O.; Knoll, W.; Bao, Z. The Effect of pH and DNA Concentration on Organic Thin-Film Transistor Biosensors. *Org. Electron.* **2012**, *13* (3), 519–524.

(5) Kaltenbrunner, M.; Sekitani, T.; Reeder, J.; Yokota, T.; Kuribara, K.; Tokuhara, T.; Drack, M.; Schwödiauer, R.; Graz, I.; Bauer-Gogonea, S.; Bauer, S.; Someya, T. An Ultra-Lightweight Design for Imperceptible Plastic Electronics. *Nature* **2013**, *499* (7459), 458–463.

(6) O'Connor, T. F.; Zaretski, A. V.; Shiravi, B. A.; Savagatrup, S.; Printz, A. D.; Diaz, M. I.; Lipomi, D. J. Stretching and Conformal Bonding of Organic Solar Cells to Hemispherical Surfaces. *Energy Environ. Sci.* **2014**, *7* (1), 370–378.

(7) Wang, G. J. N.; Shaw, L.; Xu, J.; Kurosawa, T.; Schroeder, B. C.; Oh, J. Y.; Benight, S. J.; Bao, Z. Inducing Elasticity through Oligo-Siloxane Crosslinks for Intrinsically Stretchable Semiconducting Polymers. *Adv. Funct. Mater.* **2016**, *26* (40), 7254–7262.

(8) Shin, M.; Oh, J. Y.; Byun, K. E.; Lee, Y. J.; Kim, B.; Baik, H. K.; Park, J. J.; Jeong, U. Polythiophene Nanofibril Bundles Surface-Embedded in Elastomer: A Route to a Highly Stretchable Active Channel Layer. *Adv. Mater.* **2015**, *27* (7), 1255–1261.

(9) Koch, F. P. V.; Rivnay, J.; Foster, S.; Müller, C.; Downing, J. M.; Buchaca-Domingo, E.; Westacott, P.; Yu, L.; Yuan, M.; Baklar, M.; Fei, Z.; Luscombe, C.; McLachlan, M. A.; Heeney, M.; Rumbles, G.; Silva, C.; Salleo, A.; Nelson, J.; Smith, P.; Stingelin, N. The Impact of Molecular Weight on Microstructure and Charge Transport in Semicrystalline Polymer Semiconductors-poly(3-Hexylthiophene), a Model Study. *Prog. Polym. Sci.* **2013**, *38* (12), 1978–1989.

(10) Chung, J. Y.; Nolte, A. J.; Stafford, C. M. Surface Wrinkling: A Versatile Platform for Measuring Thin-Film Properties. *Adv. Mater.* **2011**, *23* (3), 349–368.

(11) Dupont, S. R.; Oliver, M.; Krebs, F. C.; Dauskardt, R. H. Interlayer Adhesion in Roll-to-Roll Processed Flexible Inverted Polymer Solar Cells. *Sol. Energy Mater. Sol. Cells* **2012**, *97*, 171–175.

(12) Kim, J.-H.; Nizami, A.; Hwangbo, Y.; Jang, B.; Lee, H.-J.; Woo, C.-S.; Hyun, S.; Kim, T.-S. Tensile Testing of Ultra-Thin Films on Water Surface. *Nat. Commun.* **2013**, *4*, 2520.

(13) Savagatrup, S.; Printz, A. D.; Rodriquez, D.; Lipomi, D. J. Best of Both Worlds: Conjugated Polymers Exhibiting Good Photovoltaic Behavior and High Tensile Elasticity. *Macromolecules* **2014**, *47* (6), 1981–1992.

(14) Root, S.; Arya, G.; Lipomi, D. J. Mechanical Properties of Organic Electronic Materials : A Coarse-Grained Molecular Dynamics Study P3HT Amorphous Generation Effect of Alkyl Side-Chain Length Coarse-Grained Models Uniaxial Tensile Deformation Uniaxial Tensile Deformation Support. **2015**, *117*, 4663.

(15) Printz, A. D.; Zaretski, A. V.; Savagatrup, S.; Chiang, A. S.-C.; Lipomi, D. J. Yield Point of Semiconducting Polymer Films on Stretchable Substrates Determined by Onset of Buckling. *ACS Appl. Mater. Interfaces* **2015**, *7*, 23257–23264.

(16) Savagatrup, S.; Makaram, A. S.; Burke, D. J.; Lipomi, D. J. Mechanical Properties of Conjugated Polymers and Polymer-Fullerene Composites as a Function of Molecular Structure. *Adv. Funct. Mater.* **2014**, *24* (8), 1169–1181.

(17) Rodriquez, D.; Savagatrup, S.; Valle, E.; Proctor, C. M.; McDowell, C.; Bazan, G. C.; Nguyen, T.-Q.; Lipomi, D. J. Mechanical Properties of Solution-Processed Small-Molecule Semiconductor Films. *ACS Appl. Mater. Interfaces* **2016**, *8*, 11649–11657.

(18) Brinkmann, M. Structure and Morphology Control in Thin Films of Regioregular poly(3-Hexylthiophene). *J. Polym. Sci. Part B Polym. Phys.* **2011**, *49* (17), 1218–1233.

(19) McCullough, R. D. The Chemistry of Conducting Polythiophenes. *Adv. Mater.* **1998**, *10* (2), 93–116.

(20) Kline, R. J.; McGehee, M. D.; Kadnikova, E. N.; Liu, J.; Frechet, J. M. J. Controlling the Field-Effect Mobility of Regioregular Polythiophene by Changing the Molecular Weight. *Adv. Mater.* **2003**, *15* (18), 1519–1522.

(21) Kline, R. J.; Mcgehee, M. D.; Kadnikova, E. N.; Liu, J.; Frechet, J. M. J.; Toney, M. F. The Dependence of Regioregular Poly (3-Hexylthiophene) Film Morphology and Field-Effect Mobility on Molecular Weight. *Macromolecules* **2004**, *38* (December), 3312–3319.

(22) Noriega, R.; Rivnay, J.; Vandewal, K.; Koch, F. P. V; Stingelin, N.; Smith, P.; Toney, M. F.; Salleo, A. A General Relationship between Disorder, Aggregation and Charge Transport in Conjugated Polymers. *Nat. Mater.* **2013**, *12* (11), 1038–1044.

(23) Koch, F. P. V; Smith, P.; Heeney, M. "Fibonacci'S Route" To Regioregular Oligo(3-Hexylthiophene)S. *J. Am. Chem. Soc.* **2013**, *135* (37), 13695–13698.

(24) Bruner, C.; Miller, N. C.; McGehee, M. D.; Dauskardt, R. H. Molecular Intercalation and Cohesion of Organic Bulk Heterojunction Photovoltaic Devices. *Adv. Funct. Mater.* **2013**, *23*, 2863–2871.

(25) Likhtman, A. E.; Ponmurugan, M. Microscopic Definition of Polymer Entanglements. *Macromolecules* **2014**, *47* (4), 1470–1481.

(26) Bruner, C.; Dauskardt, R. Role of Molecular Weight on the Mechanical Device Properties of Organic Polymer Solar Cells. *Macromolecules* **2014**, *47*, 1117–1121.

(27) Cranston, E. D.; Eita, M.; Johansson, E.; Netrval, J.; Salajková, M.; Arwin, H.; Wågberg, L.; Salajkov, M.; Arwin, H.; Lars, W. Determination of Young' S Modulus for Nanofibrillated Cellulose Multilayer Thin Films Using Buckling Mechanics. *Biomacromolecules* **2011**, *12* (4), 961–969.

(28) Huang, H.; Chung, J. Y.; Nolte, A. J.; Stafford, C. M. Characterizing Polymer Brushes via Surface Wrinkling. *Chem. Mater.* **2007**, *19* (26), 6555–6560.

(29) Awartani, O. M.; Zhao, B.; Currie, T.; Kline, R. J.; Zikry, M. A.; O'Connor, B. T. Anisotropic Elastic Modulus of Oriented Regioregular Poly(3-Hexylthiophene) Films. *Macromolecules* **2016**, *49* (1), 327–333.

(30) Zhao, B.; Awartani, O.; O'Connor, B.; Zikry, M. A. A Direct Correlation of X-Ray Diffraction Orientation Distributions to the in-Plane Stiffness of Semi-Crystalline Organic Semiconducting Films. *Appl. Phys. Lett.* **2016**, *108* (18), 108–111.

(31) Kuila, B. K.; Nandi, A. K. Physical, Mechanical, and Conductivity Properties of poly(3-Hexylthiophene) -Montmorillonite Clay Nanocomposites Produced by the Solvent Casting Method. *Macromolecules* **2004**, *37* (23), 8577–8584.

(32) Kuila, B. K.; Nandi, A. K. Structural Hierarchy in Melt-Processed poly(3-Hexyl Thiophene)- Montmorillonite Clay Nanocomposites: Novel Physical, Mechanical, Optical, and Conductivity Properties. *J. Phys. Chem. B* **2006**, *110* (4), 1621–1631.

(33) Müller, C.; Goffri, S.; Breiby, D. W.; Andreasen, J. W.; Chanzy, H. D.; Janssen, R. A. J.; Nielsen, M. M.; Radano, C. P.; Sirringhaus, H.; Smith, P.; Stingelin-Stutzmann, N. Tough, Semiconducting Polyethylene-poly(3-Hexylthiophene) Diblock Copolymers. *Adv. Funct. Mater.* **2007**, *17* (15), 2674–2679.

(34) Printz, A. D.; Chiang, A. S. C.; Savagatrup, S.; Lipomi, D. J. Fatigue in Organic Semiconductors: Spectroscopic Evolution of Microstructure due to Cyclic Loading in poly(3-Heptylthiophene). *Synth. Met.* **2016**, *217*, 144–151.

(35) Tummala, N. R.; Risko, C.; Bruner, C.; Dauskardt, R. H.; Bredas, J. L. Entanglements in P3HT and Their Influence on Thin-Film Mechanical Properties: Insights from Molecular

Dynamics Simulations. *J. Polym. Sci. Part B Polym. Phys.* **2015**, *53* (13), 934–942.

(36) Jones, M. L.; Huang, D. M.; Chakrabarti, B.; Groves, C. Relating Molecular Morphology to Charge Mobility in Semicrystalline Conjugated Polymers. *J. Phys. Chem. C* **2016**, *120*, 4240–4250.

(37) Huang, D. M.; Faller, R.; Do, K.; Moul, A. J. Coarse-Grained Computer Simulations of Polymer / Fullerene Bulk Heterojunctions for Organic Photovoltaic Applications. *J. Chem. Theory Comput.* **2010**, *6*, 526–537.

(38) Root, S. E.; Savagatrup, S.; Pais, C. J.; Arya, G.; Lipomi, D. J. Predicting the Mechanical Properties of Organic Semiconductors Using Coarse-Grained Molecular Dynamics Simulations. *Macromolecules* **2016**, *49* (7), 2886–2894.

(39) Lipomi, D. J.; Chong, H.; Vosgueritchian, M.; Mei, J.; Bao, Z. Toward Mechanically Robust and Intrinsically Stretchable Organic Solar Cells: Evolution of Photovoltaic Properties with Tensile Strain. *Sol. Energy Mater. Sol. Cells* **2012**, *107*, 355–365.

(40) Tahk, D.; Lee, H. H.; Khang, D.-Y. Elastic Moduli of Organic Electronic Materials by the Buckling Method. *Macromolecules* **2009**, *42* (18), 7079–7083.

(41) Awartani, O.; Lemanski, B. I.; Ro, H. W.; Richter, L. J.; DeLongchamp, D. M.; O'Connor, B. T. Correlating Stiffness, Ductility, and Morphology of Polymer:Fullerene Films for Solar Cell Applications. *Adv. Energy Mater.* **2013**, *3* (3), 399–406.

(42) O'Connor, B.; Chan, E. P.; Chan, C.; Conrad, B. R.; Richter, L. J.; Kline, R. J.; Heeney, M.; McCulloch, I.; Soles, C. L.; DeLongchamp, D. M. Correlations between Mechanical and Electrical Properties of Polythiophenes. *ACS Nano* **2010**, *4* (12), 7538–7544.

(43) Kim, J. S.; Kim, J. H.; Lee, W.; Yu, H.; Kim, H. J.; Song, I.; Shin, M.; Oh, J. H.; Jeong, U.; Kim, T. S.; Kim, B. J. Tuning Mechanical and Optoelectrical Properties of Poly(3-Hexylthiophene) through Systematic Regioregularity Control. *Macromolecules* **2015**, *48* (13), 4339–4346.

(44) Landel, R. F.; Nielsen, L. E. *Mechanical Properties of Polymers and Composites*, Second Edi.; CRC Press, 1993.

(45) Johnston, I. D.; McCluskey, D. K.; Tan, C. K. L.; Tracey, M. C. Mechanical Characterization of Bulk Sylgard 184 for Microfluidics and Microengineering. *J. Micromech. Microeng.* **2014**, *24*, 35017.

(46) Selby, K.; Miller, L. Fracture Toughness and Mechanical Behaviour of an Epoxy Resin. *J. Mater. Sci.* **1975**, *10*, 12–24.

(47) Drozdov, A. D.; Christiansen, J. de C. Thermo-Viscoelastic and Viscoplastic Behavior of High-Density Polyethylene. *Int. J. Solids Struct.* **2008**, *45* (14–15), 4274–4288.

(48) Zen, A.; Pflaum, J.; Hirschmann, S.; Zhuang, W.; Jaiser, F.; Asawapirom, U.; Rabe, J. P.;

Scherf, U.; Neher, D. Effect of Molecular Weight and Annealing of poly(3-Hexylthiophene)s on the Performance of Organic Field-Effect Transistors. *Adv. Funct. Mater.* **2004**, *14* (8), 757–764.

(49) Siddiqui, S.; Spano, F. C. H- and J-Aggregates of Conjugated Polymers and Oligomers. *Chem. Phys. Lett.* **1999**, *308* (1–2), 99–105.

(50) Spano, F. C. Modeling Disorder in Polymer Aggregates: The Optical Spectroscopy of Regioregular poly(3-Hexylthiophene) Thin Films. *J. Chem. Phys.* **2005**, *122* (23).

(51) Clark, J.; Chang, J. F.; Spano, F. C.; Friend, R. H.; Silva, C. Determining Exciton Bandwidth and Film Microstructure in Polythiophene Films Using Linear Absorption Spectroscopy. *Appl. Phys. Lett.* **2009**, *94* (16), 2007–2010.

(52) Spano, F. C.; Clark, J.; Silva, C.; Friend, R. H. Determining Exciton Coherence from the Photoluminescence Spectral Line Shape in poly(3-Hexylthiophene) Thin Films. *J. Chem. Phys.* **2009**, *130* (7).

(53) Wohlgenannt, M.; Jiang, X. M.; Vardeny, Z. V.; Janssen, R. A. J. Conjugation-Length Dependence of Spin-Dependent Exciton Formation Rates in Π-Conjugated Oligomers and Polymers. *Phys. Rev. Lett.* **2002**, *88* (19), 197401.

(54) Karayiannis, N. C.; Kröger, M. Combined Molecular Algorithms for the Generation, Equilibration and Topological Analysis of Entangled Polymers: Methodology and Performance. *Int. J. Mol. Sci.* **2009**, *10*, 5054–5089.

(55) Shanbhag, S.; Kröger, M. Primitive Path Networks Generated by Annealing and Geometrical Methods: Insights into Differences. *Macromolecules* **2007**, *40* (8), 2897–2903.

(56) Kröger, M. Shortest Multiple Disconnected Path for the Analysis of Entanglements in Two- and Three-Dimensional Polymeric Systems. *Comput. Phys. Commun.* **2005**, *168* (3), 209–232.

(57) Hoy, R. S.; Foteinopoulou, K.; Kröger, M. Topological Analysis of Polymeric Melts: Chain-Length Effects and Fast-Converging Estimators for Entanglement Length. *Phys. Rev. E - Stat. Nonlinear, Soft Matter Phys.* **2009**, *80* (3), 14–16.

Chapter 4

Measurement of Cohesion and Adhesion of Semiconducting Polymers by Scratch Testing: Effect of Side-Chain Length and Degree of Polymerization

Daniel Rodriquez,[1] James G. Kohl,[2] Pierre Morel,[4] Kyle Burrows,[4] Grégory Favaro,[5] Samuel E. Root,[1] Julian Ramirez,[1] Mohammad A. Alkhadra,[1] Cody W. Carpenter,[1] Zhuping Fei,[3] Pierre Boufflet,[3] Martin Heeney,[3] Darren J. Lipomi*,[1]

[1]*Department of NanoEngineering, University of California San Diego*

9500 Gilman Drive, Mail Code 0448, La Jolla, CA 92093-0448

[2]*Department of Mechanical Engineering, Shiley-Marcos School of Engineering,*

University of San Diego, San Diego, CA, 92110-2492

[3]*Department of Chemistry and Centre for Plastic Electronics, Imperial College London,*

Exhibition Rd, London, SW7 2AZ, United Kingdom

[4]*TriTec, Anton Paar USA, Inc., 10215 Timber Ridge Drive, Ashland, VA 23005*

[5]*TriTec, Anton Paar SA, CH-2034 Peseux, Switzerland*

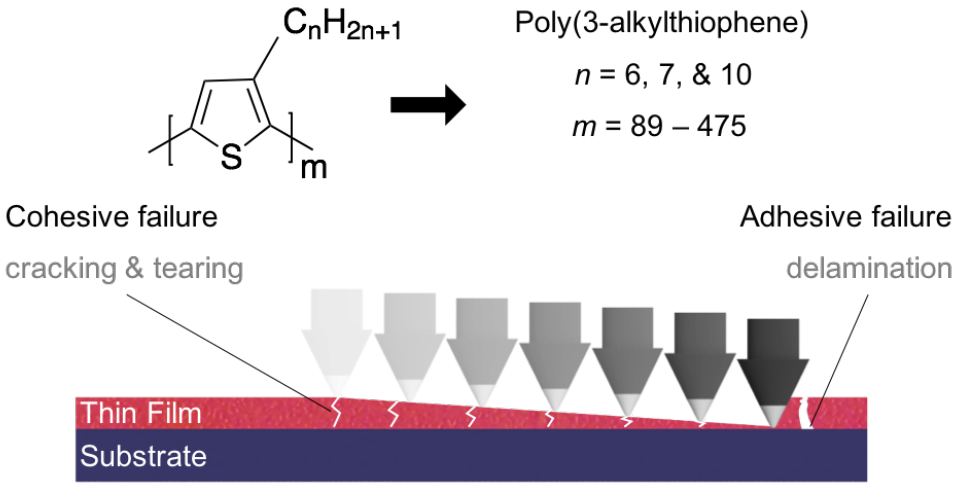

Figure 4.1. Graphical abstract.

Abstract

Most advantages of organic electronic materials are enabled by mechanical deformability, as flexible (and stretchable) devices made from these materials must be able to withstand roll-to-roll printing and survive mechanical insults from the external environment. Cohesion and adhesion are two properties that dictate the mechanical reliability of a flexible organic electronic device. In this paper, progressive-load scratch tests are used for the first time to correlate the cohesive and adhesive behavior of poly(3-alkylthiophenes) (P3ATs) with respect to two molecular parameters: length of the alkyl side chain and molecular weight. In contrast to metrological techniques based on buckling or pull testing of pseudo-freestanding films, scratch tests reveal information about both the cohesive and adhesive properties of thin polymeric films from a single procedure. Our data show a decrease in cohesion and adhesion—i.e., a decrease in overall mechanical robustness—with increasing length of the side chain. This behavior is likely due to increases in free volume and concomitant decreases in the glass transition temperature. In contrast, we observe increases in both the cohesion and adhesion with increasing molecular weight. This behavior is attributed to an increased density of entanglements with high molecular weight, which manifests as increased extensibility. These observations are consistent with the results of molecular dynamics

simulations. Interestingly, the normal (applied) forces associated with cohesive and adhesive failure are directly proportional to the average degree of polymerization—as opposed to simply the molecular weight—as the length of the alkyl side chain increases the molecular weight without increasing the degree of polymerization.

4.1 Introduction

Organic electronic materials have applications ranging from ultrathin organic photovoltaic (OPV) devices[1,2] and organic field-effect transistors (OFETs)[3,4] to wearable sensors[5,6] and actuators.[7] The electronic properties of these materials—e.g., as manifested in the efficiency of solar cells[8] and the charge-carrier mobility in thin-film transistors[9]—have improved dramatically, at least in devices fabricated at the laboratory scale. It is possible, however, that the performance at production scale could be limited by the mechanical reliability of a real device, which comprises multiple materials and interfaces.[10] In this study, we used progressive-load scratch testing for the first time to measure the cohesion and adhesion—in thin films of poly(3-alkylthiophene)s (P3ATs) as functions of two parameters: length of the alkyl side chain and molecular weight (and thus the degree of polymerization). Strong cohesion can improve mechanical stability by increasing the resistance to the formation and propagation of fracture. (We use "cohesion" to refer to the films resistance to tearing under the applied load and the sum of the intermolecular forces, rather than specifically to the "cohesive fracture energy," an extensive property measured using the four-point bending[11] or double-cantilever beam test.[12]) Furthermore, since these devices are typically supported or encapsulated by a substrate, and composed of several layers, good adhesive strength is necessary to prevent delamination. Organic semiconductors, however, tend to exhibit poor adhesion as illustrated by recent studies on roll-to-roll printed OPV devices that determined the

dominant mechanism of failure in these devices was delamination at the electrode-semiconductor interface.[12–14]

Scratch testing is an attractive method of characterizing the cohesion and adhesion of thin films on substrates, in a single test. The greatest strength of scratch testing is its practicality. Moreover, the sample used for testing can be made to isolate aspects of a real device: for example, the material of interest can be measured on realistic substrates, as opposed to on water or silicone rubber. During a scratch test, the initial indentation of the film is purely elastic.[15] As the force is increased, a critical load is reached that exceeds the elastic limit of the soft film and plastic deformation begins to occur (assuming the hardness of the indenter tip is much greater than the film).[15] Cohesive failure then occurs due to tensile stress behind the stylus tip and is observed as cracking or tearing in the film. Similarly, adhesive failure occurs due to compressive stress in front of the stylus tip, leading to delamination of the film by buckling or spallation. Schwarzer analyzed the stress distribution in scratch tests using the concept of the effective indenter and extended Hertzian theory.[16] In scratch tests both the cohesive and adhesive failure of thin films are thickness dependent, but saturate above a critical thickness (bulk value).[15] A prior study showed that cohesion and adhesion increased linearly with thickness for silicone elastomer coatings, until the bulk value was reached.[17] By assessing the type of crack propagation (i.e., tensile, conformal, Hertz) and spallation (i.e., buckling, compressive, gross) the mechanical failure mode (i.e., brittle vs. ductile) may be identified.[18] Since scratch testing can characterize cohesive and adhesive behavior, as well as brittleness and ductility, it may be used as a complement or even replacement for existing methods of metrology.

We selected P3ATs as the model materials. P3ATs are the most commonly studied subset of conjugated polymers and have been central to the development of organic electronics.[19] The

mechanical properties (elastic modulus, yield strength, ductility, and toughness),[20] electronic properties (charge-carrier mobility),[21] and thermal transitions[22] of P3ATs are well known. Moreover, the quasi-living nature of the synthesis of P3ATs permits control over the molecular weight and dispersity, and the length of the alkyl side chain is similarly easy to control when preparing the monomer. We selected alkyl side chain lengths of n = 6, 7, and 10 since the glass transition temperatures (T_g) of these materials are around (n = 6, P3HT), below (n = 7, P3HpT), and well below (n = 10, P3DT) room temperature. Similarly, we chose molecular weights that spanned a range with the previously reported entanglement molecular of P3HT (35 kDa)[22] roughly in the center. To eliminate effects caused by large deviations in molecular weight we selected dispersities in a narrow range.

A schematic illustration of a typical setup for scratch testing is depicted in **Figure 4.2a**. In a progressive-load scratch test, a stylus is dragged across the surface of a sample with an applied load that increases linearly with position, as described in **Figure 4.2b**. The location at which the film exhibits critical failure (Lc_i) and the corresponding normal force (Fn_i) are recorded during the experiment. The failure events are identified by the operator with assistance from optical microscopy, acoustic emission, and image analysis software.[23] The Lc_i associated with the failure of a film is a function of the adhesion between the film and the substrate, the thickness of the film, the rate of loading, the shape of the stylus tip, and the mechanical properties of both the substrate and the film.[17,24] Additionally, surface treatments affect the adhesion of the films to a substrate (i.e. silanes or oxygen plasma). If these properties (thickness, loading rate, stylus tip, substrate, surface treatment) are held constant, however, Fn_i may be used as the basis for a comparative analysis of the films.[15] Typically, the applied force is recorded at three distinct positions which are indicative of critical failure, as shown in **Figure 4.2c**. Lc_1 is the location in the direction of

displacement where the stylus first tears the surface of the film, but has not touched the substrate. In our tests, Lc_1 was identified by a change in the appearance of the film (from dark orange to bright orange) in the scratch channel which signaled tearing, **Figure 4.2d**. (An AFM image of this region of the scratch channel is given in **Figure D.1.**) The normal force measured at this position, Fn_1, is a measure of the samples resistance to cohesive failure. The region to the left of Lc_1 is the residual penetration depth of the stylus, which is due to plastic deformation of the film. Lc_2 is the location at which the stylus scratches through the sample completely and contacts the substrate; this position signals the onset of adhesive failure, **Figure 4.2e**. Finally, Lc_3 is the position at which gross delamination begins to occur, **Figure 4.2f**. The forces corresponding to positions Lc_2 and Lc_3 are used to compare the adhesion of materials to substrates.

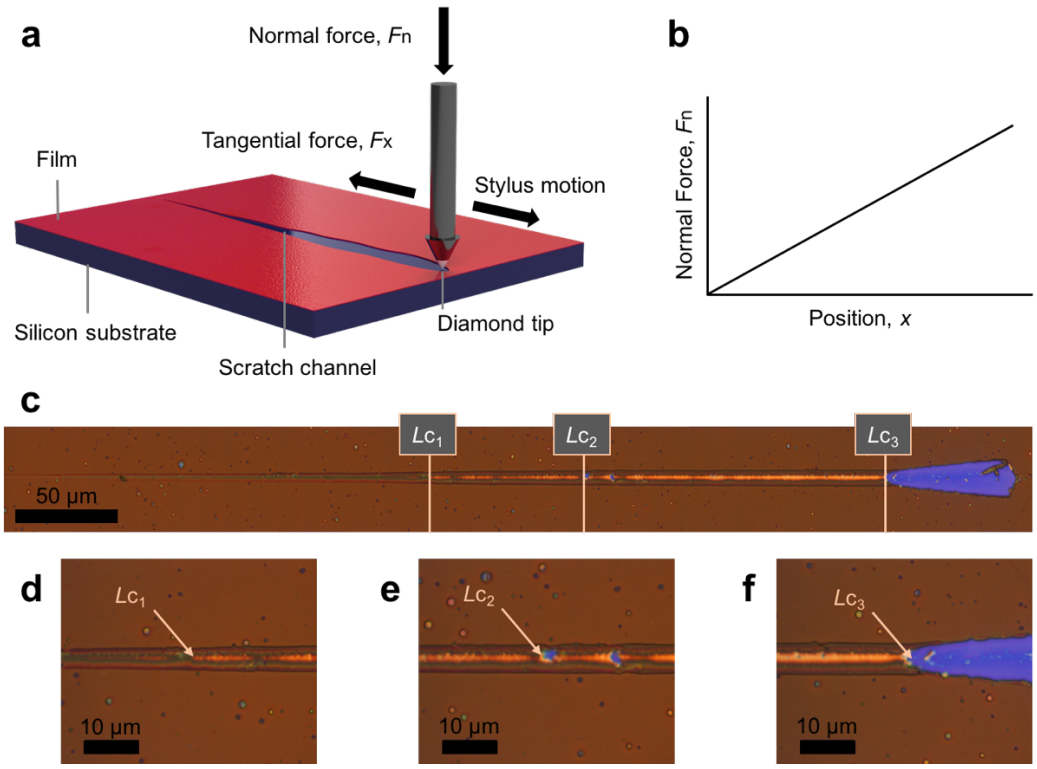

Figure 4.2. Scratch testing of thin films and coatings. (a) Schematic representation of a typical setup for scratch testing. (b) Profile of force versus position for a progressive-load scratch test. (c) Image of a scratch channel labeled with locations of critical failure, Lc_1, Lc_2, and Lc_3. (d) Magnified images of Lc_1, (e) Lc_2, and (f) Lc_3.

4.2 Results and Discussion

Results from the scratch testing of P3ATs, **Figure 4.3a**, show a decrease in cohesion as a function of the length of the alkyl side chain n (probability value (P) ≤ 0.001 between $n = 6$ and 10). The effect of n on the mechanical properties of thin films of P3ATs was previously examined both experimentally[25] and computationally:[26] the ductility increases, whereas the elastic modulus decreases, as a function of n. This effect was a manifestation of the glass transition temperature, T_g, changing from near room temperature to well below it as n changed from 6 to 7.[25] The decrease in the T_g is a result of increased free volume in the polymer film with increasing n. Since van der Waals forces are dependent on the inverse sixth power of interchain distance, small changes in separation between the main chains (decreased density) will produce large decreases in the

intermolecular forces and decreased cohesion.[27] To examine the effect of increasing *n* on aggregation behavior, which is known to influence mechanical properties,[28] we obtained UV-vis spectra. We found that an increase in *n* corresponded to a decrease in the conjugation length and the fraction of aggregates in the films, as determined using the weakly interacting H-aggregate model[29–31] (**Figure D.2** and **Table D.1**). Decreased adhesion of P3ATs with increasing *n*, ($P \leq 0.01$ between $n = 6$ and 10) as shown in **Figure 4.3b**, is also consistent with reduced density (the Hamaker constant, which characterizes the adhesion between solids, is proportional to density). A prior study has shown that the surface energy of P3AT thin films decreased with *n*, as measured by an increase in water contact angle.[25]

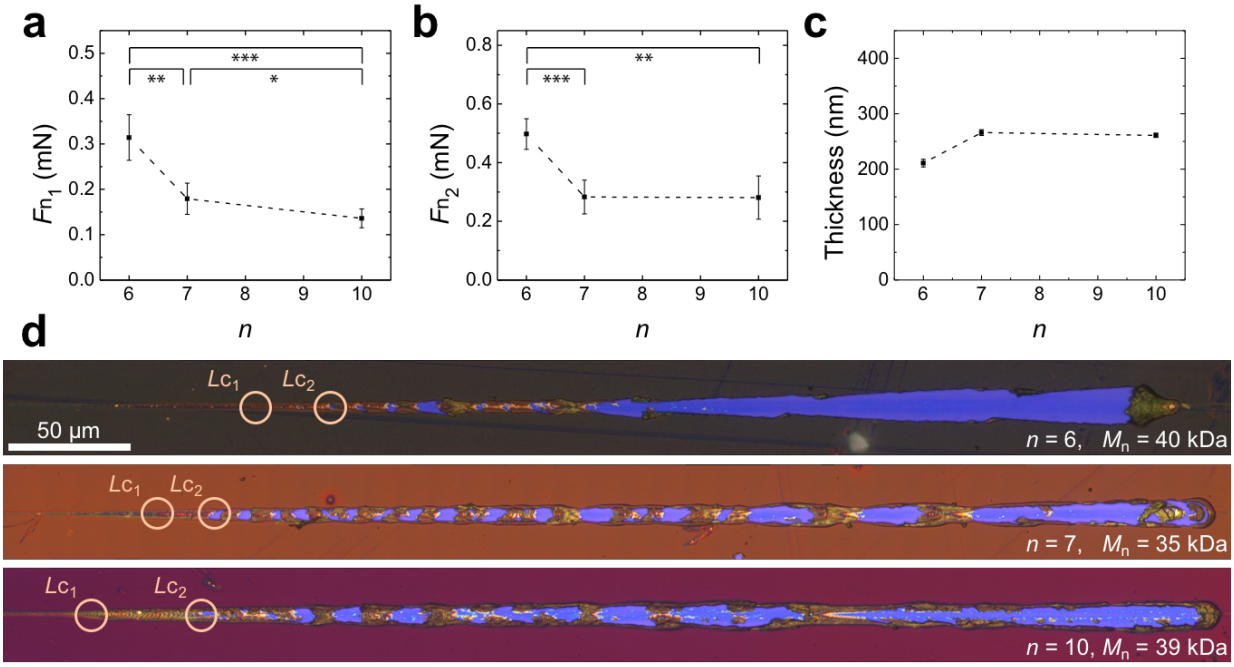

Figure 4.3. Results from scratch testing of P3ATs as a function of the length of the side chain *n*. (a, b,) Normal forces recorded at each critical location, Lc_i. Data points represent means ± s.d. ($i = 5$). *$P \leq 0.05$, **$P \leq 0.01$, ***$P \leq 0.001$, ****$P \leq 0.0001$. (c) Thickness measurements of each film under study. (d) Scratch channel images of each P3AT tested. Color variation in the samples arise from changes in *n* which affect the optical behavior of the films.

The normal forces recorded at the beginning of gross delamination (Fn_3) did not exhibit a clearly observable trend and contained a considerable amount of error. The error was due to ambiguity in the labeling of Fn_3 for $n = 7$ and 10. Therefore, we did not consider measurements of Fn_3 in our analysis. Upon visual inspection, however, it appears that films of $n = 7$ and 10 exhibit lower adhesive strength than $n = 6$ (the films fail adhesively further to the left). **Figure 4.3c** plots the thickness of each film as a function of n. **Figure 4.3d** shows the scratch channel for each of the P3ATs tested as a function of n. The images qualitatively show a decrease in the normal force required to induce failure by observing that the initiation of Lc_1 and Lc_2 occurred earlier in the scratch test (Fn_i increased linearly).

It is well known that the molecular weight of conjugated polymers strongly influence the density of entanglements and therefore the mechanical properties.[20,22] We thus performed scratch tests on P3HT having a range of M_n. The results show an increase in the cohesion as a function of M_n, **Figure 4.4a**. ($P \leq 0.0001$ between $M_n = 15$ and 80 kDa). By way of comparison, critical forces measured for the P3HT (80 kDa) sample correspond to the following data obtained by tensile testing: modulus, 0.27 GPa; toughness, 13.17 MJ m^{-3}; tensile strength, 17.1 MPa, **Table 4.1**.[20] For regioregular P3HT, increases in M_n lead to physical linking of polymer chains (entanglements) and tie molecules that traverse multiple crystallites, which increase the connectivity between chains.[32] This effect is magnified once the polymer length exceeds the entanglement molecular weight. It thus has a direct impact on the cohesive strength of conjugated polymers as it raises the energy required for chain disentanglement and chain pullout.[11] Similar results showing an increase in the cohesive strength of P3HT:fullerene bulk heterojunction films as a function of M_n, have been reported.[11] Additionally, prior studies have shown that extensibility and toughness increase with increasing molecular weight of P3HT, Table 4.1.[20,22]

Table 4.1. Tabulated values of the mechanical properties of P3HT in a range of molecular weights as determined by tensile testing. The tests were conducted in a prior study.[20]

Mechanical Properties of P3HT

M_n (kDa)	Tensile modulus (GPa)	Strain at fracture (%)	Toughness (MJ/m^3)	Tensile strength (MPa)
15	0.203 ± 0.014	4.5 ± 0.3	0.14 ± 0.01	4.5 ± 0.3
40	0.263 ± 0.015	13.0 ± 1.2	0.99 ± 0.08	10.5 ± 0.5
63	0.261 ± 0.020	58.7 ± 6.5	6.80 ± 0.78	12.6 ± 0.2
80	0.270 ± 0.012	95.6 ± 7.7	13.17 ± 0.97	17.1 ± 0.6

It has been hypothesized that the M_n of a polymer may have a significant impact on the adhesion of the material to a substrate.[33] Our results support this premise as the adhesion of P3HT increased as a function of M_n, shown in **Figure 4.4b, 4.4c.** ($P \leq 0.0001$ between M_n = 15 and 80 kDa). Since the thickness of the samples was held relatively constant, **Figure 4.4d**, thickness dependence may be eliminated as the dominating factor for the observed increase in Fn_2 and Fn_3. The increase in adhesion may be explained, in part, by the presence of a "liquid-like" skin layer near the free surfaces of the polymer films which dissipates stress. In this region, the polymer chains are highly mobile and less entangled than the bulk. To simulate the number of entanglements as they vary with the Z-height of a thin film we performed coarse-grained molecular dynamics using a well-established model for P3HT that contains three coarse-grained sites per monomer,[34] **Figure 4.4e**. The number of entanglements is estimated from the intersections of the primitive paths of the polymer chains, i.e., the number of interior kinks per chain.[26] The results show that for a 40 nm thin film of P3HT (300 repeat units), the density of entanglements is initially low and then increases sharply 5 nm into the film (on both the top and bottom surfaces). For sufficiently thin films, the skin layer has a thickness on the same order of magnitude as the length of individual polymer chains. Using the same model, the predicted trend for the RMS radius of

gyration $\langle R_g^2 \rangle^{1/2}$ and RMS end-to-end distance $\langle E2E^2 \rangle^{1/2}$ as a function of the average number of repeat units in the polymer chain $\langle m \rangle$ is shown in **Figure 4.4f**. Our results suggest that—for a film thickness of 120 nm—the skin region comprises approximately 10% of the total film thickness for P3HT with low M_n and approximately 30% of the total film thickness for P3HT with high M_n. For high M_n polymers, it can be expected that the larger volume of the skin layer will lead to a greater capacity to dissipate mechanical energy during the adhesive failure process, resulting in increased adhesion.

It should also be noted that all the results from scratch testing involve some level of cooperativity between cohesive strength and adhesion. During a scratch test, for a film to fail adhesively, it must first fail cohesively by cracking through the thickness of the film. The initiation and propagation of such a crack will lead to early adhesive failure by gross delamination, as seen in the low M_n P3HT film, **Figure 4.4g**. In high M_n samples, however, ductility increases and crack propagation is hindered by the plastic dissipation zone, a region near the crack tip that dissipates energy through plastic deformation.[35] It is then reasonable to assume that any observed increase in adhesion (Fn_3 and Lc_3) is partly a consequence of the increased cohesive strength of P3HT films with greater M_n, and their ability to dissipate mechanical energy.

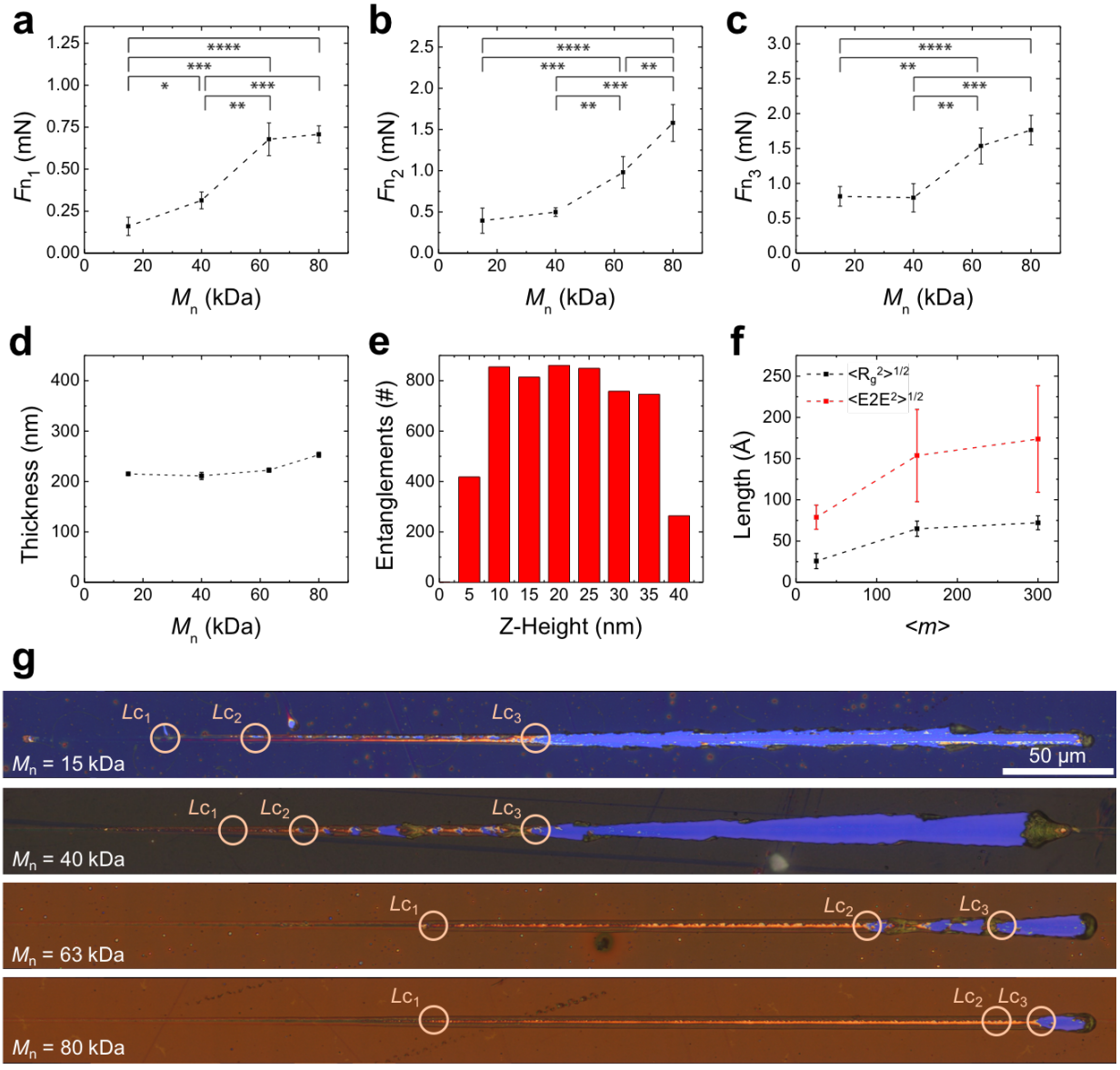

Figure 4.4. Scratch testing results for P3HT as a function of M_n. (a, b, c) Normal forces recorded at each critical location, Lc_i. Data points represent means ± s.d. (i = 5). *P ≤ 0.05, **P ≤ 0.01, ***P ≤ 0.001, ****P ≤ 0.0001. (d) Thickness measurements of each M_n tested. (e) Coarse-grained molecular dynamics estimation of the number of "entanglements"—calculated as the number of interior kinks per chain[26]—as a function of Z-height in a 40 nm P3HT thin film (300 repeat units). (f) Coarse-grained molecular dynamics predictions of the RMS radius of gyration (<R_g^2>$^{1/2}$) and the RMS end-to-end distance (<$E2E^2$>$^{1/2}$) for three representative chain lengths. (g) Scratch channel images of each M_n tested. Color differences between the samples arise from changes in aggregation behavior with increasing M_n which affect the optical behavior of the films, see Figure D.2 and Table D.1.

Figure 4.5a and **4.5b** plot the normal force associated with cohesion and adhesion as a function of the average number of repeat units <m>. We chose <m> for our analysis, as opposed

to M_n, since two polymers of the same M_n may have different degrees of polymerization, depending on the mass of the monomer (i.e., P3HT vs P3DT). Interestingly, there is a linear correlation between <*m*> and the forces required for failure for all polymers above the entanglement molecular weight, regardless of *n*. We note that one data point was excluded, P3HT (M_n = 15 kDa), since this sample was below the entanglement molecular weight. In P3ATs, the length of the side chain seems to play a secondary role to the length of the main chain once the entanglement molecular weight has been surpassed. This is a seemingly desirable result since the charge-carrier mobility of P3HT generally improves with increasing M_n and plateaus once the entanglement M_n is surpassed.[36] The increase in electronic performance arises from favorable changes in morphology in the films. At low M_n, the polymer chains exist as non-interconnected chain extended crystals and charge transport is hindered by grain boundaries that create energetic trap states.[22] At high M_n the polymer chains exhibit a larger degree of self-folding and tie molecules that connect crystalline regions of the polymer film; this morphology results in improved charge transport.[21,22,36,37]

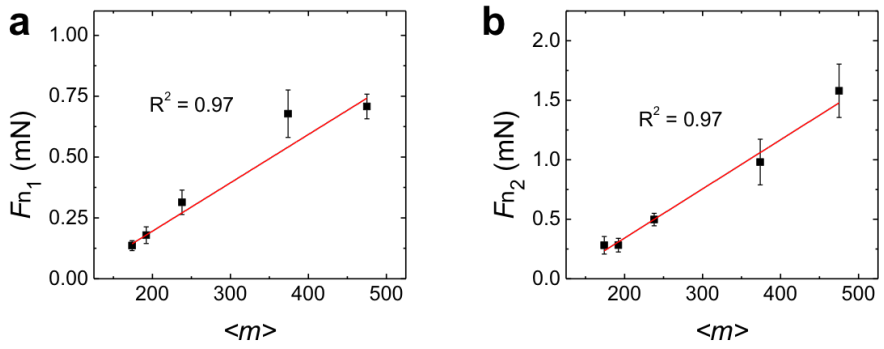

Figure 4.5. Plots showing the linear relationship between average degree of polymerization <*m*> and the force required for failure. (a) Fn_1 and (b) Fn_2 versus <*m*>.

4.3 Conclusions

These results suggest that progressive-load scratch testing has considerable value in measuring the cohesion and adhesion of conjugated polymers. In particular, measurements of

P3ATs as a function of the length of the side chain *n* and P3HT in a range of M_n have shown that cohesion and adhesion decreased as a function of *n* for P3ATs and increased with M_n for P3HT. When the results are plotted as a function of repeat units <*m*>, for all polymers above the entanglement molecular weight, we observed a linear relationship between <*m*> and the associated normal forces of failure. This work demonstrates the practicality of scratch testing as a method of characterizing the cohesive and adhesive behavior of organic semiconductors. Our findings could inform the design of conjugated polymers that exhibit greater mechanical reliability in organic electronic devices.

Supporting Information

Experimental methods, UV-vis absorption spectra, H-aggregate analysis, and AFM images of a scratch channel.

Acknowledgements

This research was supported primarily by the Air Force Office of Scientific Research (AFOSR) grant number FA9550-16-1-0220. D.R. and J.R. acknowledge support provided by the National Science Foundation Graduate Research Fellowship Program under Grant No. DGE-1144086. Computational resources to support this work were provided by the Extreme Science and Engineering Discovery Environment (XSEDE) Program through the National Science Foundation grant number ACI-1053575.

References

(1) Kim, T.; Kim, J.-H.; Kang, T. E.; Lee, C.; Kang, H.; Shin, M.; Wang, C.; Ma, B.; Jeong, U.; Kim, T.-S.; Kim, B. J. Flexible, Highly Efficient All-Polymer Solar Cells. *Nat.*

Commun. **2015**, *6* (May), 8547.

(2) Jean, J.; Wang, A.; Bulović, V. In Situ Vapor-Deposited Parylene Substrates for Ultra-Thin, Lightweight Organic Solar Cells. *Org. Electron. physics, Mater. Appl.* **2016**, *31*, 120–126.

(3) Young Oh, J.; Rondeau-Gagné, S.; Chiu, Y.-C.; Chortos, A.; Lissel, F.; Nathan Wang, G.-J.; Schroeder, B. C.; Kurosawa, T.; Lopez, J.; Katsumata, T.; Xu, J.; Zhu, C.; Gu, X.; Bae, W.-G.; Kim, Y.; Jin, L.; Won Chung, J.; B-H Tok, J.; Bao, Z. Intrinsically Stretchable and Healable Semiconducting Polymer for Organic Transistors. *Nat. Publ. Gr.* **2016**, *539* (7629), 411–415.

(4) Kaltenbrunner, M.; Sekitani, T.; Reeder, J.; Yokota, T.; Kuribara, K.; Tokuhara, T.; Drack, M.; Schwödiauer, R.; Graz, I.; Bauer-Gogonea, S.; Bauer, S.; Someya, T. An Ultra-Lightweight Design for Imperceptible Plastic Electronics. *Nature* **2013**, *499* (7459), 458–463.

(5) Roh, E.; Hwang, B.; Kim, D.; Kim, B.; Lee, N. Stretchable, Transparent, Ultrasensitive, and Patchable Strain Sensor for Human - Machine Interfaces Comprising a Nanohybrid of Carbon Sensor and Conductive Elastomers. *ACS Nano* **2015**, *9* (6), 6252–6261.

(6) Bihar, E.; Roberts, T.; Ismailova, E.; Saadaoui, M.; Isik, M.; Sanchez-Sanchez, A.; Mecerreyes, D.; Hervé, T.; De Graaf, J. B.; Malliaras, G. G. Fully Printed Electrodes on Stretchable Textiles for Long-Term Electrophysiology. *Adv. Mater. Technol.* **2017**, 1600251.

(7) Lim, S.; Son, D.; Kim, J.; Lee, Y. B.; Song, J. K.; Choi, S.; Lee, D. J.; Kim, J. H.; Lee, M.; Hyeon, T.; Kim, D. H. Transparent and Stretchable Interactive Human Machine Interface Based on Patterned Graphene Heterostructures. *Adv. Funct. Mater.* **2015**, *25* (3), 375–383.

(8) Huang, J.; Wang, H.; Yan, K.; Zhang, X.; Chen, H.; Li, C. Z.; Yu, J. Highly Efficient Organic Solar Cells Consisting of Double Bulk Heterojunction Layers. *Adv. Mater.* **2017**, *29* (19), 1–9.

(9) Liu, J.; Dong, H.; Wang, Z.; Ji, D.; Cheng, C.; Geng, H.; Zhang, H.; Zhen, Y.; Jiang, L.; Fu, H.; Bo, Z.; Chen, W.; Shuai, Z.; Hu, W. Thin Film Field-Effect Transistors of 2,6-Diphenyl Anthracene (DPA). *Chem. Commun.* **2015**, *51* (59), 11777–11779.

(10) Root, S. E.; Savagatrup, S.; Printz, A. D.; Rodriquez, D.; Lipomi, D. J. Mechanical Properties of Organic Semiconductors for Stretchable, Highly Flexible, and Mechanically Robust Electronics. *Chem. Rev.* **2017**, *117* (9), 6467–6499.

(11) Bruner, C.; Dauskardt, R. Role of Molecular Weight on the Mechanical Device Properties of Organic Polymer Solar Cells. *Macromolecules* **2014**, *47*, 1117–1121.

(12) Dupont, S. R.; Oliver, M.; Krebs, F. C.; Dauskardt, R. H. Interlayer Adhesion in Roll-to-Roll Processed Flexible Inverted Polymer Solar Cells. *Sol. Energy Mater. Sol. Cells* **2012**,

97, 171–175.

(13) Finn, M.; Martens, C. J.; Zaretski, A. V.; Roth, B.; Søndergaard, R. R.; Krebs, F. C.; Lipomi, D. J. Mechanical Stability of Roll-to-Roll Printed Solar Cells under Cyclic Bending and Torsion. *Sol. Energy Mater. Sol. Cells* **2017**, *174* (June 2017), 7–15.

(14) Brand, V.; Bruner, C.; Dauskardt, R. H. Cohesion and Device Reliability in Organic Bulk Heterojunction Photovoltaic Cells. *Sol. Energy Mater. Sol. Cells* **2012**, *99*, 182–189.

(15) Benjamin, P.; Weaver, C. Measurement of Adhesion of Thin Films. *Proc. R. Soc. London A Math. Phys. Eng. Sci.* **1960**, *254* (1277), 163–176.

(16) Schwarzer, N. Completely Analytical Tools for the Next Generation of Surface and Coating Optimization. *Coatings* **2014**, *4* (2), 253–281.

(17) Kohl, J. G.; Singer, I. L.; Schwarzer, N.; Yu, V. Y. Effect of Bond Coat Modulus on the Durability of Silicone Duplex Coatings. *Prog. Org. Coatings* **2006**, *56* (2–3), 220–226.

(18) Tomastik, J.; Ctvrtlik, R. Nanoscratch Test — A Tool for Evaluation of Cohesive and Adhesive Properties of Thin Films and Coatings. *EPJ Web Conf.* **2013**, *48*, 00027.

(19) Kleinschmidt, A. T.; Root, S. E.; Lipomi, D. J. Poly(3-Hexylthiophene) (P3HT): Fruit Fly or Outlier in Organic Solar Cell Research? *J. Mater. Chem. A* **2016**, *00* (c), 1–5.

(20) Rodriquez, D.; Kim, J.-H.; Root, S. E.; Fei, Z.; Boufflet, P.; Heeney, M.; Kim, T.-S.; Lipomi, D. J. Comparison of Methods for Determining the Mechanical Properties of Semiconducting Polymer Films for Stretchable Electronics. *ACS Appl. Mater. Interfaces* **2017**, *9* (10), 8855–8862.

(21) Kline, R. J.; McGehee, M. D.; Kadnikova, E. N.; Liu, J.; Frechet, J. M. J. Controlling the Field-Effect Mobility of Regioregular Polythiophene by Changing the Molecular Weight. *Adv. Mater.* **2003**, *15* (18), 1519–1522.

(22) Koch, F. P. V.; Rivnay, J.; Foster, S.; Müller, C.; Downing, J. M.; Buchaca-Domingo, E.; Westacott, P.; Yu, L.; Yuan, M.; Baklar, M.; Fei, Z.; Luscombe, C.; McLachlan, M. A.; Heeney, M.; Rumbles, G.; Silva, C.; Salleo, A.; Nelson, J.; Smith, P.; Stingelin, N. The Impact of Molecular Weight on Microstructure and Charge Transport in Semicrystalline Polymer Semiconductors-Poly(3-Hexylthiophene), a Model Study. *Prog. Polym. Sci.* **2013**, *38* (12), 1978–1989.

(23) Sekler, J.; Steinmann, P. A.; Hintermann, H. E. The Scratch Test: Different Critical Load Determination Techniques. *Surf. Coatings Technol.* **1988**, *36* (1–2), 519–529.

(24) Kohl, J. G.; Randall, N. X.; Schwarzer, N.; Ngo, T. T.; Shockley, M. J.; Nair, R. P. An Investigation of Scratch Testing of Silicone Elastomer Coatings with a Thickness Gradient. *J. Appl. Polym. Sci.* **2011**, *124*, 2978–2986.

(25) Savagatrup, S.; Makaram, A. S.; Burke, D. J.; Lipomi, D. J. Mechanical Properties of

Conjugated Polymers and Polymer-Fullerene Composites as a Function of Molecular Structure. *Adv. Funct. Mater.* **2014**, *24* (8), 1169–1181.

(26) Root, S. E.; Savagatrup, S.; Pais, C. J.; Arya, G.; Lipomi, D. J. Predicting the Mechanical Properties of Organic Semiconductors Using Coarse-Grained Molecular Dynamics Simulations. *Macromolecules* **2016**, *49* (7), 2886–2894.

(27) Jenekhe, S. A.; Roberts, M. F. Effects of Intermolecular Forces on the Glass Transition of Polymers. *Macromolecules* **1993**, *26* (18), 4981–4983.

(28) Awartani, O.; Lemanski, B. I.; Ro, H. W.; Richter, L. J.; DeLongchamp, D. M.; O'Connor, B. T. Correlating Stiffness, Ductility, and Morphology of Polymer:Fullerene Films for Solar Cell Applications. *Adv. Energy Mater.* **2013**, *3* (3), 399–406.

(29) Clark, J.; Chang, J. F.; Spano, F. C.; Friend, R. H.; Silva, C. Determining Exciton Bandwidth and Film Microstructure in Polythiophene Films Using Linear Absorption Spectroscopy. *Appl. Phys. Lett.* **2009**, *94* (16), 2007–2010.

(30) Siddiqui, S.; Spano, F. C. H- and J-Aggregates of Conjugated Polymers and Oligomers. *Chem. Phys. Lett.* **1999**, *308* (1–2), 99–105.

(31) Spano, F. C. Modeling Disorder in Polymer Aggregates: The Optical Spectroscopy of Regioregular Poly(3-Hexylthiophene) Thin Films. *J. Chem. Phys.* **2005**, *122* (23).

(32) Brinkmann, M.; Rannou, P. Molecular Weight Dependence of Chain Packing and Semicrystalline Structure in Oriented Films of Regioregular Poly(3-Hexylthiophene) Revealed by High-Resolution Transmission Electron Microscopy. *Macromolecules* **2009**, *42* (4), 1125–1130.

(33) Choi, G. Y.; Zurawsky, W.; Ulman, A. Molecular Weight Effects in Adhesion. *Langmuir* **1999**, *15* (24), 8447–8450.

(34) Huang, D. M.; Faller, R.; Do, K.; Moul, A. J. Coarse-Grained Computer Simulations of Polymer / Fullerene Bulk Heterojunctions for Organic Photovoltaic Applications. *J. Chem. Theory Comput.* **2010**, *6*, 526–537.

(35) Alkhadra, M. A.; Root, S. E.; Hilby, K. M.; Rodriquez, D.; Sugiyama, F.; Lipomi, D. J. Quantifying the Fracture Behavior of Brittle and Ductile Thin Films of Semiconducting Polymers. *Chem. Mater.* **2017**, *29*, 10139–10149.

(36) Noriega, R.; Rivnay, J.; Vandewal, K.; Koch, F. P. V; Stingelin, N.; Smith, P.; Toney, M. F.; Salleo, A. A General Relationship between Disorder, Aggregation and Charge Transport in Conjugated Polymers. *Nat. Mater.* **2013**, *12* (11), 1038–1044.

(37) Kline, R. J.; Mcgehee, M. D.; Kadnikova, E. N.; Liu, J.; Frechet, J. M. J.; Toney, M. F. The Dependence of Regioregular Poly (3-Hexylthiophene) Film Morphology and Field-Effect Mobility on Molecular Weight. *Macromolecules* **2004**, *38* (December), 3312–3319.

Appendix A

Supporting Information for Chapter 1

[70]PCBM and incompletely separated grades of methanofullerenes produce bulk heterojunctions with increased robustness for ultra-flexible and stretchable electronics

Suchol Savagatrup,[a] Daniel Rodriquez,[a] Adam D. Printz,[a] Alexander B. Sieval,[b] Jan C. Hummelen,[b,c] and Darren J. Lipomi[a]

[a] *Department of NanoEngineering, University of California, San Diego, 9500 Gilman Drive Mail Code 0448, La Jolla, CA 92093-0448.*

[b] *Solenne BV, Zernikepark 6-8, 9747 AN Groningen, Netherlands*

[c] *Stratingh Institute for Chemistry and Zernike Institute for Advanced Materials, University of Groningen, Nijenborgh 4, 9747 AG Groningen, Netherlands*

A.1 UV-vis absorption of P3HT:methanofullerene films on different substrates

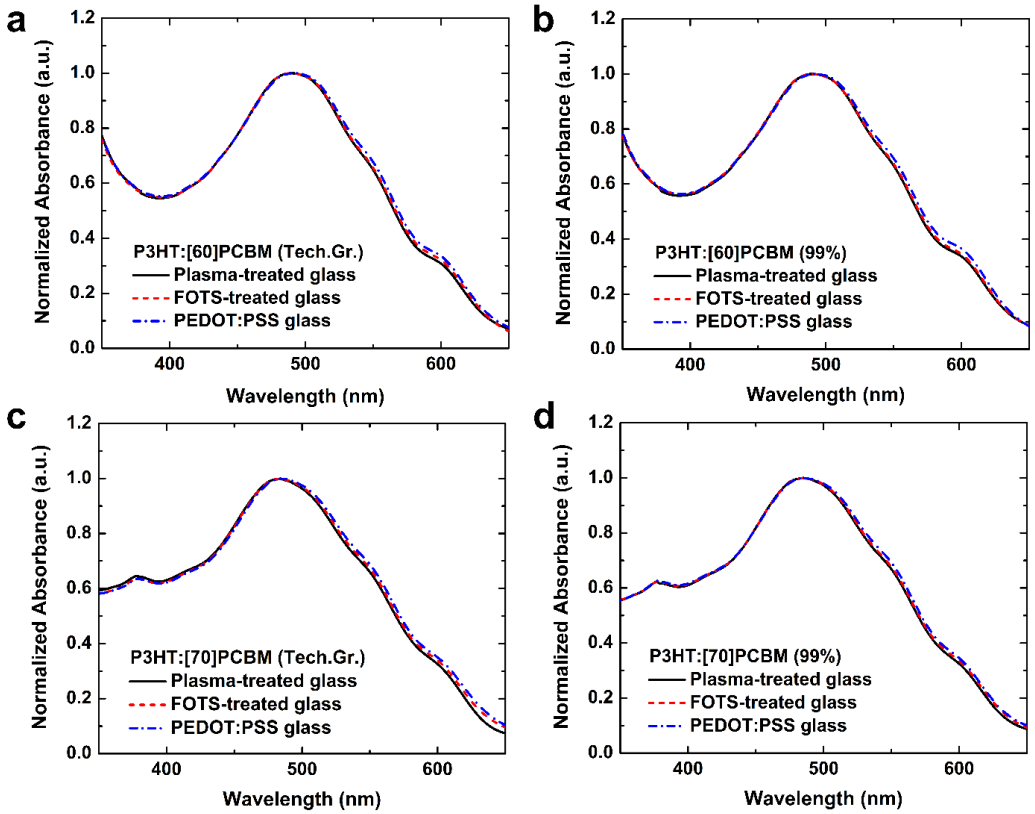

Figure A.1 UV-vis absorption of P3HT:methanofullerene thin films (~150 nm) on plasma-treated glass, FOTS-treated glass, and PEDOT:PSS films. The spin-coating parameters and solution concentration were kept constant through-out all samples. The complete overlaps observed in the normalized absorbance suggest that the differences in the microstructure resulted in these films are minimal.

A.2 Photovoltaic characteristic of P3HT:methanofullerenes with 1:1 mixture of [60]PCBM and [70]PCBM

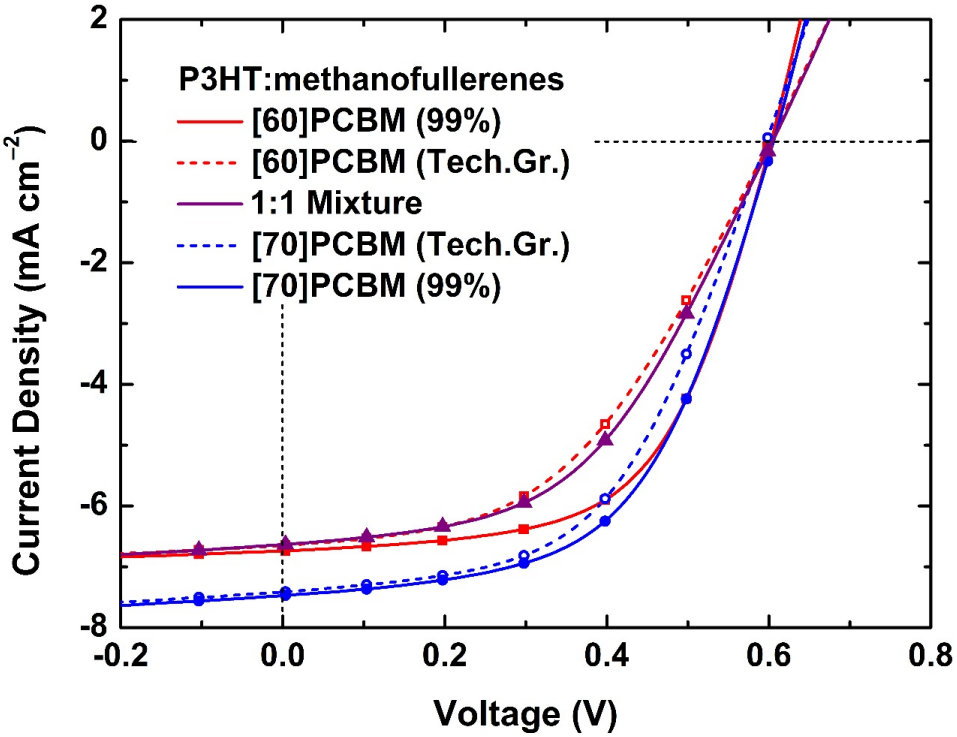

Figure A.2. Photovoltaic characteristic of averaged devices (N ≥ 8) with an active layer of 1:1 blend of P3HT and respective methanofullerenes. The architecture of the devices was PEDOT:PSS/P3HT:methanofullerene/EGaIn.

Table A.1. Summary of the photovoltaic figures of merit for P3HT:methanofullerene solar cells fabricated in this work (N ≥ 8) [†]

Device	V_{OC} (mV)	J_{SC} (mA cm^{-2})	*FF* (%)	*PCE* (%)
P3HT:[60]PCBM (99%)	602 ± 5.5	6.74 ± 0.2	59 ± 3.0	2.36 ± 0.2
P3HT:[60]PCBM (Tech. Gr.)	602 ± 3.7	6.60 ± 0.4	48 ± 4.8	1.89 ± 0.2
P3HT: 1:1 Mixture	605 ± 1.6	6.63 ± 0.5	50 ± 3.4	1.98 ± 0.1
P3HT:[70]PCBM (Tech. Gr.)	598 ± 11.2	7.41 ± 0.3	53 ± 1.7	2.35 ± 0.1
P3HT:[70]PCBM (99%)	606 ± 7.5	7.47 ± 0.4	55 ± 1.3	2.48 ± 0.1

[†]The solar cell device architecture was PEDOT:PSS/P3HT:methanofullerene/EGaIn. PEDOT:PSS, doped with 7% DMSO and 0.1% Zonyl, was spin-coated to create a layer of ~150 nm thick. The active layer was spin-coated from a solution of 1:1 P3HT:methanofullerene in ODCB (40 mg mL^{-1}) and thermally annealed at 125 °C in an inert atmosphere. EGaIn droplets were extruded to create the active area of ~0.02 cm^{-2}.

A.3. Buckling methodology

To measure the tensile moduli of the pure fullerene films, we tested the bilayer systems comprising a layer of PEDOT:PSS with known tensile modulus and a layer of pure fullerene film with unknown modulus. We obtained the characteristic buckling wavelengths for different thicknesses of the bilayer systems, while keeping the thickness ratio of the PEDOT:PSS and the fullerene film constant. The examples of the optical micrograph of the buckles are shown in Figure A.3. The buckling wavelengths were then plotted against the overall thickness of the bilayer system as shown in Figure A.4. The effective modulus of the bilayer (E_{eff}) was then calculated using equation 1:

$$E_{\text{eff}} = 3E_{\text{s}}\left(\frac{1-\upsilon_{\text{f}}^2}{1-\upsilon_{\text{s}}^2}\right)\left(\frac{\lambda_{\text{b}}}{2\pi d_{\text{f}}}\right)^3 \quad (\mathbf{1})$$

Where the fitted slope from Figure A.4 is used as the ratio between buckling wavelength, λ_{b}, and the thickness of the film, d_{f}; E_{s} is the tensile modulus of the PDMS substrate; the Poisson's ratios of the bilayer and the substrate, υ_{f} and υ_{s}, were 0.35 and 0.5, respectively.

From the known modulus of the PEDOT:PSS films ($E_{\text{f,1}}$) and the effective modulus of the bilayer (E_{eff}), we used equation 2 to calculated the modulus of the pure fullerene film ($E_{\text{f,2}}$). In all of our experiment, the ratio between the thickness of the PEDOT:PSS and the pure fullerene films were kept constant at 1. The examples of the curve of equation 2 are shown in Figure A.5. The output, the modulus of the pure fullerene film, are plotted against the modulus of the bilayer system for different values of the PEDOT:PSS. In our experiment, the modulus of the PEDOT:PSS was kept constant at 3 GPa.

$$E_{\text{eff}} = \frac{1+m^2n^4+2mn(2n^2+3n+2)}{(1+n)^3(1+mn)}E_{\text{f,1}};\ \text{where}\ m=\frac{E_{\text{f,2}}}{E_{\text{f,1}}},\ n=\frac{d_{\text{f,2}}}{d_{\text{f,1}}} \quad (\mathbf{2})$$

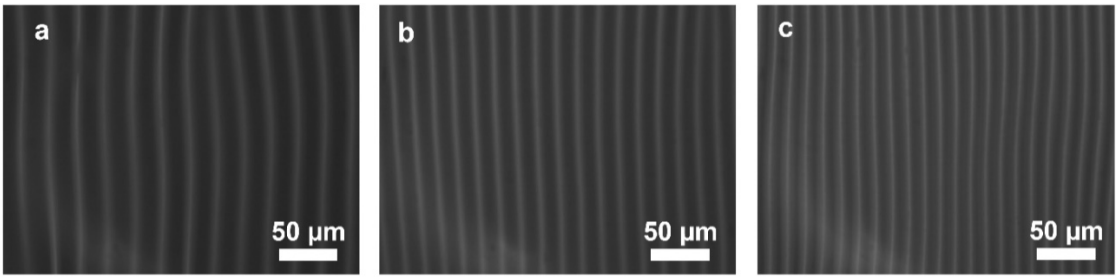

Figure A.3. Examples of the optical micrograph of the buckles obtained from the bilayer systems comprising PEDOT:PSS and pure fullerene films at different thicknesses.

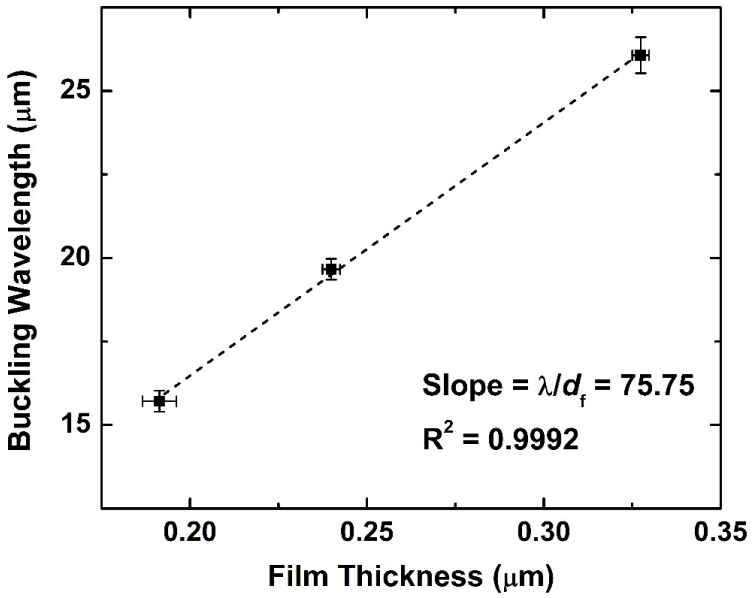

Figure A.4. An example of buckling wavelength vs. film thickness plot for a bilayer system. The slope of the fitted linear line was used as the ratio of the buckling wavelength and film thickness in equation 1.

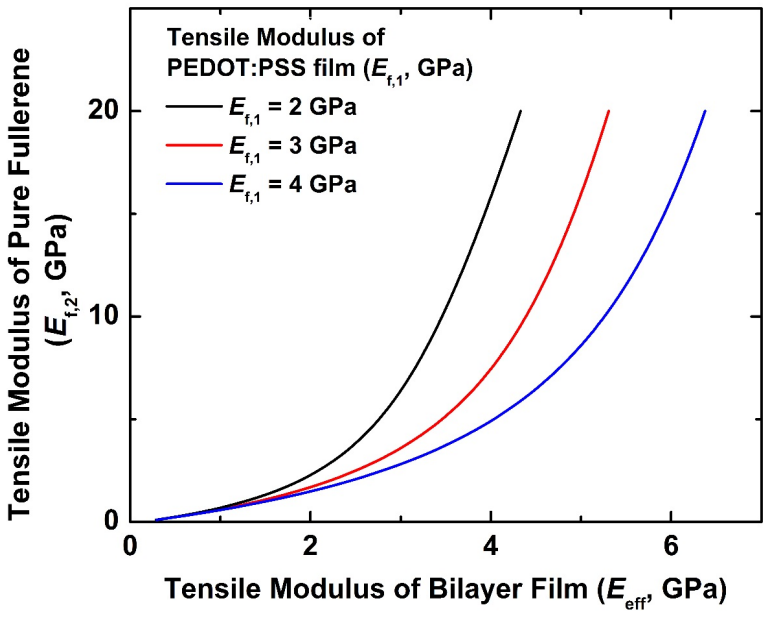

Figure A.5. Plot of the output tensile modulus of the pure fullerene films vs. the obtained tensile modulus of the bilayer films (PEDOT:PSS and pure fullerene) when the ratio of the thickness of the PEDOT:PSS and the pure fullerene film is kept constant at 1.

Appendix B

Supporting Information for Chapter 2

Mechanical Properties of Solution-Processed Small-Molecule Semiconductor Films

Daniel Rodriquez,[1] Suchol Savagatrup,[1] Eduardo Valle,[1] Christopher M. Proctor[2], Caitlin McDowell,[2] Guillermo C. Bazan,[2] Thuc-Quyen Nguyen,[2] and Darren J. Lipomi[1]*

[1]*Department of NanoEngineering, University of California, San Diego*

9500 Gilman Drive, Mail Code 0448, La Jolla, CA 92093-0448

[2]*Center for Polymers and Organic Solids, Department of Chemistry and Biochemistry,*

University of California Santa Barbara, CA 93106-9510

B.1 Photovoltaic properties of small-molecule BHJs with HPI-BT as the acceptor

Figure B.1 shows the performance of small-molecule BHJs with HPI-BT as the acceptor. We did not investigate the photovoltaic performance of these devices under strain because of their low PCE values. The most efficient solar cells, those containing $PC_{71}BM$ as the acceptor, were not measured under strain since they cracked at relatively low strains. Cracking leads to failure by disconnecting the active regions from the electrodes, shorting of the electrodes through the film, or both.

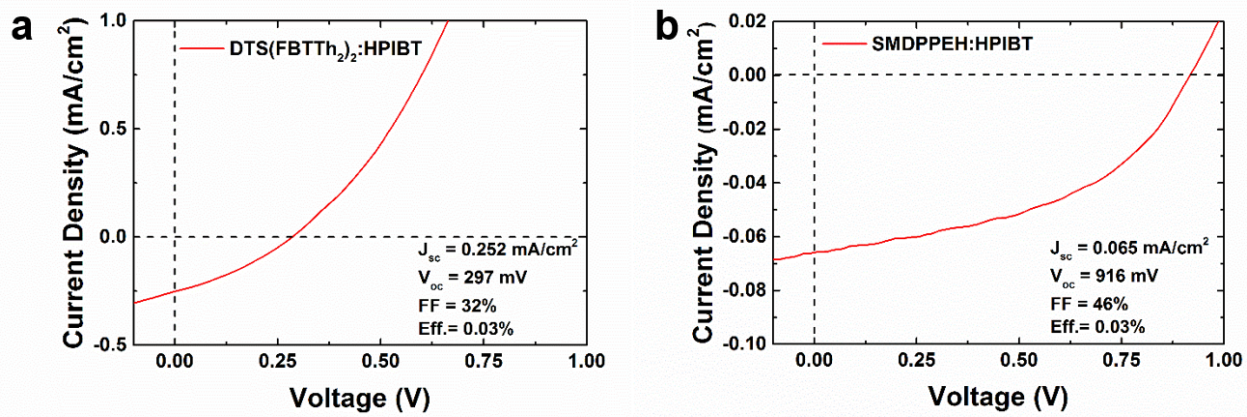

Figure B.1. Photovoltaic plots of (a) $DTS(FBTTh_2)_2$:HPI-BT and (b) SMDPPEH:HPIBT bulk heterojunction solar cells. The curves represent average values of $N = 3$ devices for both (a) and (b), the inset shows the values from the best performing solar cells.

B.2 Thermal properties of small-molecule semiconductors

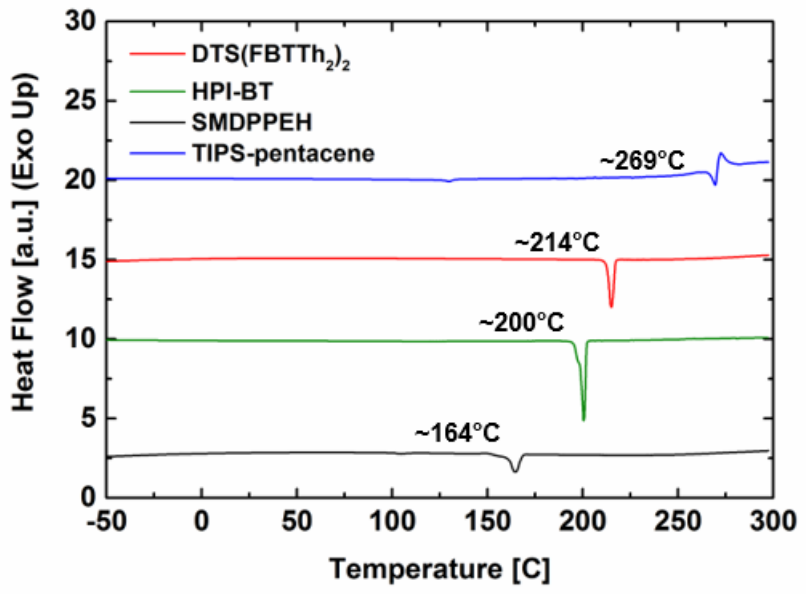

Figure B.2. DSC thermograms showing the melting temperature of DTS(FBTTh$_2$)$_2$, SMDPPEH, TIPS-pentacene, and HPI-BT.

B.3 Optoelectronic properties of small-molecule semiconductors

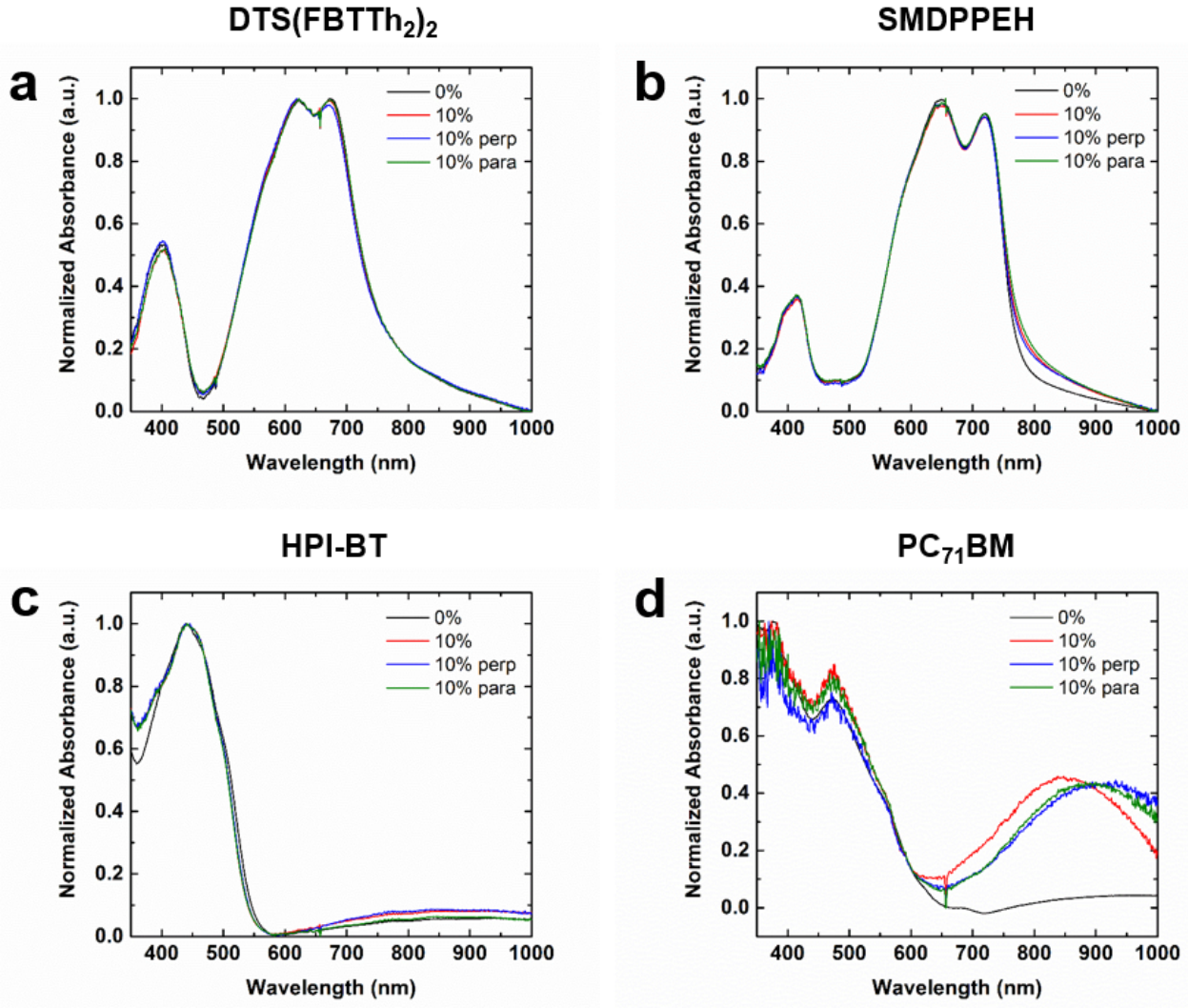

Figure B.3. Absorption spectra of as-cast pure (a) DTS(FBTTh$_2$)$_2$, (b) SMDPPEH, (c) HPI-BT, and (d) PC$_{71}$BM thin films. All films were analyzed on PDMS with a device architecture of PDMS/PEDOT:PSS/Film. Spectra was first collected from unstrained films and sequentially after being strained to 10% with no polarization and with polarization both perpendicular (perp) and parallel (para) to the axis of strain.

Appendix C

Supporting Information for Chapter 3

Comparison of Methods for Determining the Mechanical Properties of Semiconducting Polymer Films for Stretchable Electronics

Daniel Rodriquez,[1†] Jae-Han Kim,[2†] Samuel E. Root,[1] Zhuping Fei,[3] Pierre Boufflet,[3] Martin Heeney,[3] Taek-Soo Kim,*[,2] and Darren J. Lipomi*[,1]

(†These authors contributed equally.)

[1]Department of NanoEngineering, University of California, San Diego

9500 Gilman Drive, Mail Code 0448, La Jolla, CA 92093-0448

[2]Department of Mechanical Engineering, Korea Advanced Institute of Science and Technology (KAIST), Yuseong-gu, Daejeon 34141, Korea.

[3]Department of Chemistry and Centre for Plastic Electronics, Imperial College London, Exhibition Rd, London, SW7 2AZ, UK

C.1 Effect of modulus mismatch on crack-onset strain measurements

When conducting crack onset measurements of thin film materials, the mechanical properties of the underlying elastomeric substrate have a direct effect on the crack behavior. Both the elastic modulus and the adhesion of the thin films to the substrate must be considered. To illustrate the effects of the substrate on the crack behavior of the P3HT thin films we conducted a series of tests on PDMS and varied the curing ratio (5:1, 10:1, and 20:1). Our results indicate that as the elastomer becomes softer and more adhesive the films exhibit a lower crack onset and a higher crack density at the same applied strain. This is in part due to the growing mismatch in elastic modulus as the PDMS base:crosslinker ratio is increased. This suggests that matching the modulus of the substrate to the film under study is the best way to optimize the crack behavior in FOE methods. However, if the PDMS curing ratio is too low the adhesion is compromised and the thin films will not adhere to the substrate. Therefore, a balance between good adhesion and modulus matching must be achieved for the best results.

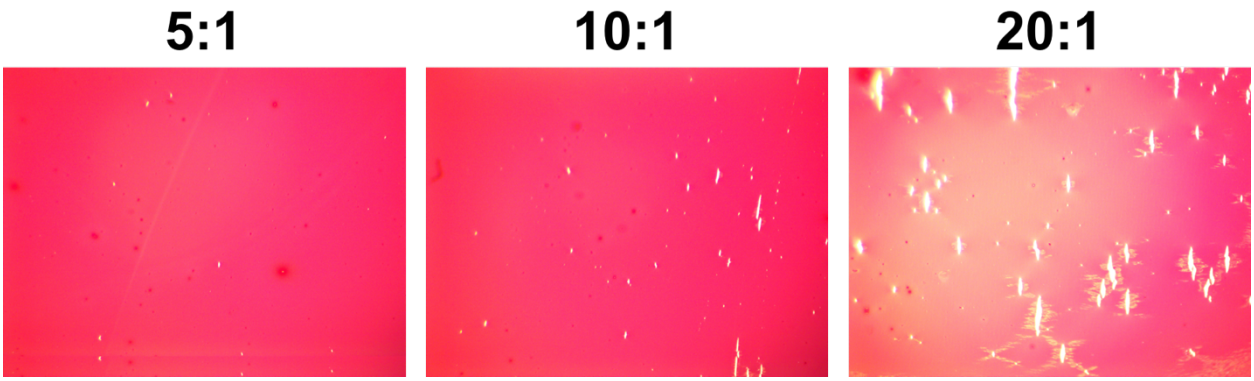

Figure C.1. Crack density at 20% strain of a 40 kDa P3HT sample on PDMS. The PDMS curing ratio was variable at 5:1, 10:1, and 20:1.

C.2 Experimental section:

C.2.1 Synthesis of materials.

Samples of regioregular poly(3-hexylthiophene) (P3HT) were synthesized according to the GRIM method.[1] The molecular weight was controlled by varying the amount of catalyst (dichloro[1,3-bis(diphenylphosphino)propane]nickel) added to the solution of freshly prepared Grignard reagent (prepared by the reaction of 2,5-dibromo-3-hexylthiophene and 0.98 equivalents of titrated isopropylmagnesium chloride lithium chloride complex solution (1.3M in THF). After catalyst addition, the reaction was refluxed for 4 h. After cooling to room temperature, the reaction mixture was poured into MeOH/HCl (4/1, v/v) mixture and filtered through a Soxhlet thimble. The polymer was extracted with methanol, acetone, hexane and chloroform. The chloroform solution was concentrated and reprecipitated into methanol. The precipitate was dried under vacuum to afford the final polymer. Number-average (M_n) and weight-average (M_w) molecular weights were determined by Agilent Technologies 1200 series GPC running in chlorobenzene at 80 °C, using two PL mixed B columns in series, and calibrated against narrow polydispersity polystyrene standards. The number average molecular weights of P3HTs are 15, 40, 63, and 80 $kgmol^{-1}$ with a dispersity (Đ) of 1.4, 1.7, 1.7 and 1.6, respectively. Regioregularity, as measured by integration of the methylene region of the 1H NMR was >95% in all cases.

C.2.2 Preparation of glass substrates.

Glass slides were cut into 2.54 cm squares with a diamond-tipped scribe. The slides were then successively washed in Alconox solution (2 mg mL^{-1}), deionized water, acetone, and isopropyl alcohol (IPA) in an ultrasonic bath for 10 min each and dried with compressed air. The glass slides were then plasma treated at ~30 W for 3 min at a pressure of 200 mTorr under ambient

air to remove any residual organic material and activate the surface. In the FOW method the glass slides were used after this step. For the FOE methods the glass slides were treated with ~100 μL of Tridecafluoro-1,1,2,2-tetrahydrooctyl)-1-trichlorosilane (FOTS) and placed under house vacuum for 3 h to passivate the surface. The surface was then thoroughly rinsed with IPA to remove any excess FOTS. The finished surface had a water contact angle of 110°.

C.2.3 Preparation of P3HT films.

Solutions of P3HT were prepared at a concentration of 15 mg mL^{-1} in chloroform and allowed to stir overnight. After mixing the solutions were filtered with a 1 μm syringe filter prior to spin coating. The films were spun onto the substrates at a speed of 500 rpm (250 rpm s^{-1} ramp) for 120 s followed by 30 s at a speed of 2000 rpm (1000 rpm s^{-1} ramp). After spinning the films were allowed to dry in air for 20 min and then annealed on a hotplate for 10 min at 110 °C. For the FOE buckling measurements two additional P3HT films were spun at speeds of 1000 rpm (500 rpm s^{-1} ramp) and 1500 rpm (750 rpm s^{-1} ramp).

C.3 Film on elastomer (FOE) methods

C.3.1 Mechanical buckling.

Poly(dimethylsiloxane) (PDMS) was chosen as the elastomer for all FOE based experiments. The PDMS was mixed at a base to crosslinker ratio of 10:1 and allowed to cure at room temperature for 48 h before use in any experiment. After curing the PDMS was cut into rectangular strips (l = 10 cm, w = 1 cm, h = 0.3 cm) for use in the FOE experiments. For mechanical buckling the PDMS was prestrained to 2-4% on a linear actuator and fixed to glass slides. Thin films of P3HT at three different thicknesses were transferred to PDMS substrates and

the pre-strain was released which caused the film to form buckles on the surface. The buckles were analyzed under a Leica DM2700M microscope in various parts of the film and divided by the length of the image to give λ_b. The thickness of the films, d_f, was measured using a Veeco Dektak stylus profilometer. The elastic modulus of the PDMS, E_s, was measured using an Instron pull tester. The Poisson's ratio of the PDMS substrate, V_s, and the P3HT thin films, V_f, were estimated to be 0.5 and 0.35, respectively. When the Poisson's ratio is estimated at these values mechanical buckling produces moduli that agree well with other methods. The resulting values were then used in Equation 1 to obtain the elastic modulus of each P3HT thin film. This process has been reported in detail elsewhere.[2]

$$E_f = 3E_s\left(\frac{1-v_f^2}{1-v_s^2}\right)\left(\frac{\lambda_b}{2\pi d_f}\right)^3 \quad (\mathbf{1})$$

C.3.2 Yield point (onset of buckling).

P3HT was transferred to precut strips of PDMS and imaged under a microscope to ensure a clean transfer prior to conducting the test. To determine the yield point the films were strained and relaxed in increments of 1% (i.e., 0%→1%→0%→2%→0%→3%→0%, etc.) until the onset of wrinkles could be observed in the microscope. After the onset of buckles the image and the strain was recorded. A more detailed explanation of this process has been reported elsewhere.[3]

C.3.3 Crack onset.

Crack onset measurements were performed by transferring thin films of P3HT to unstrained strips of PDMS. The PDMS strips were strained on a linear actuator in increments of 1% and observed under a microscope until the formation of cracks or pinholes appeared. The crack

onset was labelled as the first appearance of cracks in brittle samples and the appearance of new pinholes or the enlargement of existing pinholes in ductile samples.

C.4 Film on water (FOW) method

To perform the tensile testing of P3HT thin films, the P3HTs were spin-coated onto PEDOT:PSS/glass substrates. The dog-bone-shaped tensile testing specimen was prepared using a femtosecond laser patterning technique. To afloat the specimen on the water surface, the PEDOT:PSS was used as a sacrificial layer. By dissolving the PEDOT:PSS layer at the water surface, the P3HT thin film was delaminated from the glass substrate and subsequently the film was afloat on the water surface. For the specimen manipulation on the water surface, PDMS-coated Al grips were attached to the specimen gripping areas using van der Waals adhesion. The tensile test was performed by applying tensile strain using a linear stage. During the tensile test, stress and strain data are obtained by a load cell and a DIC camera, respectively. A detailed description of these methods has been previously reported.[4]

C.5 Computational methods

All molecular dynamics simulations were performed using the open-sourced LAMMPS software.[5] All visualization was performed using OVITO.[6] A detailed description of the coarse-grained model employed can be found elsewhere.[7,8] A detailed description of the simulation protocols employed can be found elsewhere.[9] For the low molecular weight simulations (50 units) a total of 400 chains were used. For the high molecular weight simulations (300 units) a total of 600 chains were used. Higher molecular weight simulations require more chains to ensure that they do not wrap in and out of the periodic boundary conditions and produce unphysical results.

References

(1) Loewe, R. S.; Khersonsky, S. M.; McCullough, R. D. A Simple Method to Prepare Head-to-Tail Coupled, Regioregular Poly(3-Alkylthiophenes) Using Grignard Metathesis. *Adv. Mater.* **1999**, *11* (3), 250–253.

(2) Savagatrup, S.; Makaram, A. S.; Burke, D. J.; Lipomi, D. J. Mechanical Properties of Conjugated Polymers and Polymer-Fullerene Composites as a Function of Molecular Structure. *Adv. Funct. Mater.* **2014**, *24* (8), 1169–1181.

(3) Printz, A. D.; Zaretski, A. V.; Savagatrup, S.; Chiang, A. S.-C.; Lipomi, D. J. Yield Point of Semiconducting Polymer Films on Stretchable Substrates Determined by Onset of Buckling. *ACS Appl. Mater. Interfaces* **2015**, *7*, 23257–23264.

(4) Kim, J.-H.; Nizami, A.; Hwangbo, Y.; Jang, B.; Lee, H.-J.; Woo, C.-S.; Hyun, S.; Kim, T.-S. Tensile Testing of Ultra-Thin Films on Water Surface. *Nat. Commun.* **2013**, *4*, 2520.

(5) Plimpton, S. Fast Parallel Algorithms for Short-Range Molecular Dynamics. *J. Comput. Phys.* **1995**, *117* (1), 1–19.

(6) Stukowski, A. Visualization and Analysis of Atomistic Simulation Data with OVITO–the Open Visualization Tool. *Model. Simul. Mater. Sci. Eng.* **2009**, *18* (1), 15012.

(7) Jones, M. L.; Huang, D. M.; Chakrabarti, B.; Groves, C. Relating Molecular Morphology to Charge Mobility in Semicrystalline Conjugated Polymers. *J. Phys. Chem. C* **2016**, *120*, 4240–4250.

(8) Huang, D. M.; Faller, R.; Do, K.; Moul, A. J. Coarse-Grained Computer Simulations of Polymer / Fullerene Bulk Heterojunctions for Organic Photovoltaic Applications. *J. Chem. Theory Comput.* **2010**, *6*, 526–537.

(9) Root, S. E.; Savagatrup, S.; Pais, C. J.; Arya, G.; Lipomi, D. J. Predicting the Mechanical Properties of Organic Semiconductors Using Coarse-Grained Molecular Dynamics Simulations. *Macromolecules* **2016**, *49* (7), 2886–2894.

Appendix D

Supporting Information for Chapter 4

Measurement of Cohesion and Adhesion of Semiconducting Polymers by Scratch Testing: Effect of Side-Chain Length and Degree of Polymerization

Daniel Rodriquez,[1] James G. Kohl,[2] Pierre Morel,[4] Kyle Burrows,[4] Grégory Favaro,[5] Samuel E. Root,[1] Julian Ramirez,[1] Mohammad A. Alkhadra,[1] Cody W. Carpenter,[1] Zhuping Fei,[3] Pierre Boufflet,[3] Martin Heeney,[3] Darren J. Lipomi[*,1]

[1]*Department of NanoEngineering, University of California San Diego*

9500 Gilman Drive, Mail Code 0448, La Jolla, CA 92093-0448

[2]*Department of Mechanical Engineering, Shiley-Marcos School of Engineering,*

University of San Diego, San Diego, CA, 92110-2492

[3]*Department of Chemistry and Centre for Plastic Electronics, Imperial College London,*

Exhibition Rd, London, SW7 2AZ, United Kingdom

[4]*TriTec, Anton Paar USA, Inc., 10215 Timber Ridge Drive, Ashland, VA 23005*

[5]*TriTec, Anton Paar SA, CH-2034 Peseux, Switzerland*

D.1 AFM images and UV-vis absorption spectra

During scratch tests, there may be local ordering within the scratch channel due to shear-induced ordering of the polymer chains that give rise to changes in the optical behavior of the films during cohesive failure. To further investigate this effect we performed AFM measurements within the scratch channel for P3HT (63 kDa). It is difficult to clearly identify any ordering of the polymer chains. However, it is possible to see features in the bottom of the channel running parallel to the scratch direction (reminiscent of crazing) and pileup (raised zones) along the edges. These features would be consistent with plastic deformation and shear-induced failure of the polymers.

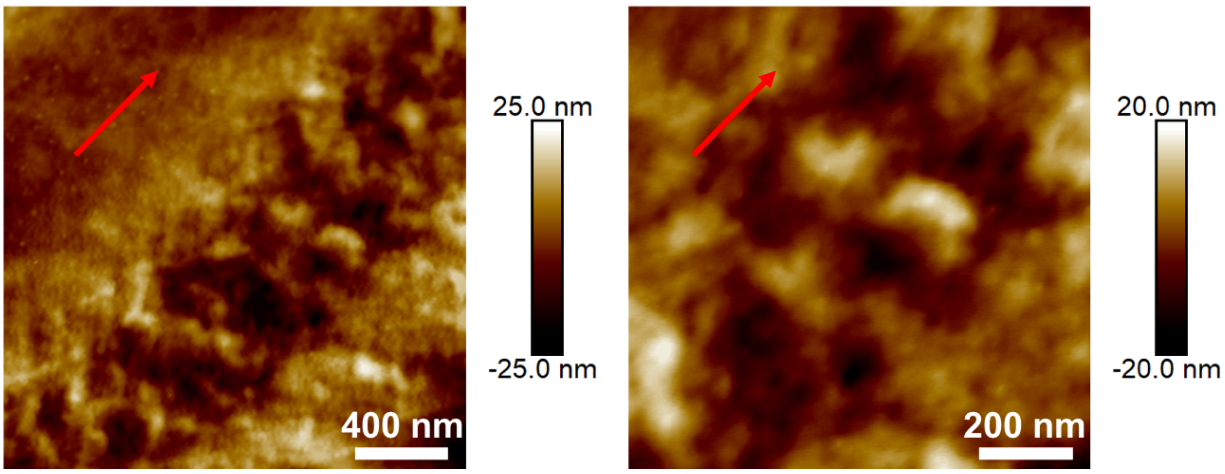

Figure D.1. Surface morphology of the scratch channel for P3HT (63 kDa). The arrow indicates the direction of the scratch.

The absorption of P3ATs is strongly affected by changes in the side chain length and the molecular weight. To quantify these changes we performed UV-vis absorption measurements as a function of *n* for P3ATs and molecular weight for P3HT. The results are shown in **Figure D.2.** Furthermore, we quantified the aggregation behavior of the films using the weakly interacting H-aggregate model and summarized the results in **Table D.1.** Overall, the conjugation length (W^{-1}) (the inverse of the exciton bandwidth, W) decreased from P3HT (8.333) to P3HpT (5.587) and increased slightly for P3DT (5.814). The conjugation length increased with molecular weight of

P3HT from M_n = 15 kDa (7.143) to M_n = 80 kDa (10.000). The fraction of aggregates initially decreased from 0.593 to 0.554 as the molecular weight of P3HT increased from M_n = 15 kDa to M_n = 63 kDa, respectively, then increased for M_n = 80 kDa (0.578). The fraction of aggregates is similar for n = 6 (0.564) and n = 7 (0.566) and decreased for n = 10 (0.510).

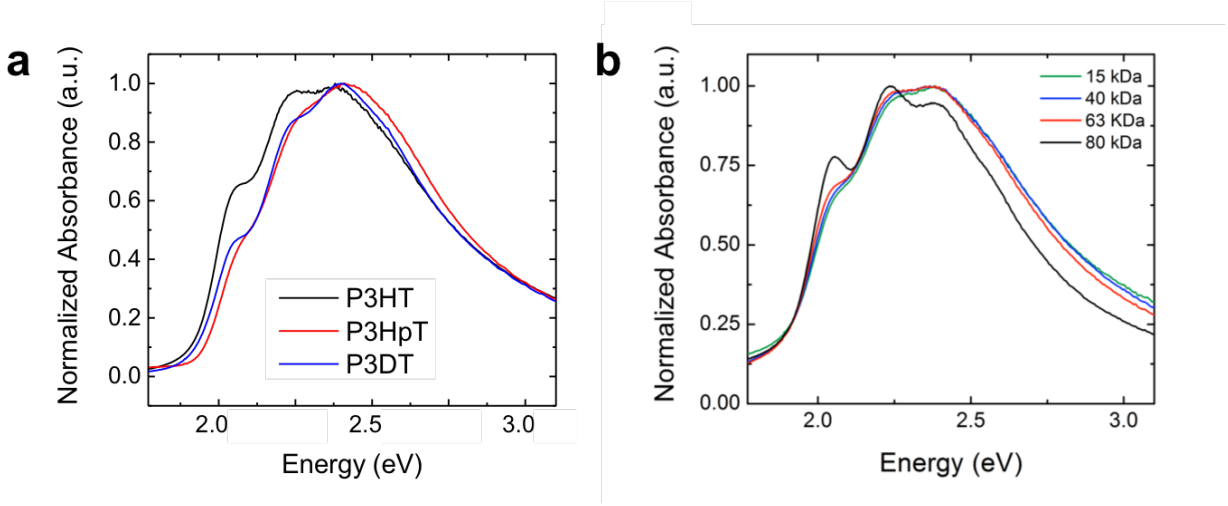

Figure D.2. Absorption of P3AT thin films cast from $CHCl_3$. a) As a function of the length of the side chain. b) As a function of molecular weight for P3HT, reproduced from ref [1].

Table D.1. Summary of the weakly interacting H-aggregate model parameters extracted from UV-vis absorption spectra. The values for M_n were reproduced from ref [1].

Weakly Interacting H-Aggregate Model Parameters

M_n (kDa)	W (eV)	1/W (eV^{-1})	Fraction of Aggregates
15	0.14	7.143	0.593
40	0.12	8.333	0.564
63	0.12	8.333	0.554
80	0.10	10.000	0.578
n	**W (eV)**	**1/W (eV^{-1})**	**Fraction of Aggregates**
6	0.12	8.333	0.564
7	0.18	5.587	0.566
10	0.17	5.814	0.510

D.2 Experimental methods

D.2.1 Sample preparation.

Regioregular P3HpT (M_n = 35 kg mol^{-1}, dispersity ($Đ$) = 2.2), and P3DT (M_n = 39 kg mol^{-1}, Đ = 2.1) were purchased from Rieke Metals, LLC. P3HT was synthesized using the GRIM method, with regioregularity > 95% in all cases. Values of the M_n of P3HT were 15, 40, 63, and 80 kg mol^{-1} with dispersities of 1.4, 1.7, 1.7 and 1.6, respectively. All solutions were prepared in concentrations of 15 mg mL^{-1} in chloroform and stirred overnight. Prior to spin coating, the solutions were filtered with a 1 μm PTFE syringe filter. The films were spun onto clean silicon wafers (1 cm × 1 cm) with a ≥ 200 nm thermal oxide layer at a speed of 500 rpm (250 rpm s^{-1} ramp) for 120 s followed by 30 s at a speed of 2000 rpm (1000 rpm s^{-1} ramp). After spinning, the films were dried in air for 20 min and then annealed on a hotplate for 10 min at 110 °C. Scratch tests were performed at a rate of 1 mm min^{-1} using an Anton Paar Nano Scratch Tester (NSTX). The initial load was 0.05 mN and increased linearly at a rate of 3.9 mN min^{-1} until a final load of 2 mN was reached. The rate of acquisition was 30 Hz and the spherical diamond stylus had a radius of curvature of 10 μm.

D.2.2 Computational methods.

Molecular dynamics simulations were performed using a previously described three-site coarse-grained model,[2] and simulation protocol for imitating solvent-casting.[3] Briefly, a periodic simulation box was populated with polymer chains in a low-density state and high temperature Langevin dynamics (550 K, friction factor = (180 fs)$^{-1}$) were run under constant pressure conditions (1 atm)—with a gradually increasing interaction parameter, initially reduced to 10% of its melt-phase value—until the simulation converged to a constant density melt, allowing ~100 ns

for equilibration. The simulation was then quenched into a glassy state (300 K) over the course of 10 ns. Three different simulations were prepared to model the effect of molecular weight, with chain lengths of (50, 150, 300) and corresponding total number of chains: (300, 300, 600). The highest molecular weight polymers contained more chains to keep the size of the simulation box much larger than the radius of gyration of the chains. Simulated 40 nm thin films were prepared by unwrapping the coordinates of the high molecular weight system, and then re-melting (550K) and quenching over the course of 20 ns to relax the structure of the surface. The primitive path and entanglements were computed using the Z1 code.[4] Simulations and visualizations were performed with LAMMPS[5] and OVITO,[6] respectively.

References

(1) Rodriquez, D.; Kim, J.-H.; Root, S. E.; Fei, Z.; Boufflet, P.; Heeney, M.; Kim, T.-S.; Lipomi, D. J. Comparison of Methods for Determining the Mechanical Properties of Semiconducting Polymer Films for Stretchable Electronics. *ACS Appl. Mater. Interfaces* **2017**, *9* (10), 8855–8862.

(2) Tapping, P. C.; Clafton, S. N.; Schwarz, K. N.; Kee, T. W.; Huang, D. M. Molecular-Level Details of Morphology-Dependent Exciton Migration in Poly(3-Hexylthiophene) Nanostructures. *J. Phys. Chem. C* **2015**, *119* (13), 7047–7059.

(3) Root, S. E.; Savagatrup, S.; Pais, C. J.; Arya, G.; Lipomi, D. J. Predicting the Mechanical Properties of Organic Semiconductors Using Coarse-Grained Molecular Dynamics Simulations. *Macromolecules* **2016**, *49* (7), 2886–2894.

(4) Kröger, M. Shortest Multiple Disconnected Path for the Analysis of Entanglements in Two- and Three-Dimensional Polymeric Systems. *Comput. Phys. Commun.* **2005**, *168* (3), 209–232.

(5) Plimpton, S. Fast Parallel Algorithms for Short-Range Molecular Dynamics. *J. Comput. Phys.* **1995**, *117* (1), 1–19.

(6) Stukowski, A. Visualization and Analysis of Atomistic Simulation Data with OVITO–the Open Visualization Tool. *Model. Simul. Mater. Sci. Eng.* **2009**, *18* (1), 015012.